PERIODICAL
Journal of Marine Research
v. 18-19
1959-61

DATE OF MAGAZINE	BORROWER'S NAME	TIME
MAR 11 1963	R Brown	
2/24/67	HL-Bell Udwin	

PERIODICAL
Journal of Marine Research

V. 18-19

1959-61

LIBRARY
BUR. OF COMM. FISH.
HON. BIOL. LAB.

PERIODICAL
2945
J. 3 Marine
Research
V. 18-19
1959-61

SEARS FOUNDATION FOR MARINE RESEARCH
BINGHAM OCEANOGRAPHIC LABORATORY, YALE UNIVERSITY

JOURNAL OF MARINE RESEARCH

VOLUME 18
NUMBERS 1–3

ISSUED 1959–60, NEW HAVEN, CONN., U.S.A.

JOURNAL OF MARINE RESEARCH

PUBLISHED BY

SEARS FOUNDATION FOR MARINE RESEARCH

BINGHAM OCEANOGRAPHIC LABORATORY, YALE UNIVERSITY

BOARD OF EDITORS

Chairman: A. E. PARR
American Museum of Natural History
New York, N. Y.

COLUMBUS O'D. ISELIN
Woods Hole Oceanographic Institution
Woods Hole, Mass.

DALE F. LEIPPER
A. and M. College of Texas
College Station, Texas

DANIEL MERRIMAN
Bingham Oceanographic Laboratory
New Haven, Conn.

WALTER H. MUNK
Scripps Institution of Oceanography
La Jolla, Calif.

DONALD W. PRITCHARD
Chesapeake Bay Institute
Annapolis, Maryland

ROGER REVELLE
Scripps Institution of Oceanography
La Jolla, Calif.

THOMAS G. THOMPSON
Oceanographic Laboratories
University of Washington
Seattle, Wash.

MANAGING EDITOR

YNGVE H. OLSEN
Bingham Oceanographic Laboratory
Yale University
New Haven, Conn.

The Journal is normally issued in three numbers per year constituting one volume. All income derived from subscriptions is used solely to increase the volume and improve the quality of the Journal for the benefit of its readers.

Subscription price for volumes 1 through 12, $3.00 per volume or $1.50 per number; for volumes 13 through 16, $5.00 per volume or $2.00 per number; for volume 17 and subsequent volumes, $7.00 per volume or $2.50 per number. Address all communications to the Managing Editor.

ALPHABETICAL INDEX BY AUTHOR'S NAMES

Page

M. R. ABBOTT: Boundary layer effects in estuaries 83

M. R. ABBOTT: Salinity effects in estuaries 101

RICHARD L. ARMSTRONG: See Turekian and Armstrong.

PETER COLLINS and HARVEY DIEHL: Tripyridyltriazine, a reagent for the determination of iron in sea water 152

TOWNSEND CROMWELL: Pycnoclines created by mixing in an aquarium tank 73

HARVEY DIEHL: See Collins and Diehl.

G. W. GROVES: See Roden and Groves.

R. E. KENT and D. W. PRITCHARD: At test of mixing length theories in a coastal plan estuary 62

TAIVO LAEVASTU: See Thompson and Laevastu.

JUNE G. PATTULLO: Seasonal variation in sea level in the Pacific Ocean during the International Geophysical Year, 1957–1958 168

W. J. PIERSON, JR.: On the use of time series concepts and spectral and cross-spectral analyses in the study of long-range forecasting problems 112

R. W. PREISENDORFER: Theoretical proof of the existence of characteristic diffuse light in natural waters 1

D. W. PRITCHARD: See Kent and Pritchard.

JOHN A. REED: See Weiss and Reed.

G. I. RODEN: On the heat and salt balance of the California Current region 36

G. I. RODEN and G. W. GROVES: Recent oceanographic investigations in the Gulf of California 10

THOMAS G. THOMPSON and TAIVO LAEVASTU: Determination and occurrence of cobalt in sea water 189

KARL K. TUREKIAN and RICHARD L. ARMSTRONG: Magnesium, strontium, and barium concentrations and calcite-aragonite ratios of some recent molluscan shells 133

J. E. TYLER: Observed and computed path radiance in the underwater light field 157

HERBERT V. WEISS and JOHN A. REED: Determination of cobalt in sea-water 185

SEARS FOUNDATION FOR MARINE RESEARCH
BINGHAM OCEANOGRAPHIC LABORATORY, YALE UNIVERSITY

JOURNAL OF
MARINE RESEARCH

VOLUME 18 1959 NUMBER 1

THEORETICAL PROOF OF THE EXISTENCE OF CHARACTERISTIC DIFFUSE LIGHT IN NATURAL WATERS[1]

By

RUDOLPH W. PREISENDORFER

Scripps Institution of Oceanography, University of California
La Jolla, California

ABSTRACT

This paper develops a mathematical model for the radiance distribution of light penetrating a homogeneous hydrosol on the basis of the general theory of radiative transfer. It is proved that the radiance distribution approaches an asymptotic pattern at great depths. This is in accord with previous field measurements of the directional patterns in underwater light and with L. V. Whitney's conjecture that there is at some depth in natural waters a characteristic diffuse light symmetrically distributed around the vertical. The angular form of this equilibrium light pattern is derived in terms of the mathematical model presented.

INTRODUCTION

Recent experimental evidence (Tyler, 1958) forms the basis for fresh support of the long-standing conjecture that the radiance distribution about a point in an optically deep natural hydrosol approaches, with increasing depth, a characteristic form which is independent of the external lighting conditions and of the optical state of the medium's surface and which depends only on the inherent optical

[1] This paper represents results of research which has been supported by the Bureau of Ships, U. S. Navy.

properties of the medium. This conjecture was apparently given its first definitive formulation by Whitney (1941a, 1941b), who referred to the asymptotic radiance distribution as *characteristic diffuse light.* (Some early experimental evidence for this conjecture is cited in Whitney's papers.) In this note we complement experimental evidence in favor of this conjecture by supplying a simple mathematical proof of the existence of characteristic diffuse light in all homogeneous optically deep natural waters. The paper concludes with a derivation of the integral equation governing the angular structure of characteristic diffuse light as well as a brief discussion of an interesting and tractable example for the case of isotropic scattering.

We note in passing that the applicability of Whitney's hypothesis has been widened considerably since its formulation. The problem of a limiting angular distribution has since been encountered in modern neutron transport theory, basically as an abstract mathematical problem rather than as an experimental phenomenon. A similar type of problem has long been extant in astrophysical radiative transfer. A general proof of the existence of an asymptotic radiance distribution which covers all of these contexts recently has been devised (Preisendorfer, 1958a).

However, the hypothesis still retains its greatest usefulness in the context of geophysical optics. For in this field, unlike the others mentioned above, the trend to a characteristic limiting form is a directly observable phenomenon. Furthermore, the existence of such a form is of inestimable importance to all experimental research work dealing with the determination of optical properties of natural waters. In many important instances, knowledge that an asymptotic radiance distribution exists will obviate the necessity of experimental probings to extremely large depths; for such knowledge will allow, by means of relatively simple formulae, accurate prediction of the geometrical structure of the light field in great-depth ranges. Some of these practical consequences of the asymptotic radiance hypothesis have been formulated recently (Preisendorfer 1958b).

PHYSICAL BACKGROUND OF THE METHOD OF PROOF

The argument used by Whitney in establishing experimental evidence for the asymptotic radiance hypothesis went basically as follows: he showed that when experimentally obtained plots of radiance distributions at various large depths were blown up to the same size (more precisely, the zenith readings were normalized to a common value), they formed a set of nearly congruent figures. Now, an interesting feature of such distributions is that they assume the same

shape and decrease in size with increasing depth at nearly the same exponential rate. This fact can be stated precisely as follows:[2]

$$N(z, \theta, \phi) = g(\theta, \phi)e^{-kz}. \tag{1}$$

From this we see that the asymptotic radiance hypothesis is equivalent to the statement that *the directional and depth dependence of radiance distributions multiplicatively uncouple at great depths.* That is, the radiance function N may be represented as the product of two functions: g which gives the shape or directional structure common to all distributions and an exponential function which gives the depth dependence of the distributions.

Each factor on the right-hand side of (1) has special physical significance. The function g evidentally defines the angular form of characteristic diffuse light. The exponent k of the exponential function has the following interesting interpretation.

Define *scalar irradiance* $h(z)$ at depth z as follows:

$$h(z) = \int_{\phi=0}^{2\pi} \int_{\theta=0}^{\pi} N(z, \theta, \phi) \sin \theta \, d\theta \, d\phi. \tag{2}$$

The quantity $h(z)$ is then a measure of the volume density of radiant energy at depth z. Measurements of $h(z)$ over the years in many hydrosols have shown that $h(z)$ varies essentially in an exponential manner with depth. That is, semilog plots of $h(z)$ *vs* depth show an unmistakable trend toward linearity as depth increases. In any event, $h(z)$ may be accurately represented by a general formula of the type

$$h(z) = h(o) \exp\left\{-\int_0^z k(z') \, dz'\right\}, \tag{3}$$

where $k(z)$ is the negative logarithmic derivative of $h(z)$. (Here and below, a primed symbol refers to a dummy variable of integration.) As depth increases, experimental evidence gathered in the field indicates that $k(z)$ approaches a constant value. Denote this limit value by k_∞. Now, assuming that an asymptotic radiance distribution is approached by the radiance distributions in a particular body of water, we see from (1), (2) and (3) that

$$h(z) = h(z_0)e^{-k_\infty(z-z_0)} = e^{-kz} \int_{\phi=0}^{2\pi} \int_{\theta=0}^{\pi} g(\theta, \phi) \sin \theta \, d\theta \, d\phi, \tag{4}$$

[2] It is implicit in the definition of radiance that it applies to an arbitrary but fixed wavelength of radiant flux. This is also true of all the other radiometric quantities used in this note.

where z_0 is the depth below which we may assume that $k(z) = k_\infty$. From this we conclude that

$$k = k_\infty. \tag{5}$$

Hence, under the above assumption (1) we see that, at great depths, the size of a radiance distribution plot decreases exponentially with increasing depth and that the rate of this decrease is precisely that of scalar irradiance (or energy density).

The close connection between the depth dependence of scalar irradiance and that of the radiance distributions, as summarized in (5), suggests the following mode of representation of the radiance distributions for any depth: Define, for each direction (θ, ϕ),

$$K(z, \theta, \phi) = \frac{-1}{N(z, \theta, \phi)} \frac{dN(z, \theta, \phi)}{dz}. \tag{6}$$

Then, in analogy to (3), $N(z, \theta, \phi)$ at any depth z may be represented exactly by

$$N(z, \theta, \phi) = N(0, \theta, \phi) \exp\left\{ - \int_0^z K(z', \theta, \phi)\, dz' \right\}. \tag{7}$$

Now suppose there is some depth z_0 below which we have $K(z, \theta, \phi) = k_\infty$ for all directions (θ, ϕ). Then (7) may be written

$$\begin{aligned} N(z, \theta, \phi) &= N(0, \theta, \phi) \exp\left\{ - \int_0^{z_0} K(z', \theta, \phi)\, dz' - \int_{z_0}^z K(z', \theta, \phi)\, dz' \right\} \\ &= N(z_0, \theta, \phi) \exp\{ - k_\infty (z - z_0) \}. \end{aligned}$$

If we set

$$g(\theta, \phi) = N(z_0, \theta, \phi) \exp\{k_\infty z_0\},$$

then we may write

$$N(z, \theta, \phi) = g(\theta, \phi)\, e^{-k_\infty z}, \tag{8}$$

for all depths z below z_0.

The similarity between (1) and (8) is unmistakable and it points out a method of attack we may follow in order to prove the asymptotic radiance hypothesis: we must show that the quantities $K(z, \theta, \phi)$ approach a limit as depth is increased and that this limit is independent of the directions (θ, ϕ). Furthermore, this limit, in accordance with the preceding discussion, should be none other than the limit k_∞ of $k(z)$, as defined in (3).

THE PROOF

We make use of the equation of transfer for radiance:

$$\frac{dN(z, \theta, \phi)}{dr} = -\alpha N(z, \theta, \phi) + N_*(z, \theta, \phi), \tag{9}$$

where

$$N_*(z, \theta, \phi) = \int_{\phi'=0}^{2\pi} \int_{\theta'=0}^{\pi} \sigma(\theta, \phi; \theta', \phi')\, N(z, \theta', \phi') \sin \theta'\, d\theta'\, d\phi' \tag{10}$$

defines the path function N_*; σ is the volume scattering function (which governs the law of scattering in the water) and α is the volume attenuation coefficient. The formal solution of (9) is readily obtained:

$$N(z, \theta, \phi) = N^0(z, \theta, \phi) + \int_0^r N_*(z', \theta, \phi)\, e^{-\alpha(r-r')}\, dr'. \tag{11}$$

The first term represents the component of N consisting of unscattered light. The second represents the space light over the path of length r

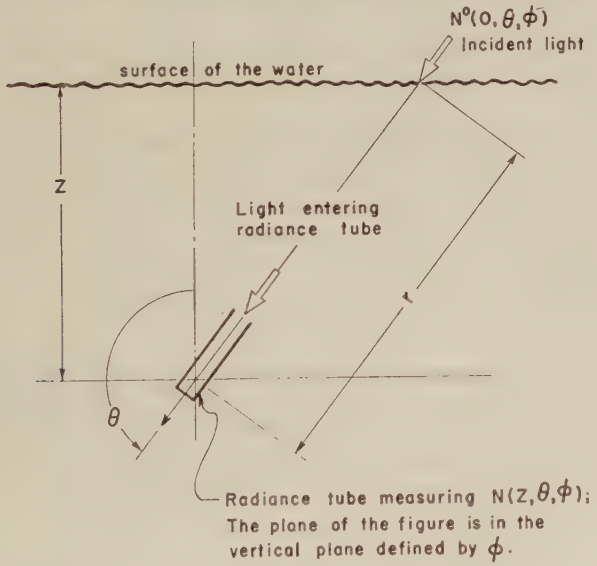

Figure 1

(Fig. 1) which has been generated by light scattered into the path of sight all along its extent. The formal solution (11) has been written for a general downward direction of flow of light (see Fig. 1) so that $N^0(z, \theta, \phi)$ is interpreted as the directly transmitted light from the upper boundary of the medium and is of the form

$$N^0(z, \theta, \phi) = N^0(0, \theta, \phi)\, e^{-\alpha r},$$

where

$$-r \cos \theta = z.$$

We now turn eq. (11) into a useful inequality by means of the following three steps:

First, since $N(z, \theta, \phi)$ clearly exceeds its spacelight component at all depths, we write

$$N(z, \theta, \phi) > \int_0^r N_*(z', \theta, \phi)\, e^{-\alpha(r-r')}\, dr'.$$

Second, using the definition of N_*, we strengthen the inequality when we write

$$N(z, \theta, \phi) > \sigma_{\min} \int_0^r h(z')\, e^{-\alpha(r-r')}\, dr',$$

where $\sigma_{\min}$ is the minimum value of the volume scattering function; that is, we have used (10) to deduce that

$$N_*(z, \theta, \phi) > \sigma_{\min} \int_{\phi'=0}^{2\pi} \int_{\theta'=0}^{\pi} N(z, \theta', \phi') \sin \theta'\, d\theta'\, d\phi' = \sigma_{\min} h(z).$$

Finally, since $h(z)$ decreases with increasing depth, we certainly strengthen the inequality by writing

$$N(z, \theta, \phi) > \sigma_{\min}\, h(z) \int^r e^{-\alpha(r-r')}\, dr'.$$

That is, we have

$$N(z, \theta, \phi) > \frac{\sigma_{\min}}{\alpha} h(z)(1 - e^{-\alpha r}) \tag{12}$$

for all depths z. From this we see that, as depth increases indefinitely, the exponential rate of decrease $K(z, \theta, \phi)$ of the radiance cannot eventually exceed the $k(z)$ of scalar irradiance and remain larger by any finite amount; if it did, the plot of N would eventually fall and remain below that of h. This observation is stated symbolically as follows:

$$\lim_{z\to\infty} K(z, \theta, \phi) \leqslant \lim_{z\to\infty} k(z) = k_\infty \tag{13}$$

for all downward directions (θ, ϕ). We now show that strict equality must hold in (13). We achieve this by initially assuming the contrary; that is, we assume that there is a nonzero solid angle Ω_0 of directions over which

$$\lim_{z\to\infty} K(z, \theta, \phi) \leqslant k_\infty - \epsilon,$$

where ϵ is *any* small positive number. Then it is clear that the radiances in this set of directions decrease at a definitely smaller rate than scalar irradiance; so much smaller in fact that, by our assumption, for some depth z_1 we must have

$$\int_{\Omega_0} N(z_1, \theta, \phi) \sin\theta \, d\theta \, d\phi > h(z_1).$$

However, this conclusion clearly contradicts (2) since a part cannot exceed the whole. We have reached a contradiction which leaves only one other possibility:

$$\lim_{z\to\infty} K(z, \theta, \phi) = k_\infty \tag{14}$$

for all downward directions (θ, ϕ). In the light of the preceding discussion [*cf* (8)], this means that the shape of the radiance distributions impinging on the upper boundaries of deep layers of water eventually assume a fixed form. But it is known that the shape of the *reflected* radiance distribution at the upper boundary of a scattering layer is determined by the shape of the incident radiance distribution at that boundary. Hence if the incident radiance distribution approaches a fixed shape, so does that of the reflected distribution. This completes the proof.

We observe that the present proof can also be applied in all natural waters which eventually become homogeneous. That is, the preceding arguments are basically unchanged if the medium is inhomogeneous over any initial finite depth range below the surface. Even more general media exist which give rise to asymptotic radiance distributions, namely media in which the ratio σ/α eventually becomes independent of depth (Preisendorfer, 1958a).

THE EQUATION FOR CHARACTERISTIC DIFFUSE LIGHT

Using the equation of transfer, definition (6), and the relation between z and r, we write the equation of transfer in the following general form:

$$N(z, \theta, \phi) = \frac{N_*(z, \phi, \theta)}{\alpha + K(z, \theta, \phi)\cos\theta}. \tag{15}$$

From (14) and (8) we see that the limiting form of (15) (as depth increases indefinitely) is

$$g(\theta, \phi) = \frac{\int_{\phi'=0}^{2\pi}\int_{\theta'=0}^{\pi} \sigma(\theta, \phi; \theta', \phi')\, g(\theta', \phi') \sin\theta' \, d\theta' \, d\phi'}{\alpha + k_\infty \cos\theta}; \tag{16}$$

this is the equation governing the angular form of characteristic diffuse light. It is a property of equations of the type shown in (16) that the function g is independent of ϕ for all real physical situations. Thus characteristic diffuse light is always represented by a surface of revolution whose axis of symmetry is vertical.

The theory of the solution of such equations as (16) is fairly well understood (*e.g.*, see Davison, 1957). The present note, therefore, will not discuss (16) in any detail. However, there is one simple special case which is immediately solved and which can shed much light on some of the salient details of the structure of the asymptotic radiance distributions. This is the case of isotropic scattering, where the volume scattering function σ is independent of direction and has the form

$$\sigma(\theta, \phi; \theta', \phi') = \frac{s}{4\pi}, \tag{17}$$

where s is the total scattering coefficient.

To observe the resulting structure of the asymptotic radiance distribution it is convenient in the present case to turn to (15). With assumption (17) and definitions (2) and (10), we have

$$N(z, \theta, \phi) = \frac{s}{4\pi} \frac{h(z)}{\alpha + K(z, \theta, \phi) \cos\theta} ,$$

which at great depths approaches the form

$$N(z, \theta, \phi) = \frac{1}{4\pi} \left(\frac{s}{\alpha}\right) \frac{h(z_0)\, e^{-k_\infty (z - z_0)}}{1 + \left(\frac{k_\infty}{\alpha}\right) \cos\theta} . \tag{18}$$

Here z_0 is the depth below which $h(z)$ decreases exponentially with increasing depth. Comparing (18) with (8), we see that for the present case

$$g(\theta, \phi) = \frac{1}{4\pi} \left(\frac{s}{\alpha}\right) \frac{h(z_0)\, e^{k_\infty z_0}}{1 + \left(\frac{k_\infty}{\alpha}\right) \cos\theta} . \tag{19}$$

We have written (19) in the indicated form to point up the following geometric fact: A polar plot of $g(\theta, \phi)$ is generally a prolate ellipsoid of revolution with vertical axis and of eccentricity k_∞/α. When there is no absorption in the medium, it is easy to deduce then that $k_\infty = 0$ and that characteristic diffuse light is represented by a sphere. On the other hand, if there is little scattering as compared to absorption, the figure assumes a narrow pencil-like shape. In the limit of no

scattering, k_∞ approaches α, and the figure degenerates into a vertical line.

The structure of the expression in (18) is related to the limiting form of a simple model for the radiance distribution discussed elsewhere (Preisendorfer, 1958c) and to a formula derived by Poole (1945). We conclude with the observation that (19) predicts a different limiting ratio of horizontal to upward radiance than that derived by Whitney (1941a) under the same circumstances (*i.e.*, isotropic scattering). Instead of the ratio 2:1, as suggested by Whitney, the present formula yields

$$\frac{g(\pi/2, \phi)}{g(0, \phi)} = 1 + \left(\frac{k_\infty}{\alpha}\right) \leqslant 2. \tag{20}$$

In other words, the ratio in (20) is not a fixed magnitude but depends on the optical properties of the medium in the manner shown.

The distribution (19) can serve as a convenient standard reference distribution against which experimentally determined radiance distributions can be compared. The amount of departure of the experimental distributions from (19) would then serve as a measure of the anisotropy of scattering in the real medium.

REFERENCES

Davison, B.

1957. Neutron transport theory. Clarenden Press, Oxford. 450 pp.

Poole, H. H.

1945. The angular distribution of submarine daylight in deep water. Sci. Proc. R. Dublin Soc., *24:* 29–42.

Preisendorfer, R. W.

1958a. A proof of the asymptotic radiance hypothesis. Visibility Laboratory Report, Scripps Institution of Oceanography, University of California. SIO Ref. 58–57.

1958b. Some practical consequences of the asymptotic radiance hypothesis. Visibility Laboratory Report, Scripps Institution of Oceanography, University of California. SIO Ref. 58–60.

1958c. Model for radiance distributions in natural hydrosols. Visibility Laboratory Report, Scripps Institution of Oceanography, University of California. SIO Ref. 58–42.

Tyler, J. E.

1958. Radiance distribution as a function of depth in the submarine environment. Visibility Laboratory Report, Scripps Institution of Oceanography, University of California. SIO Ref. 58–25.

Whitney, L. V.

1941a. The angular distribution of characteristic diffuse light in natural waters. J. Mar. Res., *4:* 122–131.

1941b. A general law of diminuation of light intensity in natural waters and the percent of diffuse light at different depths. J. opt. Soc. Amer., *31:* 714–722.

RECENT OCEANOGRAPHIC INVESTIGATIONS IN THE GULF OF CALIFORNIA

By

G. I. RODEN and G. W. GROVES

Scripps Institution of Oceanography,
La Jolla, California

ABSTRACT

Results of seven hydrographic cruises into the Gulf of California during 1956 and 1957 show that the water mass there is characteristic of Equatorial Pacific water though modified by intensive evaporation in surface layers. The combination of wind regime and complicated topographical features plays a predominant role in circulation, upwelling, distribution of temperature, and other hydrographic factors. Seasonal changes are large. An estimate of the water budget indicates that exchange between the Gulf and the Pacific Ocean is of the order of 10^6 m^3/sec. Evaporation in the Gulf is about 5×10^3 m^3/sec. Runoff and precipitation are negligible. Sea-level records were studied and interpreted in terms of geostrophic surface flow. Strong tidal currents in many parts of the Gulf are influencial in mixing the water.

Introduction. The oceanographic aspects of the Gulf of California, one of the least known marginal seas of the North Pacific, are both interesting and complex. Yet little oceanographic research has been done until recently. The Gulf is unique in that it is the only large evaporation basin in the Pacific Ocean. It is characterized by a large annual temperature range and by relatively high salinities. The tidal range at its inner end is impressive and so is the tidal bore that reaches far into the Río Colorado.

Prior to 1956, when the Scripps Institution of Oceanography in collaboration with the South Pacific Fisheries Investigations of the U. S. Fish and Wildlife Service decided to make a series of oceanographic cruises into the Gulf as part of the research conducted under the California Cooperative Oceanic Fisheries Investigations, only two hydrographic expeditions had been undertaken into this region. The first took place in 1889 with the Albatross (Tanner, 1888) and the second, almost 50 years later, with the E. W. Scripps (Sverdrup, 1941). Results from these two cruises and the meteorological aspects of the Gulf region were discussed recently (Roden, 1958).

The aims of the recent cruises into the Gulf from an oceanographic standpoint were twofold: to investigate the seasonal variation of

[1] Contribution from the Scripps Institution of Oceanography, New Series.

temperature, salinity and oxygen in the upper layers and to determine whether or not any changes in the distribution of properties had taken place in the deeper part of the sea since the last survey in 1939. In addition there were biological investigations which will not be considered here.

Tides and sea level variations in the Gulf have not been studied in detail, but since they are important in understanding the circulation, a brief description of them will be found at the end of this paper.

Data. The stations occupied and the areas covered on the seven recent cruises into the Gulf are shown in Fig. 1 and Table I, respectively. On each hydrographic station, bottle casts were made and temperatures, salinities and oxygens were determined. Bathythermographs were lowered on each station and between stations. The data were processed by the Data Collection and Processing Group of the Scripps Institution of Oceanography; the tabulated data will be published in Oceanic Observations of the Pacific, 1956 and 1957. Sea surface temperatures at coastal stations were obtained from the U.S. Coast and Geodetic Survey (1956) and meteorological information was obtained from Servicio Meteorológico Mexicano (1937, 1938).

Seasonal Variation of Temperature, Salinity and Oxygen at the Surface. One of the outstanding features of the Gulf of California is the large annual range of sea surface temperatures; at Puerto Peñasco in the north the range is about 16 C; at Cabo San Lucas in the south it is about 9 C (Table II). The pronounced seasonal temperature variation is not confined to coastal areas but occurs in offshore regions as well (Fig. 2); agreement between coastal and offshore temperatures is reasonably good. An interesting feature is an area of low temperatures around Isla Angel de la Guarda which is found throughout the year. Along the coast, temperatures are somewhat dependent upon upwelling; in winter low temperatures are generally found along the east coast and in summer along the west coast. There is little information on the year-to-year variation of temperature except that in 1957 temperatures appeared to be somewhat higher than in 1956. The seasonal variation of temperature extends downward from the surface to about 200 m, the average temperature in this depth range ranging between 14 C in winter to 18 C in summer over most of the Gulf.

The seasonal variation of salinity (Fig. 3) is surprisingly small and, except for the southernmost part, the annual range does not exceed 0.2‰. This contrasts sharply with results obtained from shore stations, where the seasonal range is of the order of 1‰ (U. S. Coast and Geodetic Survey, 1954; thus observations along the shore are not

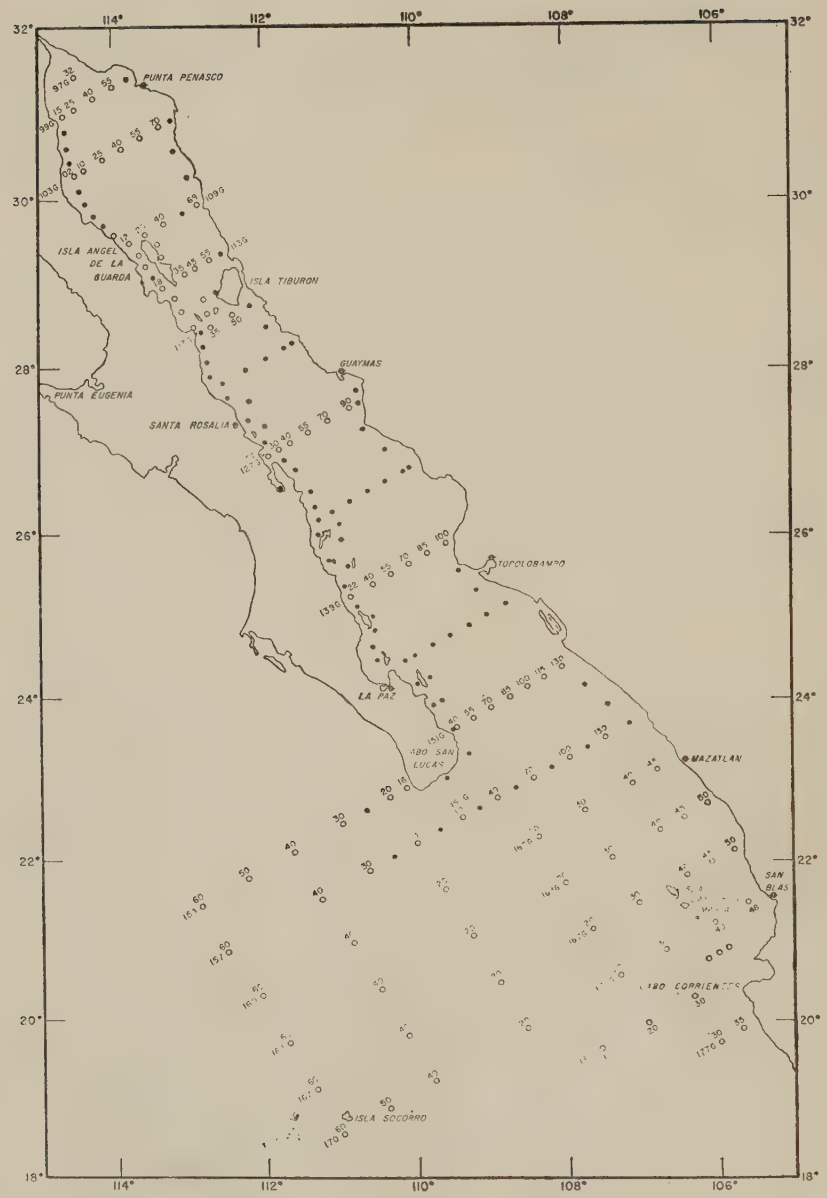

Figure 1. Stations occupied during recent Gulf cruises. Circles represent hydrographic stations, dots net-tow stations. Numbers refer to hydrographic stations.

TABLE I. Chronological list of hydrographic cruises into the Gulf of California.

Time	*Ship*	*Hydrographic casts*		*Properties observed*	*Area covered*
		Number	*to depth*		
11 Mar.–7 Apr. 1889	Albatross	28	bottom	temperature, salinity	Cabo San Lucas northward to Río Colorado.
13 Feb.–19 Mar. 1939	E. W. Scripps	53	bottom	temperature, salinity, oxygen, calcium	Cabo San Lucas northward to Río Colorado.
6 Feb.–17 Feb. 1956	Black Douglas	22	1200 m	temperature, salinity, oxygen	Cabo San Lucas northward to Isla Tiburón.
7 Apr.–23 Apr. 1956	Black Douglas	40	600 m	temperature, salinity, oxygen	Cabo San Lucas northward to Río Colorado.
26 Nov.–16 Dec. 1956	Horizon	59	bottom	temperature, salirity, oxygen	Cabo San Lucas southward to Isla Socorro and Cabo Corrientes.
8 Feb.–23 Feb. 1957	Spencer F. Baird	67	bottom	temperature, salinity, oxygen	Cabo San Lucas northward to Isla Tiburón.
7 Apr.–23 Apr. 1957	Black Douglas	37	600 m	temperature, salinity, oxygen	Cabo San Lucas northward to Río Colorado.
7 June–23 June 1957	Stranger	57	600 m	temperature, salinity, oxygen	Cabo San Lucas northward to Río Colorado.
9 Aug.–26 Aug. 1957	Stranger	57	600 m	temperature, salinity, oxygen	Cabo San Lucas northward to Río Colorado.

TABLE II. Sea surface temperatures (c) at shore stations

	Jan.	*Feb.*	*Mar.*	*Apr.*	*May*	*June*	*July*	*Aug.*	*Sept.*	*Oct.*	*Nov.*	*Dec.*	*Year*	*Range*
Puerto Peñasco, Son. (1952–1955) USCGS	14.9	15.8	17.8	20.6	23.8	26.3	29.7	31.2	31.0	28.4	22.0	17.1	23.2	16.3
Guaymas, Son. (1950–1953, 1957) USCGS	17.7	18.7	18.8	21.5	25.0	29.3	31.4	31.5	31.3	28.9	24.1	18.7	24.7	13.8
Mazatlán, Sin. (1953–1957) USCGS	21.4	20.1	20.5	21.6	24.1	28.2	29.5	30.0	29.9	28.5	25.1	22.0	25.1	9.9
Cabo San Lucas, B.C. (1957) SIO	20.8	20.5	—	20.6	23.1	23.6	25.9	28.2	29.0	—	26.2	24.4	24.2	(8.5)
La Paz, B.C. (1950–1957) USCGS	19.8	19.9	21.3	22.2	24.0	24.9	27.4	29.1	28.3	28.1	25.1	21.3	24.3	9.3

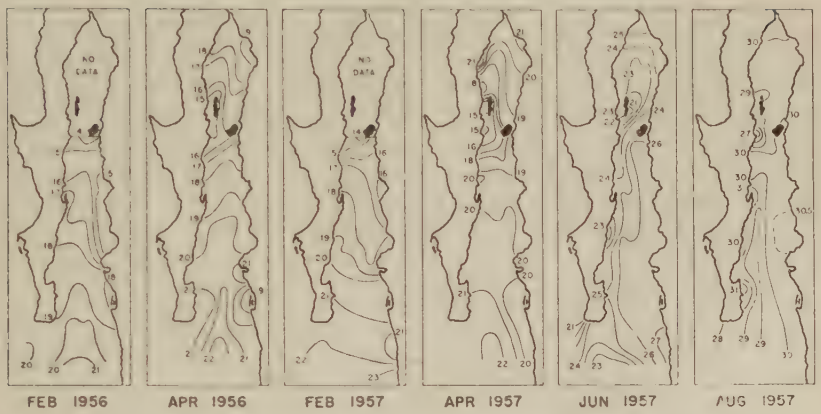

Figure 2. Horizontal distribution of temperature (°C) at 10 m.

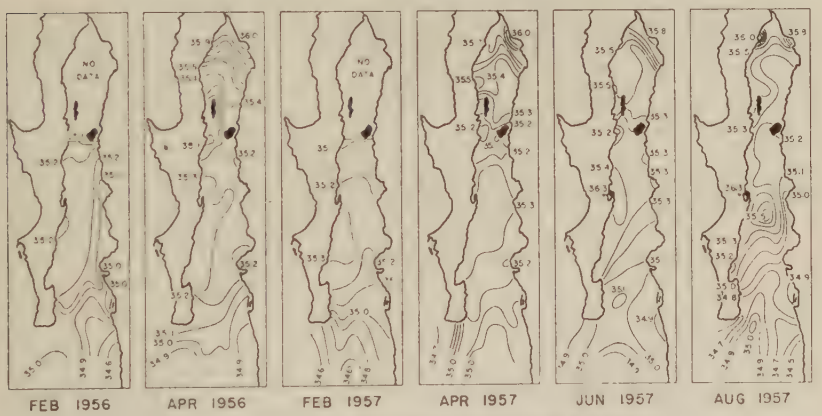

Figure 3. Horizontal distribution of salinity (‰) at 10 m.

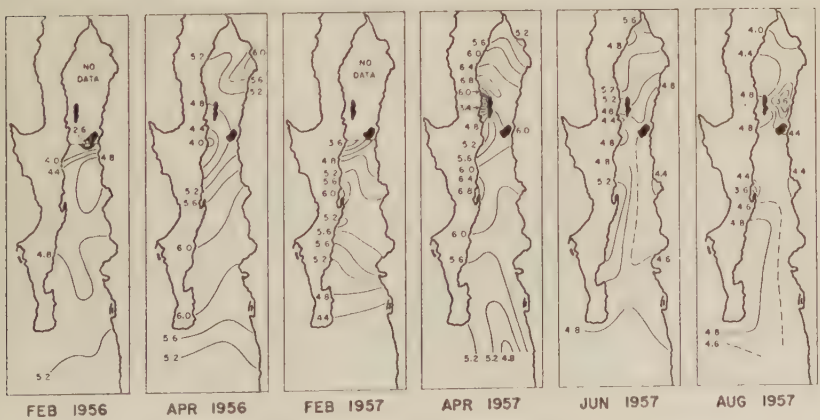

Figure 4. Horizontal distribution of oxygen (ml/1) at 10 m.

characteristic of conditions offshore. The salinity increases from the Gulf entrance to the mouth of Río Colorado. The latter has no influence upon salinity since runoff is negligible. The lowest salinities are found off river mouths in the southeastern part of the Gulf during the rainy season (July–October) whereas the highest salinities occur in shallow protected bays where evaporation is strong; such areas are Bahía Concepción, Bahía San Felipe and Bahía Adair. The average salinity of the upper 200 m shows almost no seasonal variation.

Figure 5. Upwelling areas: a) with northwesterly winds. b) with southeasterly winds. Area c is characterized by strong tidal mixing.

There is some variation of dissolved oxygen with season (Fig. 4). From the solubility of oxygen in sea water one would expect to find the highest concentrations in winter and the lowest in summer, but actually the highest concentrations occur in spring, indicating that biological activity is also important. The surface waters are generally saturated with respect to oxygen, deviations of more than 15% from the saturation value occurring only rarely. A notable exception is

found in the vicinity of Isla Tiburón and Isla Angel de la Guarda where undersaturation frequently occurs. Production of oxygen by phytoplankton during the "blooming" season occasionally leads to strong oversaturation.

Upwelling plays an important role. With northwesterly winds upwelling occurs along the east coast and with southeasterly winds along the west coast (Fig. 5). The upwelling areas are mostly found in wind lee of capes, points and islands. The upwelled water is of low temperature, and it is usually of low salinity except along the west coast. Here upwelling frequently leads to higher salinities due to the presence of an intermediate salinity maximum at a depth of about 50 m originating at the northern end of the Gulf. There is no obvious relation between oxygen concentration and upwelling.

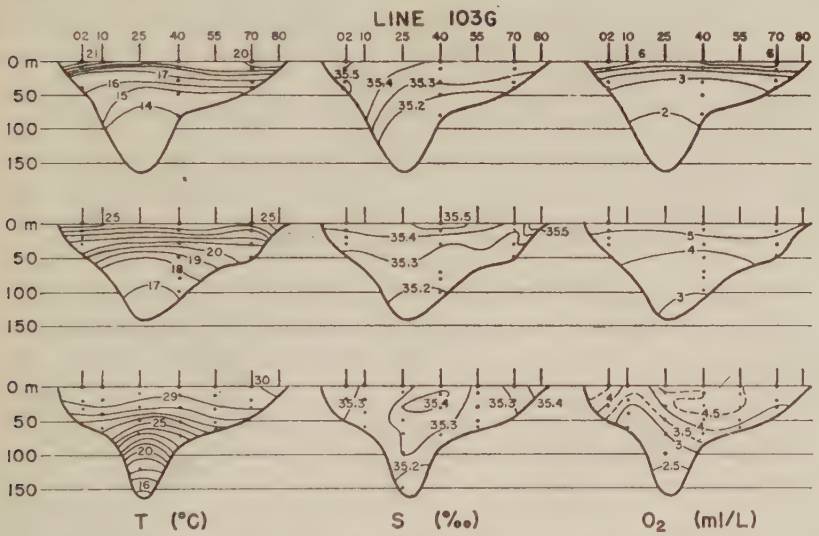

Figure 6. Distribution of temperature, salinity and oxygen in vertical section across the northern part of the Gulf for April, June, and August 1957 in descending order.

Northern Part of Gulf. This region, between Río Colorado and Isla Tiburón, lies in an arid environment which is characterized by large annual temperature ranges and strong evaporation. There is little precipitation (less than 100 mm/year) and runoff is negligible. Winds are predominantly northerly in winter and southerly in summer. The average depth is quite shallow, being about 200 m. An exception is the 1000 m deep trench between Baja California and the islands of Angel de la Guarda and San Lorenzo which is isolated from the rest of the Gulf below 250 m.

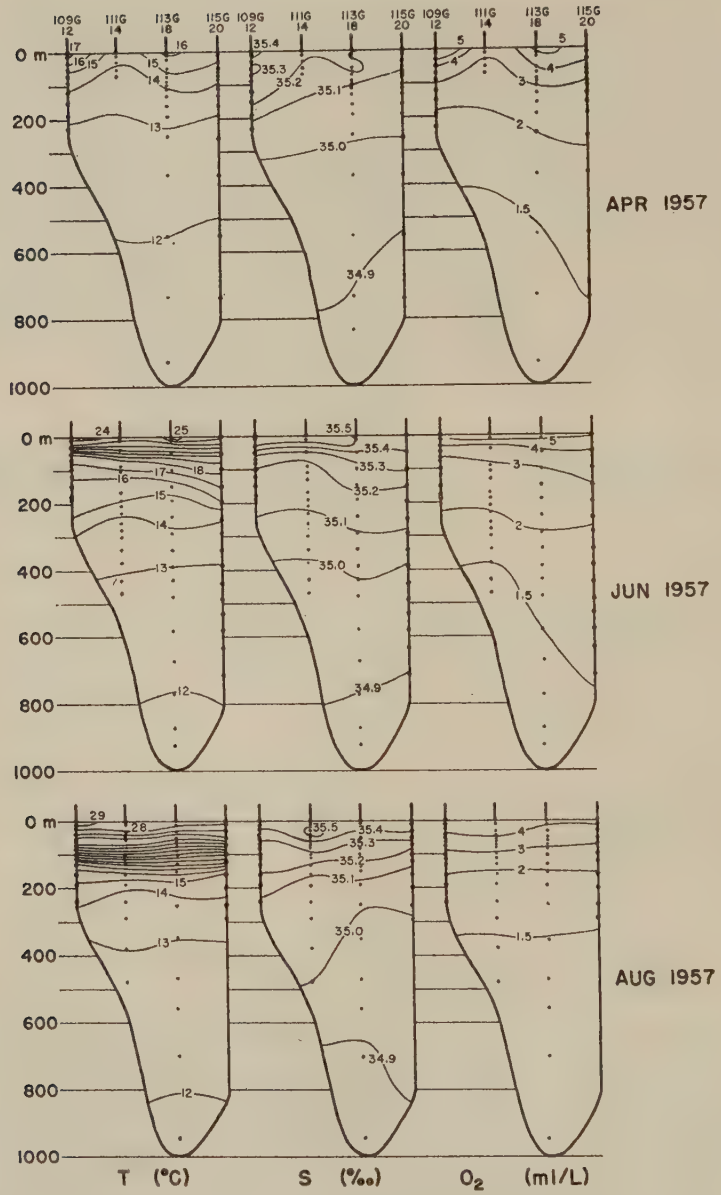

Figure 7. Distribution of temperature, salinity and oxygen in a vertical section along Ballenas Trench.

The distribution of temperature, salinity and oxygen with depth is shown in Fig. 6. Strong temperature gradients between surface and bottom are found during summer months owing to intense solar heating and lack of mixing. Winter conditions have not been thoroughly investigated, but records made at Puerto Peñasco seem to indicate that the water may be almost isothermal (14 C). Salinities, except near the coast, vary between rather narrow limits and are mostly 35.2–35.5‰.

Unusual conditions prevail in the deep trench. Surface temperatures are generally lower here than elsewhere. At depths, temperature, salinity and oxygen (Fig. 7) are much higher than in any other place at that depth. At 1000 m the temperature difference inside and outside the trench is 6°C, the salinity difference 0.4‰, and the oxygen difference 1 ml/L. These features are indicative of intensive mixing which can be attributed to strong tidal currents found there.

Central Part of Gulf. This region between Topolobampo and Isla Tiburón is in a less arid environment than that to the north. Precipitation occurs during late summer months, with the east coast receiving about twice as much as the west coast. Runoff is very slight. The depths are large and there is open communication with the ocean. Winds blow predominantly from the north during winter and from the south during summer.

The distribution of temperature, salinity and oxygen in a vertical cross-section from Santa Rosalía to Cuaymas is shown in Figs. 8 and 9. Below the thermocline the water is the same as in the Equatorial Pacific (Sverdrup, 1941). It is characterized by a salinity minimum (34.50–34.55‰) between 600 and 1000 m and an oxygen minimum (0.1–0.2 ml/L) between 400 and 800 m. The depth at which these minima occur in the gulf is somewhat less than that in the Equatorial Pacific.

Above the Equatorial Pacific water lies a water mass which is distinguished by its higher salinities and which may be called "Gulf water"; this can be looked upon as equatorial water which has been transformed at the surface by evaporation. The salinity and oxygen distributions in the upper layers are very complicated and dependent upon season. Warm temperatures in winter are slightly colder along the east than along the west coast; in summer the opposite occurs This phenomenon can be ascribed to upwelling. In late summer there appears to be, from consideration of continuity and the presence of salinity tongues, a northward flow of low salinity water along the east

coast and a southward flow of high salinity water along the west coast, both occurring at subsurface depths of about 50 m.

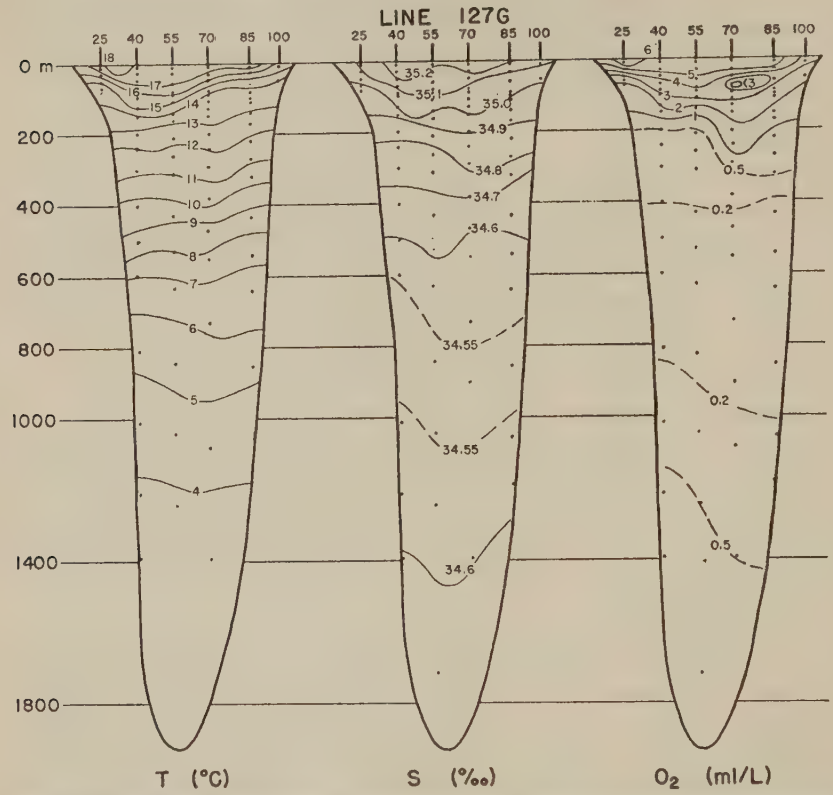

Figure 8. Distribution of temperature, salinity and oxygen in a vertical section across the central part of the Gulf for February 1957.

Southern Part of Gulf. The region between Topolobampo and Cabo Corrientes lies in a moderatley humid environment. Annual precipitation, occurring mostly in late summer and fall, varies between 500 and 1000 mm/year, with less rainfall in the northern part of this region than in the south. During the rainy season there is considerable runoff. Winds are predominantly northerly in winter and southerly in summer. The southern boundary of the Gulf is not well defined, but for oceanographic considerations it can be taken from Cabo San Lucas to Cabo Corrientes. The depths in this part of the Gulf are great, frequently exceeding 3000 m.

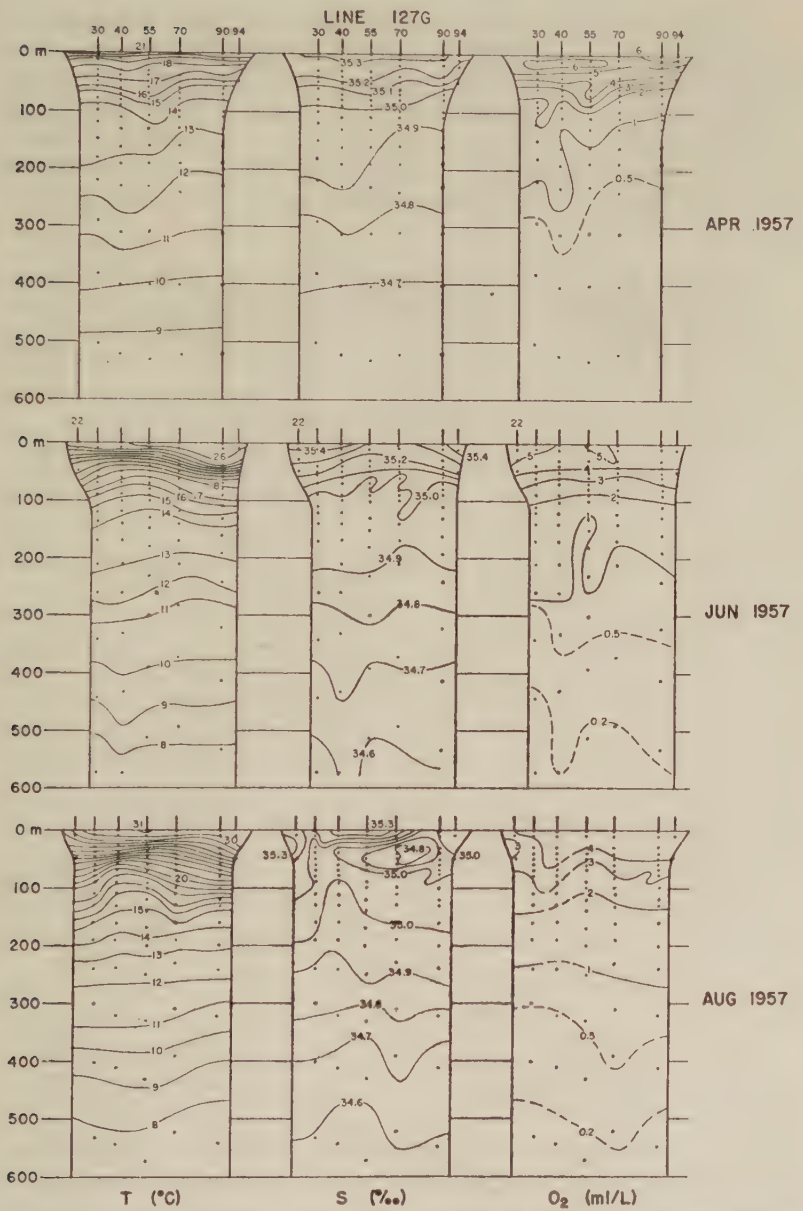

Figure 9. Distribution of temperature, salinity and oxygen in a vertical section across the central part of the Gulf.

Compared to the deep water in the central Gulf (Figs. 8, 9), the deep-water salinity and oxygen minima in this region are more pronounced. Oxygen concentrations in the southern Gulf fall below 0.1 ml/L, which has not been observed further to the north. At great depths conditions are rather uniform, so that no differences are observed between the central and southern parts. No important changes between the 1939 cruise (Sverdrup, 1941) and the 1957 cruise have been found in the deep water of the Gulf.

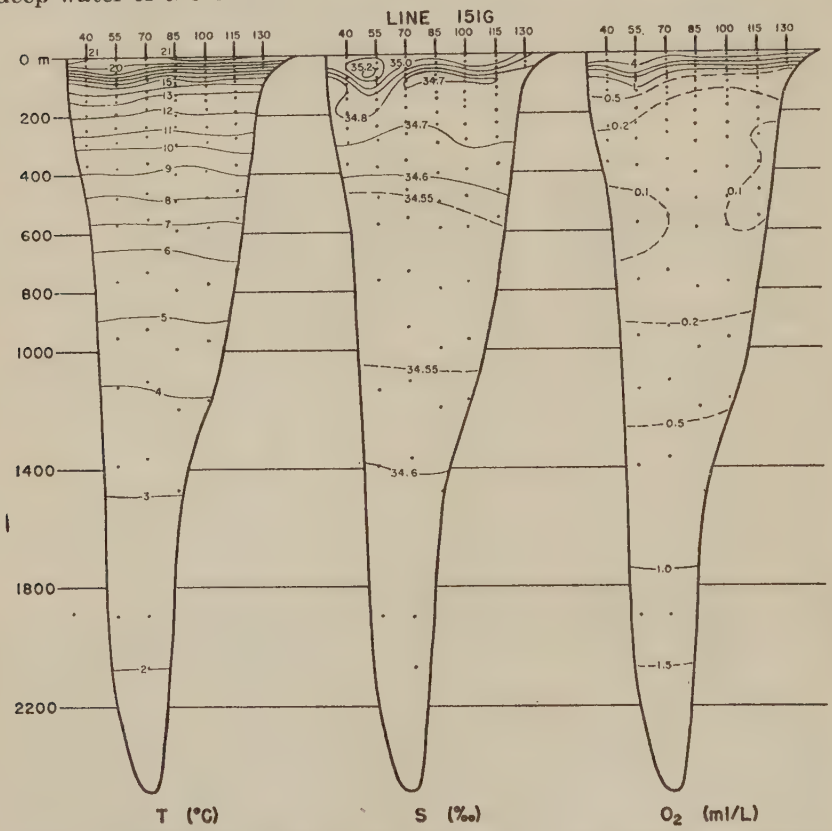

Figure 10. Distribution of temperature, salinity and oxygen in a vertical section across the southern part of the Gulf for February 1957.

In the upper 200 m the distribution of salinity and oxygen is complicated (Figs. 10, 11, 12) because of three distinct water masses: Gulf water, California Current water, and water from the eastern Tropical Pacific. The first is characterized by relatively high temperature and

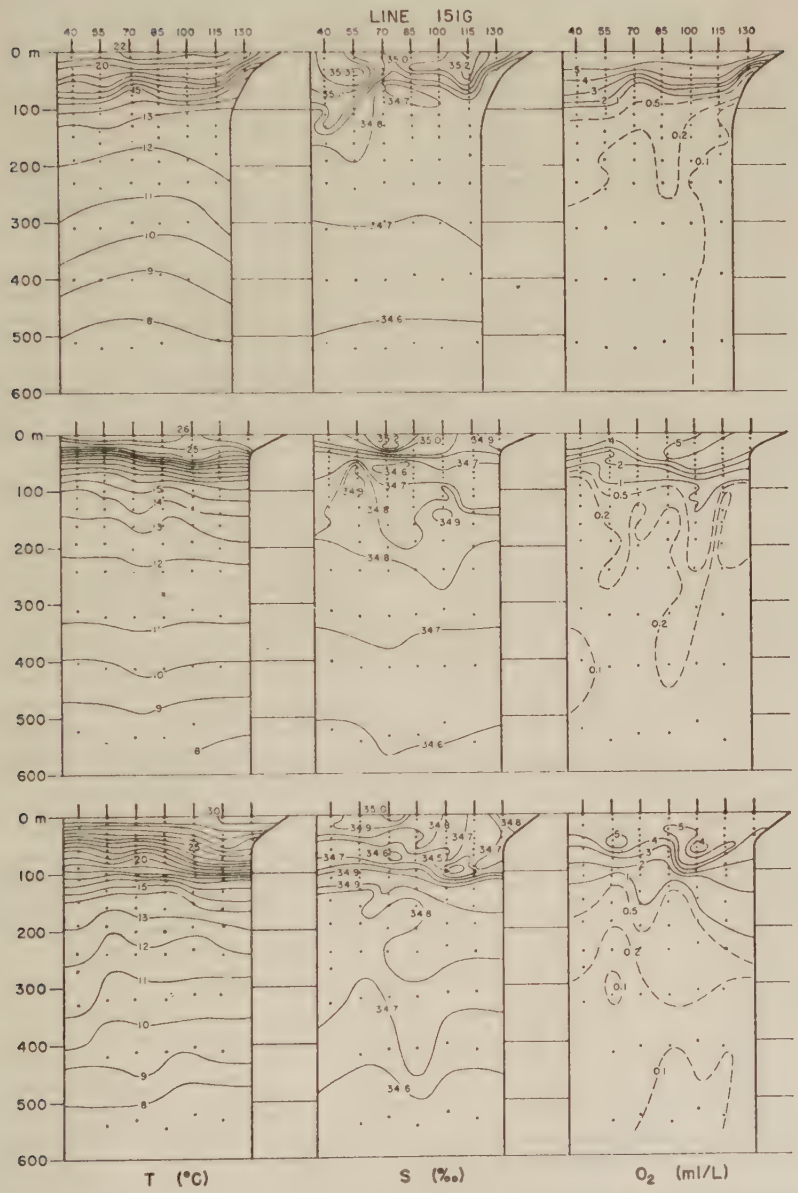

Figure 11. Distribution of temperature, salinity and oxygen in a vertical section across the southern part of the Gulf for April, June and August 1957 in descending order.

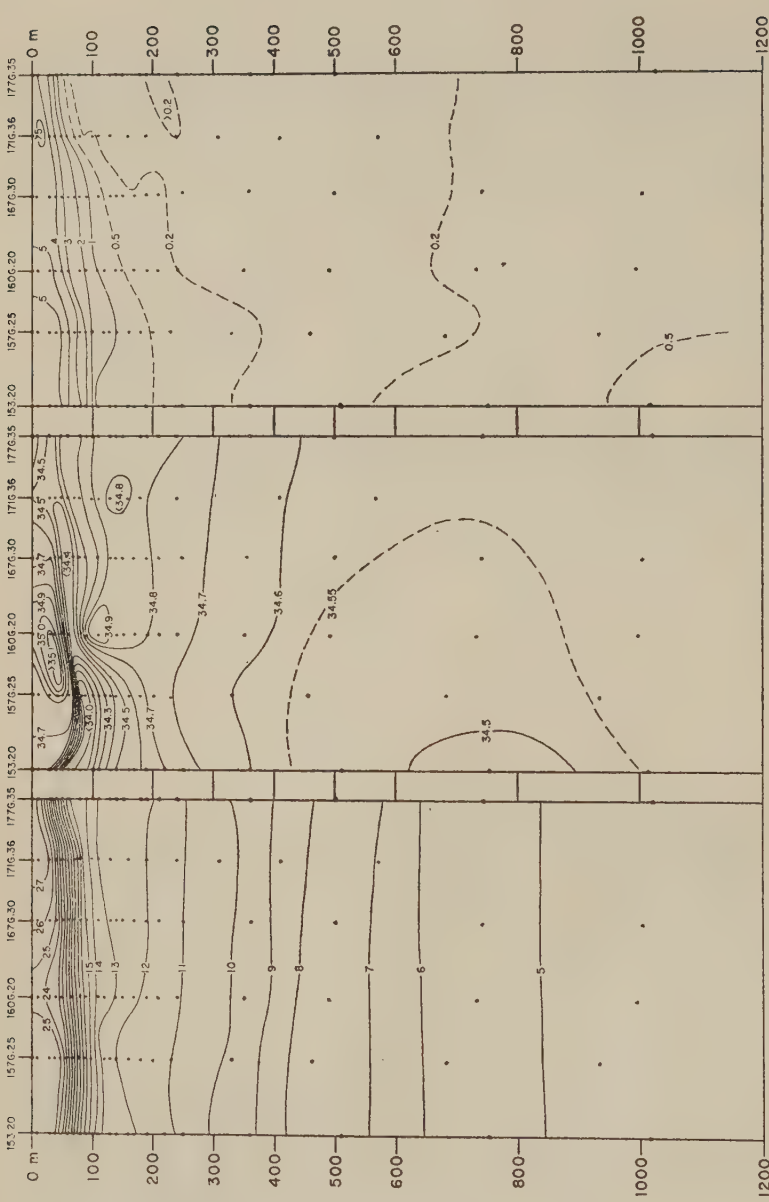

Figure 12. Distribution of temperature, salinity and oxygen in a vertical section from Cabo San Lucas to Cabo Corrientes.

salinity, the second by low temperature and salinity, and the latter by high temperature and relatively low salinity. Where these water masses meet, very sharp gradients are found. This is nearly always the case in the vicinity of Cabo San Lucas and frequently near Cabo Corrientes. The salinity distribution indicates that outflow of Gulf water seems to occur along the Baja California coast, often at depths around 50 m, and that inflow occurs mostly along the east coast and is concentrated around 100 m.

Water Balance in the Gulf. The rate of exchange of water between the Gulf and the Pacific Ocean can be estimated either by applying the geostrophic law to a hydrographic section across the mouth of the Gulf or by salt budget considerations.

The first method was applied along section 151G for the four 1957 cruises, utilizing the 500 m dynamics between adjacent stations. The region of inflowing water was computed separately from the region of outflowing water, and the totals for each, Q_i and Q_o, are tabulated in the first two lines in Table III. Exchange of water other than through the mouth of the Gulf is negligible; therefore, inflow should almost exactly balance outflow (for geostrophic flow, which represents a time average over a period of the order of a pendulum day). Otherwise, ridiculous changes in sea level would soon occur in the Gulf. The discrepancy between inflow and outflow can be ascribed to four principal defects: (1) any flow below 500 m is not accounted for; (2) dynamics based on a 500 m reference surface are in error if there is motion below; (3) there may be transients in the density field that are not geostrophically balanced; (4) the Gulf's mouth is not completely spanned by the end stations. With regard to (1) and (2), the density variation needed between 500 and 1000 m to completely balance inflow and outflow is small and could likely occur. The average salinity of the inflowing and outflowing water is defined by the relation

$$\bar{S} = \frac{\int \rho v S dx\, dz}{\int \rho v dx\, dz}, \qquad (1)$$

where v is the geostrophic velocity component normal to the section; the integration over the area of the section is confined to the region of inflowing (or outflowing) water. In making the computation, salinity and dynamic height values were interpolated linearly between stations. For three of the cruises, the outflowing water was more saline than the inflowing, but the opposite is indicated for the June cruise. Of course,

this computation is subject to all the uncertainties present in the geostrophic computation.

To apply salt budget considerations, let Q_i, Q_0, E, P and R represent inflow, outflow, evaporation, precipitation and runoff, respectively, each expressed as mass of water per unit time. Then conservation of water and salt can be expressed as follows:

$$\begin{aligned} Q_i &= (E - P - R)\bar{S}_0/(\bar{S}_0 - \bar{S}_i), \\ Q_0 &= (E - P - R)\bar{S}_i/(\bar{S}_0 - \bar{S}_i), \end{aligned} \tag{2}$$

where $\bar{S}_i$ and $\bar{S}_0$ are the mean salinities of the inflowing and outflowing water, defined by (1). These relationships need not be fulfilled at any given instant of time since there may be short-term variations in the total quantity of water and salt within the Gulf. The pertinent question to consider in such statements of conservation is "For how long a time can the substance under consideration accumulate (or be lost) at a reasonable rate until the concentration reaches an absurd value?" For conservation of water mass, this time is of the order of a seiche period of the gravest mode, or about a day. For salt, however, a time of the order of six months is needed for the average salinity in the upper 200 m to change measurably due to uncompensated evaporation. Therefore, all quantities in equations (2) must represent time averages of approximately six months, and we shall apply (2) not to each of the four 1957 cruises but only to their average.

Evaporation, E, can be estimated from the relationship

$$E = KA\rho W\Delta e, \tag{3}$$

where A is the surface area of the Gulf (cm^2), ρ the density of fresh water (g/cm^3), Δe the vapor pressure difference (mb) between the sea surface and the air above it, W the wind velocity (m/sec), and K a factor of proportionality, here taken as 0.011 (for details, see Sverdrup, 1951). The estimates of E, P, R in Table III are based on data collected during the cruises and on past weather data at the corresponding time of year (Servicio Meteorológico Mexicano, 1937).

These values can now be used to estimate the water exchange rate according to (2), provided that a suitable estimate of the average salinities $\bar{S}_i$ and $\bar{S}_0$ can be made. An objective way is to use the values from lines 3 and 4, derived from the geostrophic estimate. The resultant estimate of in- and out-flow is given in the last two lines of Table III for the average of the four 1957 cruises. This estimate, of course, depends rather critically on the salinity difference between the in- and out-flowing water, which, according to the geostrophic estimate, is 0.04‰. Actual examination of the salinity profiles across line 151G

TABLE III.

		February	*April*	*June*	*August*	*Average*
geostrophic estimate	Q_i (10^{13} g/sec)	0.9	1.6	2.2	2.8	1.9
	Q_0 (10^{13} g/sec)	1.2	1.5	1.2	1.6	1.4
	S_i (‰)	34.75	34.78	34.84	34.75	34.78
	S_0 (‰)	34.82	34.91	34.76	34.78	34.82
conservation of salt estimate	E (10^9 g/sec)	3.6	1.7	7.7	7.2	5.0
	P (10^9 g/sec)	0.4	0.1	0.2	2.2	0.7
	R (10^9 g/sec)	0.2	0.2	0.3	0.6	0.3
	Q_i (10^{13} g/sec)	—	—	—	—	3.5
	Q_0 (10^{13} g/sec)	—	—	—	—	3.5

suggests that a salinity difference 10 times greater might be more likely, and this would lead to a water exchange rate only $^1/_{10}$ as great (Roden, 1958).

It is seen that evaporation exceeds precipitation and runoff in all months examined. Precipitation amounts to less than 10% of evaporation during the first half of the year, but during the rainy season, which lasts from July to October, precipitation increases in importance. There is little runoff from the Río Colorado (Valenzuela, personal communication) and the other rivers do not discharge much water into the Gulf except during the rainy season.

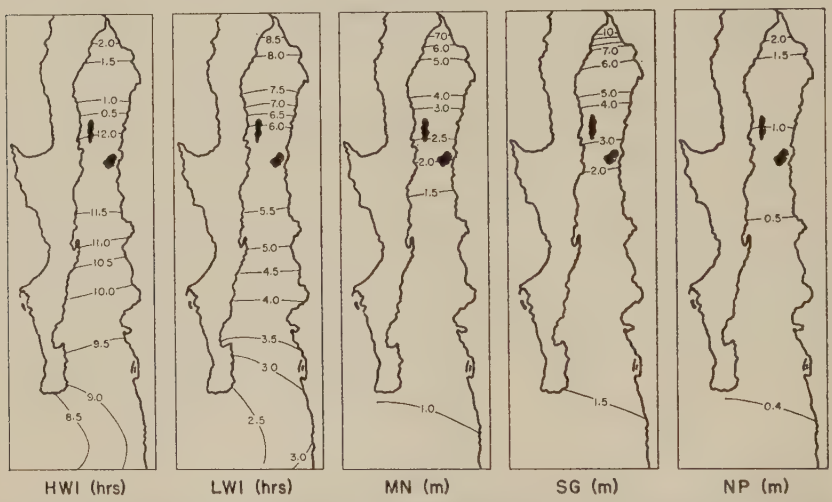

Figure 13. Tides in the Gulf of California: HWI-high water interval. LWI-low water interval. Mn mean range. Sg-spring range. Np-neap range. Time in hours; ranges in meters.

Tides. Tide observations have been recorded from very few locations in the Gulf. Generally the tide appears to be of the mixed type, with large diurnal inequalities which may predominate in some parts of the central Gulf. The composite tidal range increases gradually from the Gulf entrance to Isla Tiburón, and then rapidly toward the mouth of the Río Colorado. In this vicinity it is very large, exceeding 10 m during the spring tides. The tidal wave continues into the Rio Colorado in the form of a bore. Fig. 13 (after U. S. Coast and Geodetic Survey, 1915) shows the observed tidal ranges and high and low water intervals.

Whether the tidal oscillation within the Gulf behaves predominantly like a standing wave or like a progressive wave travelling northward depends on the amount of tidal power that is dissipated inside the Gulf.

With relatively little dissipation, most of the incoming energy would be reflected from the head of the Gulf, so that the result would appear as a standing wave. The high water interval would change rather abruptly at a node by half a tidal period. On the other hand, with relatively high dissipation, the tidal wave behaves more like a progressive wave, and we would expect the high water interval to vary smoothly with distance from the mouth of the Gulf. Evidence indicates that the time of high water gets progressively later with distance up the Gulf, with high water occurring about 5.5 hours later at its head than at its mouth; this is about the time needed for a free progressive shallow-water wave to traverse the entire length of the Gulf. But 5.5 hours is also approximately half a semidiurnal tidal period, which is the lag that would occur if the tidal wave were a pure standing oscillation. Evidence is hardly good enough to distinguish between the two alternatives.

If we neglect the small input of tidal energy by the direct action of sun and moon on the body of water in the Gulf, then the total amount of tidal power entering through the mouth is

$$P = \rho g \int h v \eta \, dx, \tag{4}$$

where h is mean water depth, η the surface elevation, v the component of orbital velocity northward along the Gulf axis, ρ the water density, and x the distance across the Gulf entrance. To get an estimate of the tidal power dissipated within the Gulf, let us assume that an ingoing progressive tidal wave is entirely dissipated. Then η and v will be in phase, and (4) gives $P = 0.4 \times 10^{18}$ ergs/sec, averaged over a tidal cycle.[2]

Let us now see if it is at all likely that such a large amount of power could be dissipated by friction of tidal currents along the bottom. The stress exerted by a tidal stream on the bottom is proportional to the square of the speed, the velocity being roughly constant from top to bottom (Taylor, 1919). The power dissipated per unit area of bottom is then proportional to the cube of the current speed, according to

$$P/A = K V^3, \tag{5}$$

where K is a numerical constant having a value near 0.0018. In Ballenas Trench (between Isla Angel de la Guarda and Baja Cali-

[2] If the tidal oscillation consists of two progressive waves, one entering and one leaving, it is possible that an even greater dissipation occurs for a given tide range at the entrance provided the phase relations are such that some cancellation between the two waves occurs (Taylor, 1919).

fornia) and off the mouth of the Río Colorado, speeds of more than 3 m/sec (6 knots) have been reported (U. S. Hydrographic Office, 1951). If currents of such magnitude occurred continuously throughout a 1000 km^2 area, then it would dissipate the same amount of power, 0.4×10^{18} ergs/sec. The area required does not seem excessively large, and so the computed amount of tidal power dissipated seems reasonable. If true, the Gulf of California would supply 3% of the tidal dissipation needed to account for the observed secular acceleration of the moon.

From the free standing-wave viewpoint (no dissipation), the semidiurnal tide has a node in the central region of the Gulf, where observations show the diurnal contribution to be relatively important. The high range observed off the mouth of the Río Colorado is due to narrowing and shoaling of the Gulf.

As a result of the high tidal range and the complicated bottom topography, tidal currents are strong, especially in narrow channels and in the vicinity of Río Colorado. The mixing effected by these strong tidal currents may have important biological consequences.

Variations of Surface Slope Across the Gulf Entrance. These variations have been studied from sea level and atmospheric pressure records made in Mazatlán, Sin., and La Paz, B.C. Monthly average values of sea level for these two stations (from 1953 into 1957) are shown in Fig. 14 (A and B); a mean annual cycle, determined from three years of record, is shown in Fig. 15. It is seen that there is a prominent seasonal cycle reaching its maximum in summer and its minimum in winter, with Mazatlán leading slightly in phase over La Paz. The range of the seasonal oscillation is from 20 to 40 cm and is noticably larger in Mazatlán than in La Paz. The double maxima which are seen in three out of four annual cycles at Mazatlán may be a characteristic local phenomenon.

In the sea, the pressure gradient at the surface is composed of two parts: (1) that arising from the gradient of the surface elevation, and (2) the atmospheric pressure gradient. Note that one millibar is equivalent to approximately one centimeter of sea water pressure. The sum of the sea-surface elevation and the atmospheric pressure, expressed as equivalent height of a column of sea water, has been referred to as *corrected sea level* (Groves, 1957). The corrected sea level for Mazatlán and La Paz was computed from the monthly mean pressures at these two places (corrected to sea level) and the monthly sea level means. The difference of corrected sea level, Mazatlán minus La Paz, is shown in Figs. 14 (C) and 15 (C). This plot can be interpreted to mean the horizontal pressure difference in centimeters of sea water between the two stations. The time variations of it are proportional

to variations in the inflowing geostrophic current. The datum is arbitrary, since the height of mean sea level at La Paz is unknown relative to mean sea level at Mazatlán because the two places have never been levelled in together. Consequently, the method gives only variations of the mean inflowing surface current and not the surface current itself.

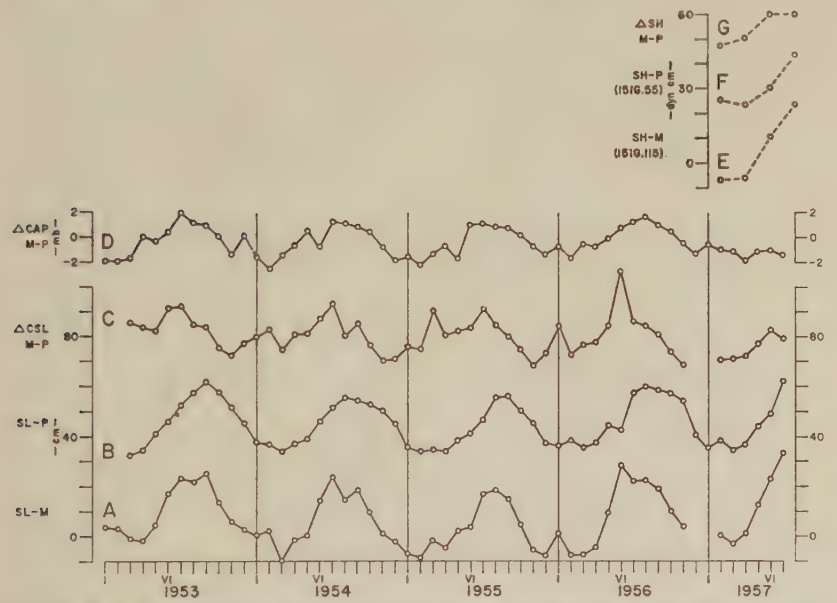

Figure 14. A—monthly mean sea level at Mazatlán; B—monthly mean sea level at La Paz; C—monthly mean difference in corrected mean sea level, Mazatlán minus La Paz; D—monthly mean difference in atmospheric pressure corrected to sea level, Mazatlán minus La Paz; E and F—steric height at stations 151G.115 and 151G.55, respectively; G—difference in steric height, station 151G.115 minus station 151G.55. Curves A, B, C, E, F, G, are plotted relative to arbitrary datum.

Mean monthly differences in atmospheric pressure (corrected to sea level), Mazatlán minus La Paz, are illustrated in Figs. 14 (D) and 15 (D). The difference is proportional to the southerly component of geostrophic wind across the entrance to the Gulf. The similarity between curves C and D in Figs. 14 and 15 might be interpreted to mean that a southerly wind across the Gulf entrance is conducive to inflow of surface waters. If it is assumed that the inflowing surface current is proportional to the surface wind from the south, the constant of proportionality can be determined by the least square method. The result is that the ratio between inflowing current and southerly wind at the sea surface is 0.0054. This value does not disagree radically with the 2% value used by navigators. The discrepancy

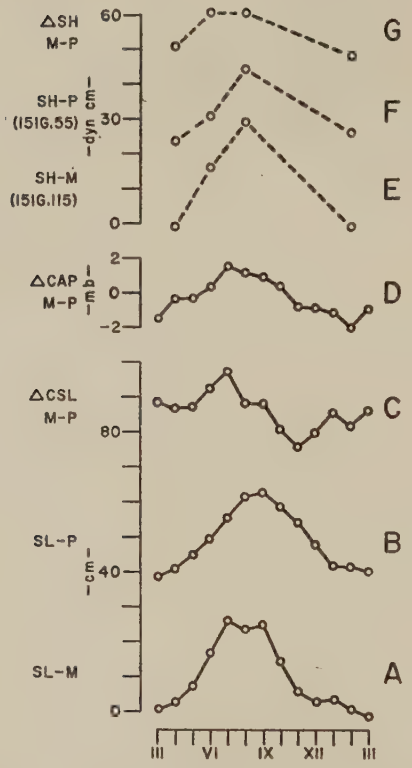

Figure 15. Curves A, B, C, D, represent an average annual cycle of the corresponding curves in figure 14. Curves E, F, G represent single observations only.

should not be taken too seriously in view of the fact that water is blown into or out of a confined basin in contrast to open ocean conditions.

Variations in *steric height* (Pattullo *et al.*, 1955) or dynamic height reflect variations in the sea surface elevation due exclusively to changes in density of sea water in a vertical column. Steric height variations across the Gulf entrance, as obtained from CCOFI stations 151G.115 (close to Mazatlán) and 151G.55 (close to La Paz), are shown in Figs. 14 (E, F) and 15 (E, F). The difference in steric height, Mazatlán minus La Paz, is shown in Figs. 14 (G) and 15 (G). Note: data for curves E, F and G represent monthly isolated instantaneous measurements, not monthly averages, and in Fig. 5 these curves are compared with other curves based on a mean annual cycle from three years of

continuous data. Consequently curves A through D deserve much more confidence than do E, F, and G. In comparing curve E with A, F with B, G with C, one can say that there is no contradiction in the supposition that the observed sea level variations at Mazatlán and La Paz are related primarily to changes in density of sea water.

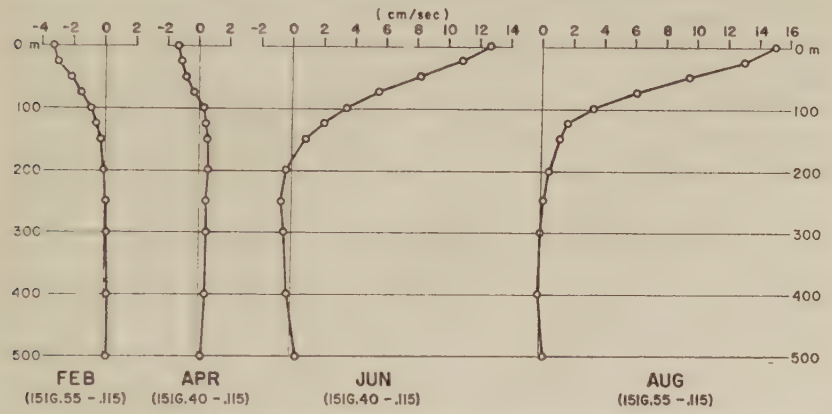

Figure 16. Horizontally averaged geostrophic current as function of depth. The plots for February and August are averaged between stations 151G.55 and 151G.115, while the plots for April and June are averaged between stations 151G.40 and 151G.115.

The horizontally averaged inflow, plotted against depth, is shown in Fig. 16. For April and June the inflow was determined from CCOFI stations 151G.115 and 151G.40 and for February and August from stations 151G.115 and 151G.55, since station 151G.40 was not occupied during the last mentioned months. It is seen that, during June and August, surface inflow is quite large and that a compensating current below 200 m is evident. February and April indicate just the opposite, with surface outflow and subsurface inflow; however, the exchange is much weaker than in summer. Exact compensation (a mean value of precisely zero, if averaged vertically) is not obtained for reasons discussed in the section on Water Balance.

In conclusion the following points seem to be borne out from observations of sea level, atmospheric pressure and density of sea water at the entrance to the Gulf of California:

(1) A southerly surface wind generates an inflowing surface current.
(2) The velocity ratio between the inflowing surface current and the southerly wind is about 0.005.
(3) Geostrophic flow at the surface is compensated by a reverse flow at depths.

Conclusions. Recent oceanographic investigations have shown that the water mass encountered in the Gulf is characteristic of Equatorial Pacific water. At the surface this water is slightly modified by extensive evaporation which increases its salinity. Seasonal temperature variations observed in the upper layers are large in the central and northern parts and moderately large in the southern part. Seasonal salinity variations are quite small. The seasonal variation of oxygen shows a maximum in spring, indicating that biological activity is of importance. The rather unusual hydrographic conditions in Ballenas Trench, between Isla Angel de la Guarda and Baja California, were attributed to isolation of the Trench and to mixing by strong tidal currents. No changes in the distribution of properties were observed in the deeper part of the Gulf since the last survey in 1939. An estimate of the water budget shows that exchange of water with the Pacific Ocean is of the order of 10^6 m^3/sec, and evaporation is about 5×10^3 m^3/sec. Runoff and precipitation are negligible. Comparison of sea level and atmospheric pressure records at La Paz, B.C. and Mazatlán, Sin. with hydrographic observations suggests that variations in sea level are primarily steric. At the surface the currents follow the winds, while at depths a compensating current opposite to the wind direction is generally indicated. The tide in the Gulf is of the mixed type with large diurnal inequalities. A large part of the tidal energy may be dissipated in the northern part of the Gulf, the tide appearing essentially as a progressive wave. The high tidal ranges in the northern part are due to narrowing and shoaling of the Gulf.

ACKNOWLEDGMENTS

The authors are indebted for valuable suggestions to E. H. Ahlstrom, M. Blackburn, T. Cromwell, J. Isaacs, W. H. Munk, J. L. Reid, Jr., and W. S. Wooster.

The authors express their thanks to the Instituto de Geofísica, Universidad Nacional Autónoma de México, the Servicio Meteorológico Mexicano, and the Comisión Internacional de Límites y Aquas entre México y Estados Unidos, for their helpful cooperation in this study.

The work carried out in this paper was partly sponsored by the Scripps Tuna Oceanographic Research Program under contract with the U. S. Fish and Wildlife Service and by the Marine Life Research program of the Scripps Institution of Oceanography.

REFERENCES

Groves, G. W.
1957. Day to day variation of sea level. Meteorol. Monogr., *2* (10): 32–45. June.

Oceanic Observations of the Pacific.
1956, 1957. University of California Press. Los Angeles and Berkeley.

Patullo, June, W. H. Munk, Roger Revelle, and Elizabeth Strong
1955. The seasonal variation in sea level. J. mar. Res., *14* (1): 88–155.

Roden, G. I.
1958. Oceanographic and meteorological aspects of the Gulf of California. Pacif. Sci., *12* (1): 21–45.

Servicio Meteorológico Mexicano.
1937, 1938. Bol. anu., Tacubaya, D.F.

Sverdrup, H. U.
1941. The Gulf of California: Preliminary discussions of the cruise of the E. W. Scripps in February and March, 1939. Proc. 6th Pac. Sci. Congr. Calif., *3:* 161–166.
1951. Evaporation from the oceans. Amer. met. Soc. Compendium of Meteorology: 1071–1081.

Taylor, G. I.
1919. Tidal friction in the Irish Sea. Philos. Trans., (A) *220:* 1–33.

Tanner, F. L.
1888. Report on investigations of the U.S. Fish Commission steamer Albatross for the year ending June 20, 1889. Rep. U.S. Comm. Fish. (1888): 395–512.

U.S. Coast and Geodetic Survey.
1915. General Tide Tables for the year 1916. Washington, D. C.
1954. Density of sea water at tide stations. Spec. Publ. 281. Washington, D. C.
1956. Surface water temperatures at tide stations: Spec. Publ. 280. Washington, D. C.

U.S. Hydrographic Office
1951. Sailing Directions (H.O. 84) West Coast of Mexico and Central America. Washington, D. C.

ON THE HEAT AND SALT BALANCE OF THE CALIFORNIA CURRENT REGION[1]

By

GUNNAR I. RODEN

Scripps Institution of Oceanography, La Jolla, California

ABSTRACT

The average monthly variation of the heat and salt balance of the upper 200 m is investigated for eight areas of the Pacific Ocean off California and Baja California. Accuracy of the method and of the nonseasonal variations of the balance is estimated. It is shown that observed heat changes are principally due to radiation and advection, the heat exchange with the atmosphere being rather small and constant. Evaluation of the advection term by two independent methods shows only little agreement. Observed salt changes seem to be related principally to advection and to a lesser degree to the excess of evaporation over precipitation.

Introduction. In recent years increased effort has been directed toward a better understanding and a more accurate evaluation of the different terms involved in calculating the heat balance. Aspects of radiation were investigated by Anderson (1952), Berliand (1952), Black (1956), Burdecki (1958) and Budyko (1956). The heat exchange of the atmosphere was dealt with by Budyko (1956), Jacobs (1951) and Sverdrup (1951). The monthly heat balance of the earth's surface was investigated by Budyko (1955) and of the oceans by Pattullo (1957). On a regional scale, Koizumi (1956) and Tabata (1958) have studied the heat balance off Japan and off the west coast of Canada, respectively.

In the region of the California Current almost no work has been done on the heat balance, mainly because the necessary data were lacking. In the past ten years, however, a great amount of information has been gathered through regular hydrographic cruises. Thus, for the first time it becomes possible to investigate the relative importance of rates of radiation, heat exchange with the atmosphere, local heating, and advection.

Radiation can be considered an important factor of the heat balance owing to the small amount of clouds usually found over the California Current region. On the other hand, turbulent heat exchange with the atmosphere will probably play only a minor part in the balance because of the rather low and constant wind velocities and the stable

[1] Contribution from the Scripps Institution of Oceanography, New Series.

stratification of the air. Advection can be expected to be important owing to the presence of the California Current and the frequent occurrence of upwelling. Since cold water is brought into the region, advection represents a loss of heat from the balance point of view.

The change of salt in the California Current region can be expected to be related primarily to advection, because both evaporation and precipitation are small. There is not sufficient runoff to alter the salt balance.

Data. Eight areas bounded by five degree squares of latitude and longitude were selected for the present investigation (Fig. 1). This rather arbitrary selection was necessary because of the limited amount of climatological data available. Air temperatures, sea surface temperatures and cloudiness were obtained from publications of the Imperial Marine Observatory in Kobe, Japan (1911–1938). Wind velocities were procured from the U. S. Hydrographic Office (1956), atmospheric pressures from unpublished records of the U. S. Weather Bureau (1899–1958). Temperatures and salinities in the upper 200 m of the ocean were obtained from cruises made by the Scripps Institution of Oceanography in collaboration with the South Pacific Fishery Investigations of the U. S. Fish and Wildlife Service (Oceanic Observations of the Pacific, in press).

The number of observations taken per month in each square is shown in Table I. Compared to about 400 to 1200 observations of air temperatures, sea surface temperatures, and cloudiness, only 0–250 are available for the average temperature and salinity of the upper 200 m.

Theoretical Considerations

A) Heat Balance. The heat used locally for changing the temperature of a water column can be expressed, according to the equation of the heat balance, as

$$Q_L = Q_r + Q_a + Q_v, \tag{1}$$

where Q_L denotes the rate of local heat change, Q_r the rate of effective radiation, Q_a the rate of exchange of heat with the atmosphere through processes of evaporation, condensation and convection, and Q_v the rate of heat brought into the region by ocean currents and by mixing. The first three terms are calculated from oceanographical and meteorological observations; the advection term is found by difference. The units used in this paper are cal cm^{-2} day^{-1}.

The method of the heat balance requires knowledge of the transmission of solar energy through the atmosphere, of the processes

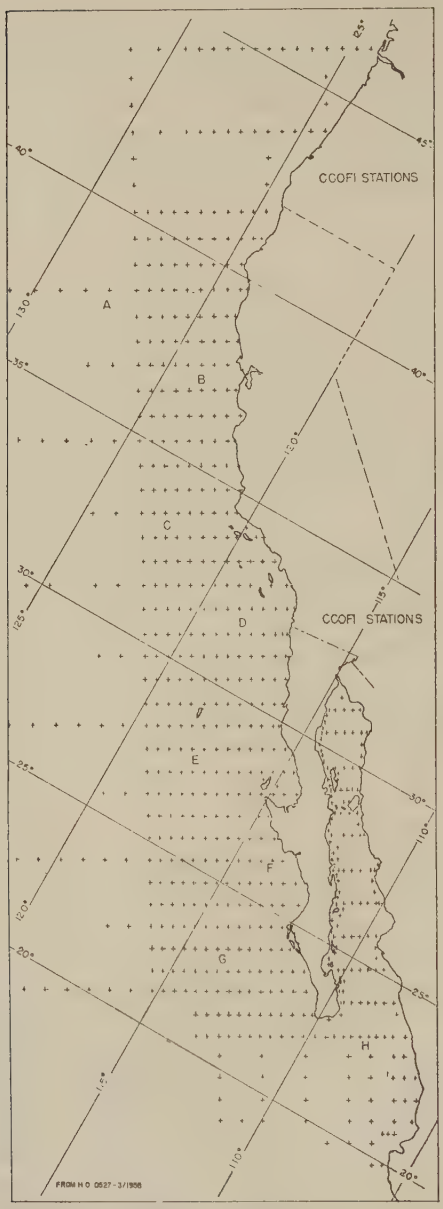

Figure 1. Stations occupied during CCOFI cruises off California and Baja California (dots) and areas used in the present investigations (letters).

TABLE I. TOTAL NUMBER OF OBSERVATIONS IN EACH FIVE DEGREE SQUARE OF LATITUDE AND LONGITUDE BY MONTHS

Square \ Month	I	II	III	IV	V	VI	VII	VIII	IX	X	XI	XII
					Air temperature, sea surface temperature, cloudiness.							
A	881	952	1046	1056	1127	1246	1216	1340	1097	1136	986	1010
B	724	728	841	945	978	1015	955	1058	948	884	777	789
C	498	451	526	491	490	505	464	575	469	495	498	530
D	696	625	717	711	683	757	678	807	710	665	675	692
E	514	471	518	530	539	530	543	577	565	454	504	508
F	419	378	427	434	422	396	399	456	441	358	417	418
G	546	512	609	562	605	557	590	668	598	499	559	602
H	641	568	633	647	625	608	676	714	647	548	609	658
					Average temperature of upper 200 meters.							
A	0	13	16	26	28	35	41	31	22	7	7	2
B	11	9	9	44	43	85	61	54	26	26	22	9
C	60	84	61	181	107	149	106	68	28	60	30	32
D	75	128	80	171	104	129	102	73	59	109	42	75
E	99	155	121	240	147	118	119	66	56	110	44	57
F	31	42	36	58	39	43	35	25	14	32	21	17
G	20	56	34	44	6	46	7	11	19	2	36	26
H	0	21	1	13	0	11	0	11	1	0	1	26
					Average salinity of upper 200 meters.							
A	0	13	16	22	24	25	12	10	20	6	4	0
B	0	9	9	35	31	80	37	24	19	19	13	0
C	33	70	43	54	85	127	59	37	18	50	21	25
D	52	110	56	147	77	103	69	51	37	88	23	56
E	64	126	88	202	103	105	85	50	44	46	34	49
F	4	33	26	47	24	30	24	17	10	25	15	15
G	19	53	31	42	4	15	2	10	1	2	36	25
H	0	25	1	21	0	11	0	11	0	0	1	25

occurring at the boundary between the sea and the atmosphere, and of the conditions in the sea itself. The processes involved are complicated and one is compelled to use many restrictive assumptions when calculating the heat balance.

The rate of local heat change, which can be calculated from a knowledge of the vertical temperature distribution in the sea, is given by the expression

$$Q_L = C_p \cdot \rho \int_0^z \frac{\partial \theta}{\partial t} d_z, \tag{2}$$

where C_p is the specific heat of sea water at constant pressure (0.94 cal/g), ρ the mean density of the water column (1.024 g/cm^3), θ its temperature (°C), t time, and z the depth at which the seasonal variation of temperature becomes small enough to be neglected. The specific heat and density have been assumed constant, i.e., they are represented by their mean values, because it is permissible to neglect the small variations with temperature and salinity. The depth of no seasonal variation is obtainable from an inspection of temperature records at different levels in the sea; this depth, in the region concerned, lies at about 200 m.

The rate of effective radiation, i.e. the difference between total heat absorbed by the water mass and total back radiation from the sea surface per unit time, can be expressed as follows, according to Budyko (1956),

$$Q_r = Q_o(1 - r)(1 - k'C) + Q_{bo}(1 - k''C^2) + 4s\sigma\theta^3(\theta_{\text{sea}} - \theta_{\text{air}}), \tag{3}$$

where Q_o is the total incoming short wave radiation with a clear sky, r the amount of radiation reflected, C the cloudiness in tenths of the sky covered, Q_{bo} the effective back radiation with a clear sky, θ the absolute temperature, s the ratio of the radiation from the sea surface to a black body, and σ the Stefan-Bolzmann constant; k' and k'' are factors depending upon latitude. The first term represents incoming radiation, the second term back radiation, and the third term the effect of stability upon back radiation (see below).

Total (direct + diffuse) incoming radiation is frequently measured by pyrheliometers at certain meteorological stations. From time series of such measurements, incoming radiation with a clear sky and with a sky covered by clouds of various amount, height and thickness may be evaluated. Upon combining measurements from many similarly located stations, an average picture of incoming radiation at different latitudes can be obtained. It has been found by Kimball (1928) and Budyko (1956) that the ratio of incoming radiation of a

clear to a cloudy day depends linearly upon cloudiness. Kimball's ratio, based upon measurements made in the United States, does not depend on latitude; but Budyko, considering all available stations in the northern hemisphere, found that this ratio decreases toward the poles. In latitudes between 25–45N, agreement between Budyko's and Kimball's ratios is very close. Another attempt to evaluate the ratio was made by Black (1956), but recently his methods have been questioned by Burdecki (1958). Average monthly values of total incoming radiation with a clear sky, as determined by Budyko (1956), are given in Table II; the latitudinal dependence of the ratio of radiation with a clear to a cloudy sky is shown in Table III.

Effective back radiation is the difference between long wave radiation from the sea surface and long wave radiation from the atmosphere. It decreases with increasing humidity and stability of the air and, for the range of humidities commonly observed at sea, it decreases also with increasing temperature (Fig. 2). Berliand (1952) has given the following semiempirical equation from which effective back radiation can be computed:

$$Q_b = -[s\sigma\theta^4 (0.39 - 0.050 \sqrt{e})(1 - k''C^2) + 4S\,\theta^3(\theta_{sea} - \theta_{air})], \quad (4)$$

where s is the ratio of the radiation of the sea surface to a black body, σ the Stefan-Bolzmann constant, θ the absolute temperature, e the vapor pressure of air (mb), k'' a constant, and C the cloudiness in tenths.

The first term, which takes into account the effect of temperature, humidity and cloudiness, varies, for the ranges generally found in oceanic regions, between 20 and 200 cal $cm^{-2}day^{-1}$. The constant k'' has been evaluated by considering also the vertical extent of clouds as well as the height of the cloud base from the surface of the earth; it was found that k'' increased from the equator to the pole (Table III) because of the decrease in cloud base heights in polar regions. The second term considers the effect of stability. Owing to the small sea-air temperature differences observed over the oceans, this term is rather small and varies for the most part only between -20 to $+20$ cal $cm^{-2}day^{-1}$.

Compared with early methods for evaluating effective back radiation (Askölf, 1920), Berliand's equation yields results that are about 50% lower than those found previously. A similar discrepancy with early methods was also found by Anderson (1952). An explanation for the disagreement between recent and early results can be sought in the fact that the constant k'' is not the same for all places but varies with latitude, depending upon the vertical dimensions of clouds.

TABLE II. Total incoming radiation with a clear sky in cal cm^{-2} day^{-1} (after Budyko, 1956)

Month / Lat	I	II	III	IV	V	VI	VII	VIII	IX	X	XI	XII	Year
Av.	293	356	486	599	706	733	719	623	508	401	317	269	501
80N	0	0	80	320	597	677	630	360	120	13	0	0	243
75N	3	20	133	340	623	693	657	410	177	57	7	0	258
70N	7	47	193	423	647	713	677	457	233	100	23	3	294
65N	27	83	253	470	670	730	700	503	297	150	50	13	329
60N	57	130	320	513	693	743	720	547	350	203	87	40	367
55N	100	187	350	553	717	757	737	590	410	257	133	77	406
50N	157	250	450	593	733	767	750	627	473	327	193	127	454
45N	220	313	513	633	753	777	763	670	533	387	257	190	501
40N	290	383	567	667	763	783	773	703	587	447	323	257	545
35N	360	453	617	700	767	783	777	727	627	503	393	320	586
30N	423	507	650	720	767	783	777	740	660	550	453	380	618
25N	477	550	677	727	763	780	770	743	683	587	500	433	641
20N	517	583	693	727	753	763	757	740	700	617	543	483	656
15N	553	610	700	720	733	740	737	727	703	640	577	523	664
10N	580	633	700	710	707	707	707	707	703	653	600	553	663
5N	600	650	693	693	680	660	670	683	693	663	620	577	657
0	617	660	680	673	640	600	623	653	680	667	633	600	644

TABLE III. Annual mean values of k' and k'' at stated latitudes

Lat.	0	5	10	15	20	25	30	35	40	45	50	55	60	65	70	75	Stockholm	U.S.A.
k'	0.65	0.66	0.66	0.67	0.67	0.68	0.68	0.68	0.67	0.66	0.64	0.62	0.60	0.55	0.50	0.42	0.61	0.71
k''	0.50	0.52	0.55	0.57	0.59	0.61	0.63	0.65	0.68	0.70	0.72	0.74	0.76	0.78	0.80	0.82	0.83	–
Source	Budyko (1956)																Asklöf (1920)	Kimball (1928)

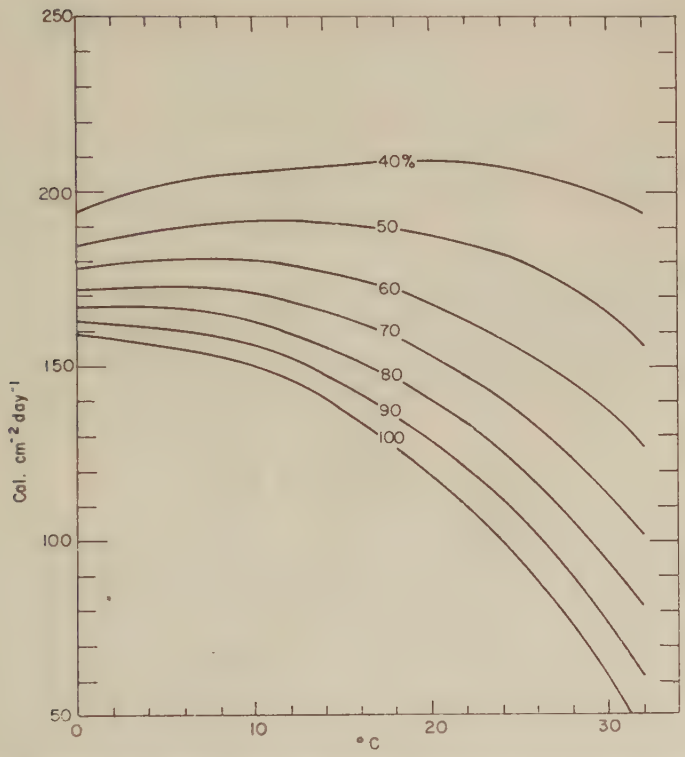

Figure 2. Effective back radiation with a clear sky and neutral stability as a function of sea surface temperature (°C) and relative humidity (%).

The amount of radiation reflected from the sea surface depends on the angle of incidence and on the roughness of the surface. Compared to a calm surface, the presence of waves reduces the amount of incoming radiation with high solar altitudes and increases it with low solar altitudes. The albedo of the sea surface for total (direct and diffuse) incoming radiation varies between 0.06 and 0.23 (Table IV), according to Budyko (1956) and Zubov (1957). Cox and Munk (1955) found that the albedo for a roughened sea surface varied between 0.02 and 0.15 for direct radiation and between 0.04 and 0.10 for diffuse radiation. For the present investigation, a value of 0.06 has been adopted.

The relation between cloud type and incident radiation has been studied by Haurwitz (1948), who found that a fully overcast day with cirrus lets 83% of a clear sky radiation through. With fog the ratio is only 18% (Table V).

TABLE IV. Albedo of the sea surface for total (direct + diffuse) radiation (after Budyko, 1956)

Lat \ Month	I	II	III	IV	V	VI	VII	VIII	IX	X	XI	XII	Year
70	—	0.23	0.16	0.11	0.09	0.09	0.09	0.10	0.13	0.15	—	—	(0.13)
60	0.20	0.16	0.11	0.08	0.08	0.07	0.08	0.09	0.10	0.14	0.19	0.21	0.13
50	0.16	0.12	0.09	0.07	0.07	0.06	0.07	0.07	0.08	0.11	0.14	0.16	0.10
40	0.11	0.09	0.08	0.06	0.06	0.06	0.06	0.06	0.07	0.08	0.11	0.12	0.08
30	0.09	0.08	0.07	0.06	0.06	0.06	0.06	0.06	0.06	0.07	0.08	0.09	0.07
20	0.07	0.07	0.06	0.06	0.06	0.06	0.06	0.06	0.06	0.06	0.07	0.07	0.06
10	0.06	0.06	0.06	0.06	0.06	0.06	0.06	0.06	0.06	0.06	0.06	0.07	0.06
0	0.06	0.06	0.06	0.06	0.06	0.06	0.06	0.06	0.06	0.06	0.06	0.06	0.06

TABLE V. RATIO OF INSOLATION WITH OVERCAST SKY TO INSOLATION WITH CLOUDLESS SKY FOR AN OPTICAL AIR MASS $m = 2.5$ (AFTER HAURWITZ, 1948)

Cloud type	*Ci*	*Cs*	*Ac*	*As*	*Sc*	*St*	*Ns*	*Fog*
Ratio	0.83	0.74	0.49	0.41	0.33	0.25	0.21	0.18

The rate of heat exchange with the atmosphere through the process of evaporation can be expressed by

$$Q_e = L\rho E, \tag{5}$$

where L is the latent heat of evaporation (cal/gm), ρ the density of water (g/cm^3), and E evaporation (cm/day). L decreases somewhat with temperature, but not much error is introduced in assuming it constant (585 cal/gm). As a first approximation, E can be expressed as a vertical flux of water vapor, viz:

$$E = -\frac{A}{\rho}\frac{d(\rho q)}{dz}, \tag{6}$$

where ρ is the density of air, q the specific humidity, z the height, and A the coefficient of turbulent heat exchange. A depends on wind velocity, height, and stability of the air; with neutral stability, A increases approximately linearly with height; with unstable stratification the increase is faster, with stable stratification slower.

The equation cannot be evaluated in the above form because of the difficulty in measuring humidity gradients at sea and because of uncertainties as to the coefficient of turbulent heat exchange. Instead, a semiempirical equation of the type

$$E = -K \cdot W\Delta e \tag{7}$$

is commonly used in climatological research (Jacobs, 1951; Sverdrup, 1951). Here Δe is the vapor pressure difference (mb) between the sea surface and the air above it, W the wind velocity (m/sec), and K a coefficient of proportionality which can be obtained from the boundary layer theory (Sverdrup, 1951). This coefficient decreases slightly with increasing wind velocity and altitude, as shown in Fig. 3.

The rate of heat exchange through conduction can be computed from the rate of evaporation (Q_e) and the "Bowen Ratio" (R) in accordance with equation

$$Q_c = R \cdot Q_e = 0.66 \times 10^{-3} p \times \frac{\Delta\theta}{\Delta e} Q_e \quad \text{(Bowen, 1926)}, \tag{8}$$

where p is the sea level atmospheric pressure and (mb) $\Delta\theta$ the sea-air temperature difference (°C); the other symbols have their previous meaning.

The heat exchange through condensation can be written formally as

$$Q_p = L \cdot \rho \cdot H, \tag{9}$$

where L is the latent heat of condensation, ρ the density of the condensed water (g/cm³), and H the height (cm) of the water layer resulting from condensation. No direct measurements of H are available from the oceans. A rough estimate of the magnitude of heat gained by this process may be obtained by considering a dense fog (liquid water content 10^{-5}g/cm³) of 100 m thickness laying above the sea surface. Even if all the water of the fog were available for condensa-

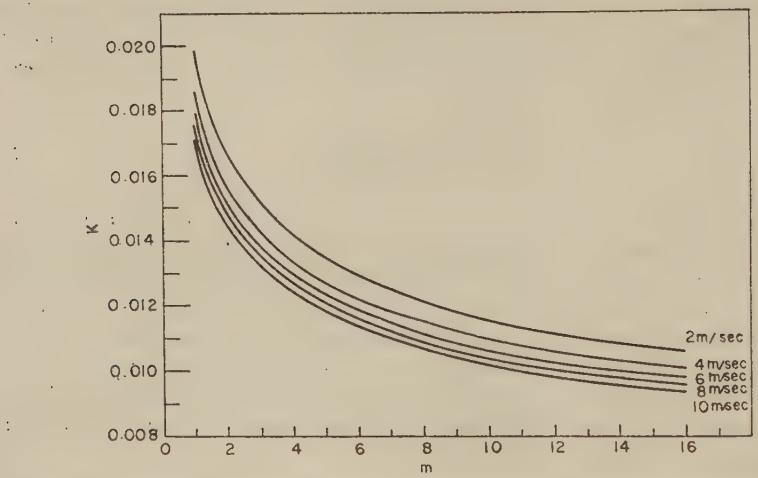

Figure 3. Evaporation coefficient K as a function of wind velocity (m/sec) and height above the sea surface (m).

tion (which certainly is not the case), the amount of heat gained would be only 60 cal/cm². It is therefore unlikely that the condensation of water vapor affects the heat balance of the sea to any extent.

The total amount of sensible heat exchange is the sum of these processes, viz.

$$Q_a = Q_e + Q_c + Q_p. \tag{10}$$

The evaporation term usually outweighs the other terms by an order of magnitude.

The rate of heat brought into the region through the process of advection can be calculated either by taking the difference from the other terms of the heat balance, viz.

$$Q_v = Q_L - Q_r - Q_a \tag{11}$$

or by using an independent expression

$$Q_v = C_p \cdot \rho \left[\int_0^z u \frac{\partial \theta}{\partial x} dz + \int_0^z v \frac{\partial \theta}{\partial y} dz + \int_0^z w \frac{\partial \theta}{\partial z} dz \right], \qquad (12)$$

where u, v, and w are the velocity components and the other terms are as stated before. By using both equations to compute Q_v and by comparing the results, a check could be made of the accuracy of the heat balance method. As a first approximation, the horizontal velocity components can be obtained from the geostrophic method, the temperature gradients from actual measurements made at sea. The vertical velocity component can be avoided by selecting ocean areas where there is reason to assume that vertical motion is unimportant. Unfortunately several attempts to compare the advection terms obtained from the difference method and from the independent method have yielded disappointing results. At the present time it is not possible to say whether the discrepancy is due to inadequacy of the difference method or to evaluation of Q_v from eq. (12), or both.

B) Salt Balance. The local change of salt in a given time interval can be written as

$$S_L = S_{e-p} + S_r + S_v, \qquad (13)$$

where S_L denotes the local rate of salt change, S_{e-p} the rate due to the excess of evaporation over precipitation, S_r the rate due to runoff, and S_v the rate due to advection. The units used are g cm^{-2} day^{-1}.

The local rate of change can be expressed for a water column of depth Z:

$$S_L = 10^{-3} \rho \int_0^z \frac{\partial S^*}{\partial t} dz, \qquad (14)$$

where ρ is the density of the water column (g cm^{-3}) and S^* its salinity (‰). The integration should be carried out to a depth where the seasonal variation of salinity becomes negligible; this depth, in the region concerned, lies at 200 m. In order to evaluate eq. (14), the salinity must be known accurately to ±0.01‰.

The rate of change due to excess evaporation over precipitation is

$$S_{e-p} = (e - p)\ 10^{-3}\ \rho\ S^*, \qquad (15)$$

where e is evaporation (cm/day), p precipitation (cm/day); the other quantities are as before.

The rate of change due to runoff is

$$S_r = -\frac{D}{A}\ 10^{-3}\ \rho\ S^*, \qquad (16)$$

where D is the discharge (cm^3 day^{-1}), and A the area (cm^2) affected by the discharge.

The advection term is generally computed as the difference from the other terms of the salt balance, since it is difficult to evaluate it independently.

The Region off California and Baja California

A) Radiation (Tables VI, VII). The rate of total (direct + diffuse) short wave radiation received at the sea surface varies with latitude and time, with annual mean values ranging from about 300 cal cm^{-2} day^{-1} off northern California to about 450 cal cm^{-2} day^{-1} off southern Baja California. Seasonal differences between the northern and southern part of the region are greatest in winter and smallest in summer. The minimum rate of radiation is always found in December, but the maximum rate may occur in spring (Central Baja California), summer (California), or fall (southern Baja California), depending on regional differences in the seasonal variation of cloudiness. The oceanic areas receive, on the whole, considerably less radiation than comparable coastal stations, as can be seen by comparing values in Tables VI and VII. The largest differences are found during the warmer part of the year when there is a sharp increase in cloudiness from the coast toward the ocean.

Back radiation shows little seasonal or latitudinal variation. About 120 cal cm^{-2} day $^{-1}$ are lost to the atmosphere on an annual average, but there is an indication that values are somewhat lower in summer than in winter.

The difference between incoming short wave and outgoing long wave radiation is the effective radiation, which shows a seasonal and latitudinal variation similar to the incoming radiation. Annual mean values range from about 200 cal cm^{-2} day^{-1} off northern California to about 350 cal cm^{-2} day^{-1} off southern Baja California. They are in good agreement with Budyko's charts (1955, 1956).

B) Sensible Heat Exchange with the Atmosphere (Table VIII). In the California Current region this is due almost entirely to evaporation, the rates due to condensation and convection being very small.

The rate of evaporation is comparatively low and does not show appreciable seasonal or latitudinal variation. This can be explained partly by the rather low and constant wind velocities. On an annual average, between 70 and 130 cal cm^{-2} day^{-1} are lost to the atmosphere; these values agree favorably with the findings of Jacobs (1951) and

TABLE VI. AVERAGE MONTHLY VARIATION OF TOTAL INCOMING RADIATION (Q_s), BACK RADIATION (Q_b) AND EFFECTIVE RADIATION (Q_r) IN CAL CM^{-2} DAY^{-1}

Area \ Month	I	II	III	IV	V	VI	VII	VIII	IX	X	XI	XII	Year
						Q_s							
A	189	226	314	363	428	438	388	379	345	266	204	156	308
B	205	242	361	410	451	462	427	379	339	285	215	181	330
C	251	288	386	433	460	470	412	367	347	316	283	243	355
D	267	307	392	426	430	438	412	388	379	326	296	250	359
E	306	328	412	427	390	367	387	378	389	369	334	286	364
F	306	344	452	492	520	515	518	519	483	403	343	290	432
G	343	391	480	516	508	501	534	534	511	452	370	322	455
H	333	403	507	538	553	547	504	504	456	452	380	322	458
						Q_b							
A	−110	−106	−109	−111	−108	−114	−94	−127	−106	−113	−112	−107	−110
B	−133	−123	−128	−129	−130	−126	−112	−101	−118	−120	−124	−131	−123
C	−136	−136	−134	−120	−128	−114	−98	−104	−127	−124	−132	−137	−124
D	−129	−138	−134	−119	−112	−112	−98	−97	−109	−121	−136	−137	−120
E	−134	−133	−131	−129	−109	−96	−100	−90	−102	−120	−137	−138	−118
F	−130	−136	−135	−136	−132	−126	−123	−111	−113	−115	−130	−136	−127
G	−126	−133	−137	−133	−138	−130	−114	−103	−100	−105	−107	−121	−121
H	−116	−132	−132	−130	−126	−115	−91	−84	−84	−93	−95	−107	−109
						Q_r							
A	79	120	205	252	320	324	294	252	239	153	92	49	198
B	72	119	233	281	321	336	315	278	221	165	91	50	207
C	115	152	252	313	332	356	314	263	220	192	151	106	231
D	138	169	258	307	318	326	314	291	270	205	160	113	239
E	172	195	281	298	281	271	287	288	287	249	197	150	246
F	176	208	317	356	388	389	395	408	370	288	213	154	305
G	217	258	343	383	370	371	420	431	411	347	263	201	334
H	217	271	375	408	427	432	413	420	372	359	285	215	349

TABLE VII. TOTAL INCOMING RADIATION IN CAL CM^{-2} DAY^{-1} AT CERTAIN SHORE STATIONS IN CALIFORNIA

Month / *Place*	*I*	*II*	*III*	*IV*	*V*	*VI*	*VII*	*VIII*	*IX*	*X*	*XI*	*XII*	*Year*
Eureka	148	196	312	367	420	446	441	387	346	254	171	139	302
San Francisco	198	253	391	478	536	579	543	486	437	337	243	179	388
Santa Maria	252	281	376	461	499	564	567	531	464	362	275	198	403
San Diego	259	307	412	462	491	525	559	543	477	379	313	235	414

TABLE VIII. AVERAGE MONTHLY VARIATION OF THE SENSIBLE HEAT EXCHANGE WITH THE ATMOSPHERE THROUGH EVAPORATION (Q_e) CONVECTION (Q_c) AND TOTAL HEAT EXCHANGE (Q_a) IN CAL CM^{-2} DAY^{-1}

Area \ Month	I	II	III	IV	V	VI	VII	VIII	IX	X	XI	XII	Year
						Q_e							
A	−88	−59	−64	−76	−88	−94	−94	−76	−64	−70	−64	−76	−76
B	−64	−59	−53	−70	−82	−88	−76	−64	−53	−70	−64	−53	−66
C	−111	−129	−117	−99	−88	−76	−94	−94	−105	−129	−111	−99	−104
D	−64	−76	−82	−76	−70	−64	−88	−88	−82	−88	−76	−59	−76
E	−105	−105	−140	−146	−158	−99	−94	−94	−76	−105	−111	−111	−112
F	−117	−117	−146	−88	−111	−82	−70	−70	−88	−129	−117	−117	−104
G	−117	−105	−105	−117	−140	−94	−76	−94	−111	−140	−123	−140	−114
H	−146	−117	−140	−140	−152	−146	−123	−99	−94	−117	−135	−140	−129
						Q_c							
A	−15	−1	5	5	7	15	10	5	11	0	−6	−5	2
B	−4	4	12	8	16	24	17	17	11	6	4	0	10
C	−2	5	7	11	7	13	8	5	14	3	7	−5	6
D	−3	2	−2	2	−1	1	−2	−2	−2	0	−2	−3	−1
E	−7	0	0	10	5	5	2	6	−2	0	−3	−9	1
F	−11	−4	1	8	6	8	7	6	3	−10	−4	−7	0
G	−11	−5	−3	7	1	10	2	−1	−3	−4	−4	−11	−1
H	−10	−6	−4	1	2	−1	−4	−5	−5	−1	−4	−10	−4
						Q_a							
A	−103	−60	−59	−71	−81	−79	−84	−71	−53	−70	−70	−81	−74
B	−68	−55	−41	−62	−66	−64	−59	−47	−42	−64	−60	−53	−56
C	−113	−124	−110	−88	−81	−63	−86	−89	−91	−126	−104	−104	−98
D	−67	−74	−84	−74	−71	−63	−90	−90	−84	−88	−78	−62	−77
E	−112	−105	−140	−136	−153	−94	−92	−88	−78	−105	−114	−120	−111
F	−128	−121	−145	−80	−105	−74	−63	−64	−85	−139	−123	−124	−104
G	−128	−110	−108	−110	−139	−84	−74	−95	−114	−144	−127	−151	−115
H	−156	−123	−144	−139	−150	−149	−127	−104	−99	−118	−139	−150	−133

Budyko (1955, 1956). The rate of evaporation is somewhat larger in the southern than in the northern part of the region.

The rate of heat exchange through convection is generally less than 10% of that through evaporation. During spring and summer months the sea gains small amounts of heat from the atmosphere whereas during fall and winter months it loses a small amount. The amounts exchanged are so small in comparison with evaporation that they can be neglected.

The rate of heat change through condensation can be completely neglected.

The rate of total exchange of sensible heat with the atmosphere is therefore approximately equal to the rate of evaporation.

C) Local Heating and Advection (Table IX). The average monthly variation of the rate of local heat change shows that heat is gained principally between July and September and lost mainly between November and January. These gains and losses are somewhat more pronounced in the southern than in the northern part of the region. The time lag in the occurrence of the maximum rate of heat gain and the maximum rate of radiation strongly suggest that advection may be an important process in the California Current region.

The rate of advection, when computed from the other terms of the heat balance, varies between about 130 and 230 cal cm^{-2} day^{-1} on a yearly average; this value is in good agreement with figures obtained by Budyko (1955, 1956), who gives 200 cal cm^{-2} day^{-1} for the southern part of the California Current region. The loss of heat through advection of cold water appears to be largest during winter and spring and smallest in fall. Only in isolated places, such as that off southern Baja California in fall, is there some gain of heat through advection of warm water.

From the other terms of the heat balance, an attempt was made to evaluate the rate of advection independently. Area E off central Baja California was chosen for this purpose because it is sufficiently far away from the coast to be markedly influenced by upwelling. It was found that on an annual average the rate of advection amounted to 203 cal cm^{-2} day^{-1} as compared to 135 cal cm^{-2} day^{-1} obtained by the difference method. However, comparison of the average monthly variation of the rate of advection (Fig. 4) shows that there is little similarity between both curves.

D) Salt Balance (Table X). The observed rate of local salt change does not show a simple seasonal variation. Off central California there is a salt gain in summer by upwelling and a gain in winter

TABLE IX. AVERAGE MONTHLY VARIATION OF LOCAL HEAT CHANGE (Q_L) AND ADVECTION (Q_v) IN CAL CM^{-2} DAY^{-1}

Area \ Month	*I*	*II*	*III*	*IV*	*V*	*VI*	*VII*	*VIII*	*IX*	*X*	*XI*	*XII*	*Year*
						Q_L							
B	−147	−83	−32	−32	6	90	102	70	52	90	12	−128	0
C	−83	−51	−46	26	77	83	102	186	198	−121	−256	−115	0
D	−141	−83	−32	−70	−26	173	237	166	128	51	−166	−237	0
E	−109	−115	−64	−20	58	128	134	90	179	83	−198	−166	0
F	−307	−205	−166	−204	−26	205	256	307	542	173	−294	−281	0
G	−154	−237	−83	51	90	90	96	230	525	−58	−467	−83	0
						Q_v (by difference)							
B	−151	−147	−224	−251	−249	−182	−154	−161	−127	−11	−19	−131	−151
C	−85	−78	−188	−199	−174	−210	−126	12	69	−187	−303	−117	−133
D	−212	−178	−206	−303	−273	−90	13	−35	−58	−66	−248	−288	−162
E	−169	−205	−205	−182	−70	−49	−61	−110	−30	−61	−281	−196	−135
F	−355	−292	−338	−480	−309	−110	−76	−37	257	24	−384	−311	−201
G	−243	−385	−318	−222	−141	−197	−250	−86	228	−261	−613	−133	−219

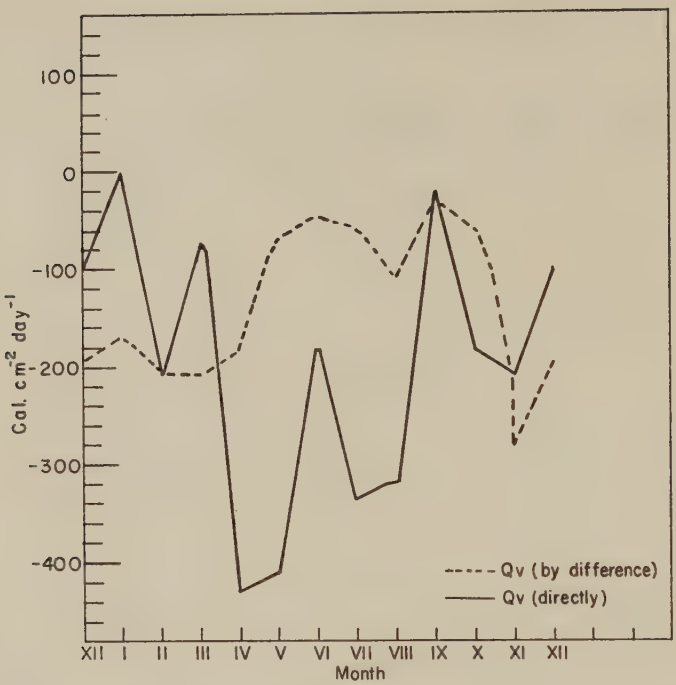

Figure 4. Average monthly variation of advection of heat (Q_v) in area E off central Baja California. Dotted curve represents Q_v found by difference from the other terms of the heat balance; solid line shows Q_v determined independently.

through advection from the west. Off southern California the gain occurs in spring and is probably related to upwelling. Off Baja California there is a gain from about May to September and again in December.

The rate of salt change due to excess evaporation over precipitation shows a summer maximum off California and a spring maximum off Baja California. Generally this represents a gain of salt, except in the northern part of the region, during winter. Annual mean values range from about 50 g cm^{-2} day^{-1} off Baja California to about -10 g cm^{-2} day^{-1} off central California.

The rate of change due to advection shows features similar to the local salt change. There is a loss of salt through advection on an annual average in all of the areas except in that off central California.

E) Errors of the Heat and Salt Balance Method. The accuracy of the heat and salt balance method depends on the soundness of

TABLE X. AVERAGE MONTHLY VARIATION OF LOCAL SALT CHANGE (S_L), SALT CHANGE DUE TO EXCESS EVAPORATION OVER PRECIPITATION (S_{e-p}) AND SALT CHANGE DUE TO ADVECTION (S_v) IN G CM^{-2} DAY^{-1}

Area \ Month	I	II	III	IV	V	VI	VII	VIII	IX	X	XI	XII	Year
						$10^4 \times S_L$							
B	67	0	−134	−201	134	201	134	134	67	−201	−268	67	0
C	−335	−67	−67	134	268	268	134	−268	−67	201	67	−268	0
D	−201	0	268	268	134	−67	−201	−67	201	0	−134	−201	0
E	0	−134	−67	−134	−134	268	335	201	134	−268	−268	67	0
F	0	−201	−268	−201	67	201	67	67	335	67	−268	134	0
G	67	−201	−67	0	201	134	0	0	67	−335	−201	335	0
						$10^4 \times S_{e-p}$							
B	−95	−75	−58	−3	27	48	44	37	24	14	−31	−88	−13
C	14	17	24	43	41	43	55	51	58	61	41	0	37
D	−14	−14	3	24	31	37	51	48	44	37	20	−24	20
E	34	31	58	75	88	58	51	44	20	51	51	27	49
F	65	65	85	51	65	48	34	20	7	68	61	48	51
G	65	48	61	68	82	54	37	7	7	71	58	44	50
						$10^4 \times S_v$							
B	162	75	−76	−198	−107	153	90	97	43	−215	−237	155	13
C	−349	−84	−91	91	227	225	79	−319	−125	140	26	−268	−37
D	−187	14	265	244	103	−104	−252	−115	157	−37	−154	−177	−20
E	−34	−165	−125	−209	−222	210	284	157	114	−319	−319	40	−49
F	−65	−266	−343	−252	2	153	33	47	328	−1	−329	86	−51
G	2	−249	−128	−68	119	80	−37	−7	60	−406	−259	291	−50

the assumptions underlying the theory, on the reliability of the data, and on the magnitude of random and systematic errors.

Accepting the theory as correct, the effect of observational errors upon the different terms is shown in Table XI. An error in estimating cloudiness by one tenth changes the rate of incoming radiation by 10% and of back radiation by 4%, on an average. The effect of an error of 0.1°C in determining the sea-air temperature difference alters the rate of back radiation by 1% and of sensible heat exchange through convection by about 3%. An error of 1 m/sec in estimating wind velocity changes the rate of evaporation between 10 and 20% for wind velocities most commonly observed in the California Current region. An error of 1% in determining humidity changes the rate of evaporation by 5% and the rate of back radiation by 1%. Small errors in determining temperature and salinity changes from one month to the next lead to appreciable errors in the rates of local heat and salt change.

Summarizing, it may be said that the rate of effective radiation calculated from the theory is accurate within 20%, the rate of exchange of sensible heat by the atmosphere within 40%, and the rate of local heat and salt change within about 20%. The advection term calculated by difference from the other terms of the balance is therefore accurate only within 80%. The error in calculating the advection term directly from the horizontal (geostrophic) velocity components and temperature gradients is estimated to be roughly 50%.

F) Nonseasonal Variations. The nonseasonal variation of heat balance terms may be estimated by taking the difference between the monthly mean and the long term mean of the same month for various contributing factors and plotting these anomalies against time.

The monthly cloudiness anomalies (tenths) for the period 1921–1938, shown in Fig. 5, vary mostly between ± 0.2 and none are greater than ± 0.4. These anomalies produce a change in the rate of incoming radiation on the order of $\pm 20\%$ and of back radiation on the order of $\pm 10\%$.

Anomalies in the northerly wind component at Lat. 30N between Long. 110W–130W and at Lat. 40N between Long. 120W–130W for the period 1920–1958 are shown in Fig. 6. The velocities, obtained from pressure differences, must be multiplied by a factor of 0.6 in order to make them applicable near the sea surface. It is seen that, near sea level, the wind anomalies are on the order of ± 2 m/sec at Lat. 30N and ± 3 m/sec at Lat. 40N. The change in the rate of

TABLE XI. PERCENTAGE ERROR OF HEAT BALANCE AND SALT BALANCE TERMS

Cloudiness	*Error in cloudiness*	*Error in incoming radiation*	*Error in back radiation*	*Sea-air temp. diff.*	*Error in sea-air temp. diff.*	*Error in back radiation*	*Error in convection*
C	ΔC	$\frac{\Delta Q_s}{Q_s}$	$\frac{\Delta Q_b}{Q_b}$	$\theta_s - \theta_a$	$\Delta(\theta_s - \theta_a)$	$\frac{\Delta Q_b}{Q_b}$	$\frac{\Delta Q_c}{Q_c}$
tenths	*tenths*	%	%	°C	°C	%	%
0.0	±0.1	∓ 7	∓ 0	1.0	±0.1	±1	±10
0.2	±0.1	∓ 8	∓ 1	2.0	±0.1	±1	± 5
0.4	±0.1	∓ 9	∓ 3	3.0	±0.1	±1	± 3
0.6	±0.1	∓12	∓ 5	4.0	±0.1	±1	± 3
0.8	±0.1	∓15	∓ 8	5.0	±0.1	±1	± 2
1.0	±0.1	∓21	∓17	6.0	±0.1	±1	± 2

Wind velocity	*Error in wind vel.*	*Error in evaporation*	*Humidity*	*Error in humidity*	*Error in evaporation*	*Error in back radiation*
		$\frac{\Delta Q_e}{Q_e}$			$\frac{\Delta Q_e}{Q_e}$	$\frac{\Delta Q_b}{Q_b}$
W	ΔW			Δ		
m/sec	*m/sec*	%	%	%	%	%
2	±1	±50	60	±1	∓ 2	∓1
4	±1	±25	65	±1	∓ 3	∓1
6	±1	±17	70	±1	∓ 3	∓1
8	±1	±13	75	±1	∓ 4	∓1
10	±1	±10	80	±1	∓ 5	∓1
12	±1	± 8	85	±1	∓ 7	∓1
14	±1	± 7	90	±1	∓10	∓1
16	±1	± 6	95	±1	∓20	∓1

Temp. diff. per mo.	*Error in temp. diff. per mo.*	*Error in local heat change*	*Salinity diff. per mo.*	*Error in sal. diff. per mo.*	*Error in local salt change*
		$\frac{\Delta Q_L}{Q_L}$			$\frac{\Delta S_L}{S_L}$
θ	$\Delta\theta$		S	ΔS	
°C	°C	%	‰	‰	%
0.2	±0.1	±50	0.02	±0.01	±50
0.4	±0.1	±25	0.04	±0.01	±25
0.6	±0.1	±17	0.06	±0.01	±17
0.8	±0.1	±13	0.08	±0.01	±13
1.0	±0.1	±10	0.10	±0.01	±10
1.2	±0.1	± 8	0.15	±0.01	± 7
1.4	±0.1	± 7	0.20	±0.01	± 5
1.6	±0.1	± 6	0.25	±0.01	± 4

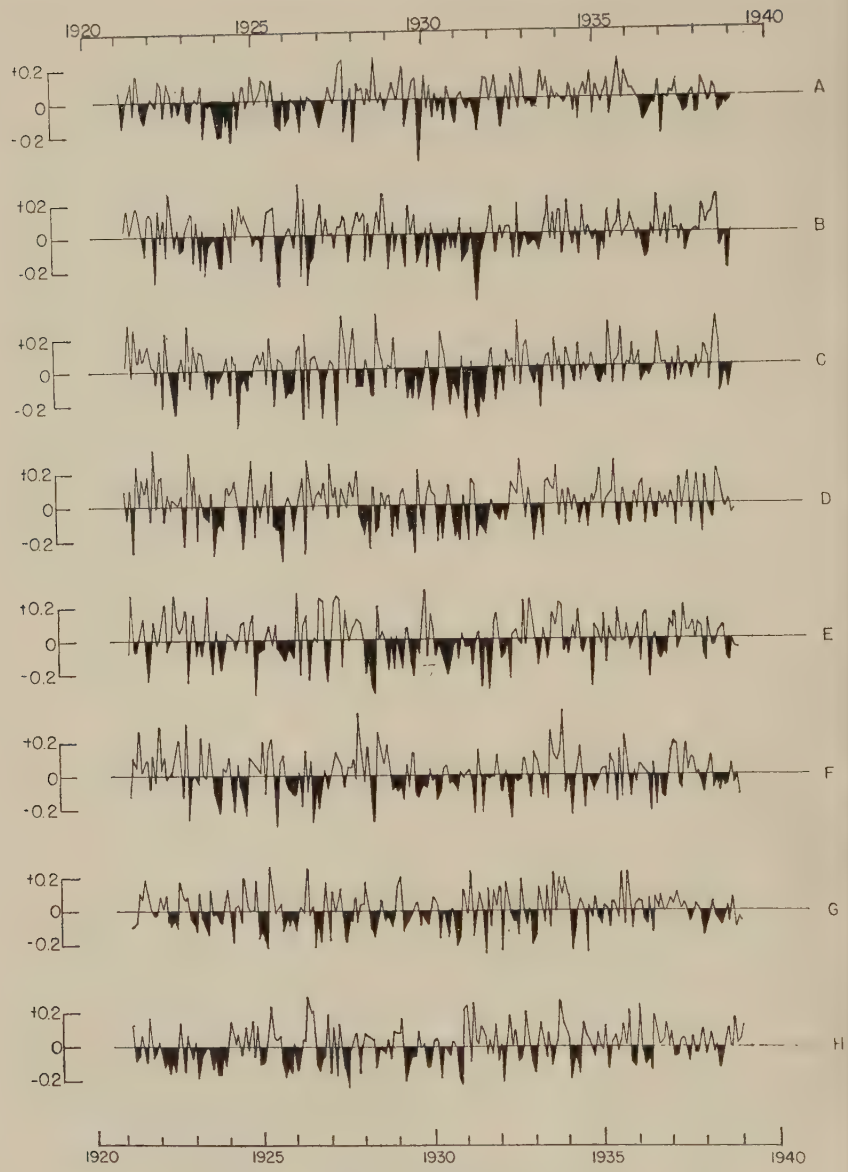

Figure 5. Monthly cloudiness anomaly in tenths.

evaporation and convection produced by these anomalies is on the order of ±50% at Lat. 30N and ±75% at Lat. 40N.

Nonseasonal variations in temperature change from one month to the next are generally within ±0.3°C/mo. The change in the rate of local heating produced by these anomalies is within ±60%.

Anomalies in salinity change per month fall mostly within ±0.02‰/mo and produce changes in the local salt content by about ±50%.

It might seem that changes produced by nonseasonal variations are not much larger than changes that could be produced by errors in observation; however, the errors discussed in the previous section apply to individual observations; by taking monthly averages of many stations, we may expect that random errors will be reduced to a

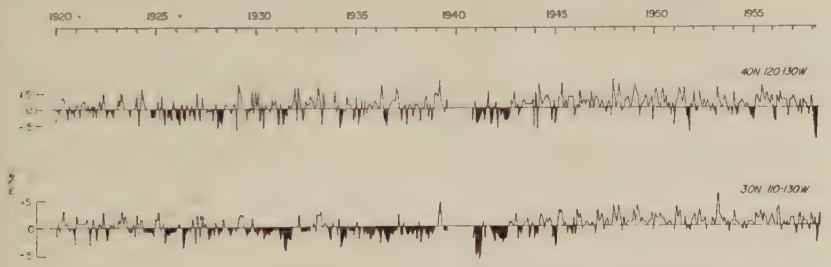

Figure 6. Monthly anomaly of northerly (geostrophic) wind component, expressed in millibars of pressure difference.

minimum and that nonseasonal changes are therefore larger than errors due to observation.

Conclusions. Investigations of the heat and salt balance in the California Current region show that the rate of local heat change is primarily related to the rate of effective radiation and the rate of advection. The rate of turbulent heat exchange with the atmosphere is rather small and constant. The rate of local salt change is influenced principally by the rate of advection and less so by the rate of excess evaporation over precipitation. The rates of radiation and local heating are accurate within 20%, and the rate of turbulent heat exchange is accurate within 40%. An attempt to evaluate the advection term independently and to compare it to the advection term obtained by difference showed disappointing results.

Acknowledgments. The author is indebted for valuable suggestions to E. H. Ahlström, R. S. Arthur, M. Blackburn, G. W. Groves, J. D. Isaacs, W. H. Munk, June Pattullo, J. L. Reid, and M. B. Schaefer.

The research carried out in this paper was sponsored in part by: Scripps Tuna Oceanographic Research under contract with the U. S. Fish and Wildlife Service; the California Academy of Sciences; the California Department of Fish and Game; Stanford University; the South Pacific Fishery Investigations of the U. S. Fish and Wildlife Service; and the Marine Life Research Program of the Scripps Institution of Oceanography of the University of California.

REFERENCES

Anderson, E. R.
1952. The exchange of energy between a body of water and the atmosphere with application to evaporation. Doctoral dissertation, University of California, Los Angeles. 121 pp.

Asklöf, Sven
1920. Über den Zusammenhang zwischen der nächtlichen Wärmeausstrahlung, der Bewölkung und der Wolkenart. Geogr. Ann., Stockh., *3:* 1–7.

Berliand, M. E. and T. G. Berliand
1952. Opredelenie effektivnovo izluchenia zemli s uchetom vlijania oblachnosti. Izv. ansssr, geophys. ser. *1.*

Black, J. N.
1956. The distribution of solar radiation over the earth's surface. Arch. Met. Geophys. (B) *7:* 166–189.

Bowen, I. S.
1926. The ratio of heat losses by conduction and by evaporation from any water surface. Phys. Rev., *27:* 779–787.

Budyko, M. I. (editor)
1955. Atlas teplovo balansa. gimiz, Leningrad.
1956. Teplovoi balans zemnoi poverkhnosti. gimiz, Leningrad. 256 pp.

Burdecki, Feliks
1958. Remarks on the distribution of solar radiation on the surface of the earth. Arch. Met. Geophys. (B) *8:* 326–335.

Cox, Charles and W. H. Munk
1955. Some problems in optical oceanography. J. mar. Res., *14*(1): 63–78.

Haurwitz, Bernhard
1948. Isolation in relation to cloud type. J. Met., *5:* 110–113.

Imperial Marine Observatory, Kobe, Japan
1911–1938. The mean atmospheric pressure, cloudiness, air and sea surface temperature in the North Pacific Ocean and the neighbouring seas.

Jacobs, W. C.
1951. The energy exchange between the sea and the atmosphere and some of its consequences. Univ. Calif. Press, Berkeley and Los Angeles. 122 pp.

Kimball, H. H.
1928. Amount of solar radiation that reaches the surface of the earth on the land and the sea. Mon. Weath. Rev., Wash., *56:* 383–389.

Koizumi, M.
1956. Researches on the variation of oceanographic conditions in the region of the ocean weather station "EXTRA" in the North Pacific Ocean (III). Pap. Met. Geophys., *6:* 273–284.
Oceanic Observations of the Pacific
(in press) Data report for 1956 and 1957. Univ. Calif. Press, Berkeley and Los Angeles.
Patullo, June G.
1957. The seasonal heat budget of the oceans. University of California, Los Angeles. Doctoral Dissertation, 104 pp.
Sverdrup, H. U.
1951. Evaporation from the oceans, in Compendium of Meteorology; Amer. met. Soc.; 1071–1081.
Tabata, Susumu
1958. Heat budget of the water in the vicinity of Triple Island, British Columbia. J. Fish. Res. Board Canada, *15*(3): 429–451.
U. S. Hydrographic Office
1956. Pilot charts for the North Pacific Ocean. Washington D. C.
U. S. Weather Bureau
(unpublished) Mean monthly sea level atmospheric pressure charts for the northern hemisphere, 1899–1958. Washington, D. C.
Zubov, N. N.
1957. Okeanologicheskie tablitsy. GIMIZ Leningrad. 408 pp.

A TEST OF MIXING LENGTH THEORIES IN A COASTAL PLAIN ESTUARY[1]

By

RICHARD E. KENT* AND D. W. PRITCHARD

Chesapeake Bay Institute, The Johns Hopkins University

ABSTRACT

Observations of vertical and horizontal variations in salinity and velocity in the James River estuary have been previously employed in the indirect determination of the vertical eddy flux of salt, $\langle v_2's' \rangle$ (Pritchard, 1954). This term is employed here to compute a mixing length after the definition of Prandtl. It is shown that this *observed* mixing length is qualitatively similar to a *theoretical* one formulated from the geometry of the system and a stability parameter related to the density stratification of the system. Several alternate hypotheses regarding the *theoretical* mixing length are tested. It is found that better quantitative agreement is obtained when the influence of surface wind waves is included in the formulation of the *theoretical* mixing length.

Prandtl (1925) proposed the mixing length theory of turbulence in an attempt to relate the rate of momentum transport to the mean flow pattern of an incompressible fluid. Despite its questionable reality concerning the mixing process, this concept has proven extraordinarily fruitful in the development of fluid mechanics and consequently has been utilized in related fields to describe the turbulent transport of properties other than momentum.

The purpose of this work is to demonstrate that the mixing length associated with vertical diffusion of salt in a stratified estuary may be formulated in terms of the stability of the system and of an adiabatic mixing length determined by the geometry of the system. This mixing length will be shown to be qualitatively compatible with the corresponding one provided by Prandtl's definition. An improved correspondence results when the effects of surface wind waves are included in the formulation of the adiabatic mixing length.

Development. Consider a stratified coastal plain estuary in which there exists a mean circulation pattern similar to that described by

[1] Contribution No. 40 from the Chesapeake Bay Institute. This work was supported by the Office of Naval Research, the State of Maryland (Department of Research and Education), and the Commonwealth of Virginia (Virginia Fisheries Laboratory).

* Present address: National Marine Consultants, Inc., Santa Barbara Airport, Goleta, California.

Pritchard (1952). Here the lateral variations in velocity and salinity are negligibly small so that the flow pattern is essentially two dimensional, consisting of a seaward flow in the upper portion of the water column and a landward flow in the lower portion. Pritchard (1954) has shown that, in this system, the salt balance is maintained primarily by a longitudinal advective salt flux and a vertical nonadvective salt flux. It is the mixing length associated with this latter flux with which we are concerned. A left-handed co-ordinate system is employed in which the x_1, x_2, and x_3 -axes are directed horizontally seaward, vertically downward and laterally across the estuary, respectively.

Consider first the mixing length for salt as given by Prandtl's proposal. Let the vertical flux of salt at a point in the estuary be expressed as

$$\langle v'_2 s' \rangle = \gamma \sqrt{\overline{v'^2_2}} \times \sqrt{\overline{s'^2}}, \tag{1}$$

where $\sqrt{\overline{v'^2_2}}$ and $\sqrt{\overline{s'^2}}$ are the local root mean squares of the turbulent fluctuations in velocity and salt, respectively, and where γ is the correlation between them. If, as Prandtl suggests, a turbulent fluctuation in property may be described in terms of a linear dimension and of a mean gradient of that property, we have for $\sqrt{\overline{s'^2}}$

$$\sqrt{\overline{s'^2}} = l_s \frac{\overline{\partial s}}{\partial x_2}. \tag{2}$$

Further, it is hypothesized that a negative correlation must exist between the velocity fluctuations perpendicular and parallel to the direction of mean flow; that is,

$$\sqrt{\overline{v'^2_2}} = -c\sqrt{\overline{v'^2_1}}. \tag{3}$$

By the same argument that led to (2), we write

$$\sqrt{\overline{v'^2_2}} = -cl_v \frac{\overline{\partial v_1}}{\partial x_2}. \tag{4}$$

Assuming for this system that $l_s = l_v = l$ and by substituting (2) and (4) into (1), we have for the vertical flux of salt

$$\langle v'_2 s' \rangle = -\gamma c l^2 \left| \frac{\overline{\partial v_1}}{\partial x_2} \right| \frac{\overline{\partial s}}{\partial x_2}. \tag{5}$$

Letting $\eta^2 = \gamma c$ be a constant in (5), we have

$$\eta^2 l^2 = -\frac{\langle v'_2 s' \rangle}{\left| \frac{\overline{\partial v_1}}{\partial x_2} \right| \cdot \frac{\overline{\partial s}}{\partial x_2}} \tag{6}$$

from which the mixing length, l, may be calculated provided that the remaining quantities are known. For future reference, let this value of l be called the *observed* mixing length.

Consider now the derivation of l in terms of an adiabatic mixing length and a stability function. For an unstratified system, Prandtl (1932) found that the mixing length in the immediate vicinity of a solid boundary is nearly a linear function of the shortest distance from the boundary; that is

$$l_\alpha = \kappa(x_2), \tag{7}$$

where l_α is the adiabatic (unstratified) mixing length, κ the universal turbulence constant, and x_2 the distance from the boundary. Montgomery (1943) generalized Prandtl's geometrical assumption so that the adiabatic mixing length for cylinders of infinite length became a linear function of the reciprocal of the average "nearness," in the plane normal to the cylinder, to the boundary. Since the ratio of width to water depth is large (200:1) for the shallow coastal plain estuary in which we are interested, the system may be regarded as being composed essentially of two parallel plane boundaries: namely, the water surface, and the river bottom. For this geometrical setup, neglecting the roughness length, Montgomery's mixing length, l_α, is found to be

$$l_\alpha = \frac{\kappa x_2}{h}\{h - x_2\}, \tag{8}$$

where h is the boundary separation (in our case the depth of water). Clearly, l_α is symmetrical about the point of mid-depth.

It is evident that the mixing length in a homogeneous system will be unlike that in a stratified system. A stable stratification will provide a damping effect on vertical turbulent motions since a portion of the energy in excess of that required to maintain the mean field is used to perform work against the density gradient. The reverse is true for an unstable stratification. Rossby and Montgomery (1935) have pointed out that for a stable stratification the mixing length is reduced; furthermore they have proposed a relationship between the adiabatic and stratified lengths.

They state that the turbulent kinetic energy per unit mass for the case of neutral stability must be equal to the sum of the turbulent kinetic energy plus the potential energy per unit mass for the stable case. The turbulent kinetic energies for the two cases are proportional to

$$l_\alpha^2 \left|\overline{\frac{\partial v_1}{\partial x_2}}\right|^2 \quad \text{and} \quad l \cdot \left|\overline{\frac{\partial v_1}{\partial x_2}}\right|^2,$$

where the mean shear is assumed to be the same in the two cases. Here l_α is the mixing length for adiabatic conditions (neutral stability) and l is the mixing length for stable conditions. The potential energy for the stable case is shown to be proportional to

$$\frac{g}{\sigma_t}\frac{\partial \sigma_t}{\partial x_2} l^2,$$

where σ_t has the conventional meaning of the density less unity times one thousand. (Note: Rossby and Montgomery treated the atmospheric case, where the potential temperature θ takes the place of σ_t.)

The expression obtained by Rossby and Montgomery relating l for the stable case with l_α is then in our notation

$$l = l_\alpha(1 + \beta Ri)^{-\frac{1}{2}}, \tag{9}$$

where Ri is the Richardson number, given by

$$Ri = \frac{g}{\sigma_t}\frac{\partial \sigma_t}{\partial x_2} \Big/ \left|\frac{\partial \bar{v}_1}{\partial x_2}\right|^2$$

and where β is an undetermined proportionality factor.

Holzman (1943)* cited other references to show evidence for a critical value of Ri above which turbulence is suppressed. He argued that l should go to zero at some finite value of Ri, a condition not satisfied by eq. (9). Holzman proposed an alternate relationship which does provide for a critical value of Ri, and further, it is more amenable to mathematic treatment. His expression, in our notation, is

$$l = l_\alpha(1 - \beta Ri)^{\frac{1}{2}}. \tag{10}$$

As stated above, Rossby and Montgomery assumed that the turbulent kinetic energy for the adiabatic case was equal to the turbulent kinetic energy plus the potential energy due to the displacement over the mixing length for the stable case. An alternate proposal is that the energies *per unit length of displacement* are equal. This proposition leads to the expression

$$l = l_\alpha(1 + \beta Ri)^{-1}. \tag{11}$$

In eq. (8), l_α is based on the assumption of rigid planar boundaries at both the bottom and surface of the estuary. Actually, turbulent energy is introduced at the free water surface by wind waves. In this case the adiabatic mixing length should be larger in the near surface layers than the values given by eq. (8). It would appear reasonable to conclude that this increase should be related to the

orbital motion induced by surface wind waves. The orbital motion induced by surface waves is proportional to the expression

$$e^{-2\pi x_2/L},$$

where L is the wave length of the surface waves and x_2 the depth, as before. A possible expression for the adiabatic mixing length is then

$$l_a = \frac{\kappa x_2}{h}\{h - x_2\}\{1 + ae^{-2\pi x_2/L}\}. \tag{12}$$

Here a is an undetermined proportionality factor.

The term $\kappa x_2\{h - x_2\}/h$ in eq. (12) is the same as in eq. (8) and depends only on the geometry of the system. This term is symmetrical about mean depth. The term $\{1 + ae^{-2\pi x_2/L}\}$ depends on the characteristics of the surface wave motion, and the effect of this term on l_a decreases rapidly with depth. Fig. 1 gives an example of l_a computed from both eq. (8) and (12). In this computation κ has been taken as 0.40, h as 7.5 m, L as 5 m, and a as 3.17. Note that eq. (8) gives an l_a which is symmetrical about a well defined maximum at mid-depth while inclusion of the effect of surface wind waves extends this area of maximum l_a into the upper half of the water column. In this particular case the two computations for l_a are essentially the same below mid-depth.

For purposes of comparison with the *observed* mixing length as determined by eq. (6), we designate the l determined by any of the equations (9), (10), or (11) as the *theoretical* mixing length. This designation will hold whether eq. (8) or eq. (12) is employed in determining l_a.

We will now compare the *observed* mixing length given by eq. (6) with the *theoretical* mixing lengths given by each of the equations (9), (10) and (11), using data collected in the James River estuary.

Eq. (6) contains the unknown constant η, and eqs. (9), (10) and (11) contain the unknown constant β. The procedure employed in this comparison involves the simultaneous solution of the two subject equations at two depths (3.5 m and 5 m) in order to obtain the constants η and β. The correspondence of the two l's at other depths is then examined.

The data here employed were collected in the James River estuary during three periods of several days each during the summer of 1950. The station is located some 17 miles upstream from the mouth of the James. For further information on the physical and chemical properties of this estuary, refer to Pritchard (1952, 1954). The data employed in the evaluation are presented in detailed reduced form by

Pritchard and Kent (1953) under the station designation J-17. From this latter reference the required values of $\langle v'_2 s' \rangle$, $\overline{\partial s}/\partial x_2$, σ_t, $\partial \sigma_t/\partial x_2$, $|\ \overline{\partial v_1}/\partial x_2\ |$, and $|\ \overline{\partial v_1}/\partial x_2\ |^2$ can be obtained directly or computed from auxiliary data.

We have first taken all three periods together as representing one set of data. The average values of the pertinent parameters were employed in comparing the *observed* with the *theoretical* mixing length.

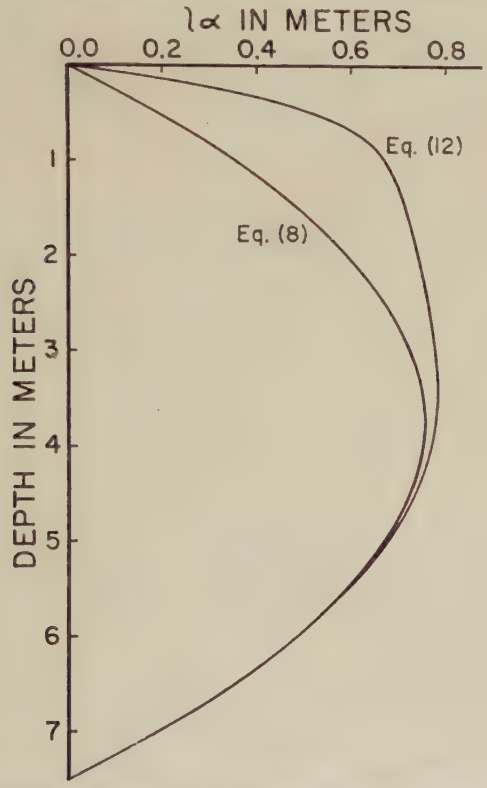

Figure 1. The adiabatic mixing length, l_α, as a function of depth as computed from eq. (8), which includes the effect of geometry only, and from eq. (12), which also includes the effect of surface wind waves.

In this initial comparison eq. (8) was employed in obtaining l_α. In comparing eq. (6), the *observed* mixing length, with eq. (9), the *theoretical* mixing length proposed by Rossby and Montgomery, we found that it was not possible to find a simultaneous solution at two depths which gave real values for η and β. In order to make some

comparison, a value 0.253 was chosen for η, and β was then found by assuming that the two pertinent equations were the same at the single depth of 3.5 m. Results are shown in Fig. 2(a). Here the *theoretical* is presented as a solid curve while the *observed* is plotted as discrete points for each one-half meter. Note that the *observed* mixing length is in general larger than the *theoretical*, except at 3.5 m, where agreement was forced by the method of determining the proportionality constant β.

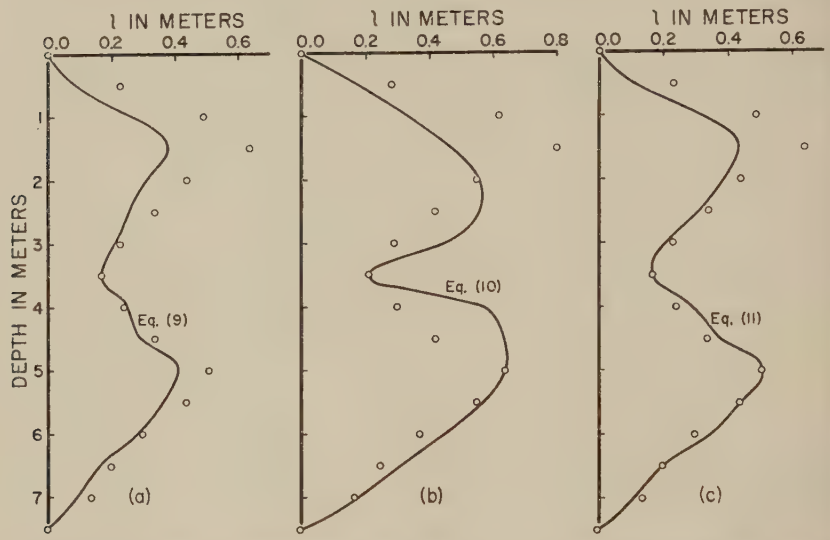

Figure 2. Comparison of *observed* mixing length given by eq. (6), plotted here as discrete points at each one-half meter depth, with the *theoretical* mixing length given by eqs. (9), (10) and (11). For these determinations, the parameter l_α is given by eq. (8).

The selection of any positive value of η would give the same relative disagreement between the *observed* and *theoretical* as shown in Fig. 2(a), when eq. (9) is employed in computing the *theoretical* mixing length. The adiabatic mixing length, l_α, required as a parameter in using eq. (9), was computed from eq. (8) for this comparison. Thus when l_α is determined on the basis of boundary geometry only, without considering the influence of wind waves, there is only fair correspondence between the mixing length based on Rossby and Montgomery's relationship and the one based on observation.

Comparison of the *observed* with the *theoretical* mixing length based on the relationship proposed by Holzman is shown in Fig. 2(b). Eqs. (6) and (10) were solved simultaneously at 3.5 and 5 m depth to obtain values for the parameters η and β. Except at these two points

of forced correspondence, the correspondence between the two lengths is not particularly good.

The value of β which results from this comparison is 0.412×10^{-3}. Eq. (10) provides for a critical value of Ri at which turbulence becomes completely damped: that is, at which the mixing length goes to zero. This condition is met when $\beta\, Ri$ equals unity: that is, when Ri equals 2.43×10^{3}.

Comparison of the mixing length determined from eq. (11) with the *observed* is shown in Fig. 2(c). Here again (6) and (11) were solved simultaneously at 3.5 and 5 m depth to obtain values of η and β. At other depths the correspondence between the two lengths is much better than that shown in Fig. 2(b) and somewhat better than that shown in Fig. 2(a). The area of greatest difference occurs in the upper layers.

These comparisons were made by using eq. (8) in the determination of the adiabatic mixing length. As pointed out above, it is reasonable to assume that the effect of surface wind waves would be to increase the mixing length in the upper layers. Thus the lack of agreement between the mixing length computed from eq. (11) and that *observed* may be due to failure to include the influence of surface waves in determining the parameter l_a.

Figs. 3(a) and 3(b) show the comparison between the *observed* mixing length and the values computed from eqs. (9) and (11), respectively, when the adiabatic mixing length is determined from eq. (12). The value of the unknown constant a in eq. (12) was taken at 3.17. This value provides for exact correspondence of the mixing length determined from eq. (11) with that observed at the maximum which occurs at 1.5 m depth. The wave length L was taken as 5 m, a value compatible with the observed mean wind.

With the influence of surface waves included in the determination of the adiabatic mixing length, it becomes possible to solve eqs. (6) and (9) simultaneously at 1.5 and 3.5 m. Correspondence between the mixing length computed from these two equations is reasonably good at all depths.

The excellent agreement shown in Fig. 3(b) between the mixing lengths determined from eqs. (11) and (6) is somewhat forced, since the constants η and β were determined to give exact correspondence at depths of 3.5 and 5.0 m; and the proportionality factor a in eq. (12) was evaluated so as to give exact agreement at 1.5 m. However, the correspondence at depths other than these three is much better than for any of the other hypotheses tested.

The evaluation discussed above was made by using the average of data collected during three periods of several days each. The data

from the individual periods show significant differences in vertical stability as well as in other parameters which enter the computations. In the following discussion the observed data from each of the three periods have been used in further testing the suitability of eq. (11) in defining a mixing length under stable conditions.

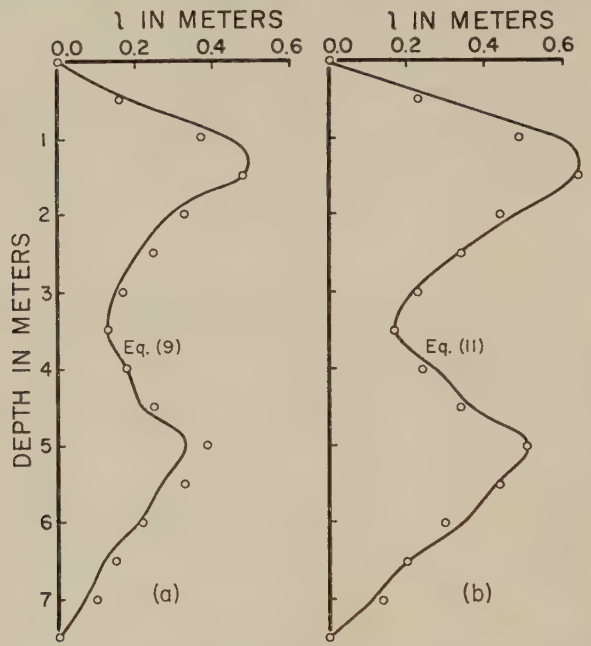

Figure 3. Comparison of *observed* mixing length as given by eq. (6), plotted here as discrete points for each one-half meter depth, with the *theoretical* mixing length given by eqs. (9) and (11), when the adiabatic mixing length is given by eq. (12).

The proportionality factors η and β should be constant if eq. (11) is a valid expression for the mixing length under stable conditions. The values of these two factors as determined from the combined data have been used in computing the *observed* and *theoretical* mixing lengths, using eq. (6) and eq. (11) respectively for each of the three periods. Results of this comparison are shown in Fig. 4. The curves for each of the three periods as computed from eq. (11) show differences, one from the other, which are also reflected in the *observed* mixing length. The correspondence of the two lengths for these three periods is quite good.

Table I summarizes the results of the various comparisons discussed above. Data available from the James River estuary indicate the following:

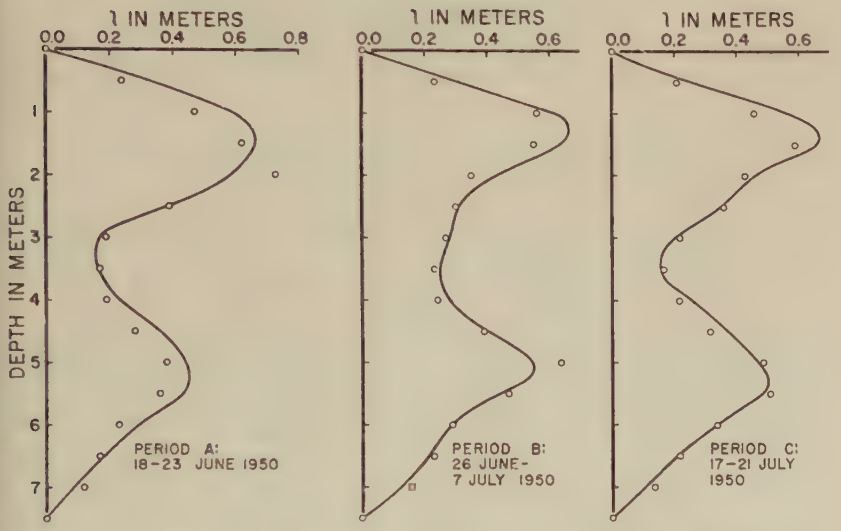

Figure 4. Curves are the mixing length computed from eq. (11), using $\beta = 1.65 \times 10^{-3}$. The circled points are the *observed* mixing length determined from eq. (6), using $\eta = 0.253$. The effect of wind waves has been included in the computation of the *theoretical* curve.

(a) The original proposal of Rossby and Montgomery for the mixing length under stable conditions is more compatible with the data than is the later proposal by Holzman.

(b) The relationship given by eq. (11) appears to provide a somewhat better correspondence with the data than that provided by the relationship of Rossby and Montgomery.

(c) The influence of surface wind waves is effective in increasing the adiabatic mixing length in the upper layers.

TABLE 1

Hypothesis	η	β	*Root mean square percentage difference, observed and theoretical mixing lengths**
Eqs. (8) and (9)	0.253	8.05×10^{-3}	29.9
	0.335	14.14×10^{-3}	23.4
Eqs. (8) and (10)	0.201	0.412×10^{-3}	41.7
Eqs. (8) and (11)	0.253	1.58×10^{-3}	28.0
Eqs. (12) and (9)	0.335	16.55×10^{-3}	16.1
Eqs. (12) and (11)	0.253	1.65×10^{-3}	15.0

* Depths at which agreement between the two lengths was "forced" by virtue of the selection of the coefficients are omitted from this evaluation.

REFERENCES

Holzman, B.
1943. The influence of stability on evaporation. Ann. N. Y. Acad. Sci., *44:* 13–18.

Montgomery, R. B.
1943. Generalization for cylinders of Prandtl's linear assumption for mixing length. Ann. N. Y. Acad. Sci., *44:* 89–103.

Prandtl, L.
1925. Bericht über Untersuchungen zur ausgebildeten Turbulenz. Z. angew. Math. Mech., *5:* 136–139.
1932. Meteorologische Anwendung der Strömungslehre. Beitr. Phys. frei. Atmos., *19:* 188–202.

Pritchard, D. W.
1952. Salinity distribution and circulation in the Chesapeake Bay estuarine system. J. mar. Res., *11*(2): 106–123.
1954. A study of the salt balance in a coastal plain estuary. J. mar. Res., *13*(1): 133–144.

Pritchard, D. W. and R. E. Kent
1953. The reduction and analysis of data from the James River operation Oyster Spat. Chesapeake Bay Inst., Tech. Rept. VI, 92 pp.

Rossby, C.-G. and R. B. Montgomery
1935. The layer of frictional influence in wind and ocean currents. Pap. phys. Oceanogr., *3*(3): 101 pp.

Note Added in Proof

I am indebted to Dr. R. B. Montgomery for pointing out to me that in the Richardson number the factor $(1/\sigma_t)(\partial\sigma_t/\partial x_2)$ should more correctly be $(1/\rho)(\partial\rho/\partial x_2)$. In the text this change would affect only the values of β, which should be multiplied by the factor 1.47×10^2. Thus the value of $\beta = 1.65 \times 10^{-3}$ should be corrected to $\beta = 0.242$, etc.

PYCNOCLINES CREATED BY MIXING IN AN AQUARIUM TANK

By

TOWNSEND CROMWELL

Inter-American Tropical Tuna Commission
Scripps Institution of Oceanography

Foreword

The experiments described in this paper were carried out by the author before his death in an airplane crash near Guadalajara, Mexico, 2 June 1958. We had planned to collaborate in studying the results from the standpoint of possible model similarity between events in the experimental tank and in the ocean, possibly repeating some of the experiments or devising new ones. But I was unable to find many of the pertinent numerical data in Mr. Cromwell's files.

It was the general opinion of our colleagues that Mr. Cromwell's interesting experiments had shed considerable light on the problem of thermocline formation and that a qualitative description would be of value even without a detailed discussion of the results. Fortunately, Mr. Cromwell had finished writing a preliminary draft and had prepared several figures. The present article consists entirely of that draft, with few minor changes by myself.

Considering the possibility of performing further experiments on pycnocline formation, Mr. Cromwell and I agreed that the initial linear density gradient herein used was probably an unnessary complication; the fluid above the pycnocline was shown to be sensibly homogeneous, and apparently only a thin layer of fluid immediately below participates in the process at any given time. Rouse and Dodu (1955), using the simpler initial state of two homogeneous layers, kept the pycnocline in the same relative position by allowing water to flow into the lower layer and out of the upper. It would be even simpler to eliminate the flow and allow the pycnocline to descend during the experiment. Then a thorough investigation of the effects of all parameters influencing the experiment, including mesh size, agitation frequency and amplitude, distance from mesh to pycnocline, etc., would be enlightening. Or, it might be possible to devise parameters that come closer to de-

scribing the turbulence introduced than those mentioned, thus facilitating comparison with an ocean where there is no oscillating mesh.

The loss of Townsend Cromwell was a great loss to the science of the oceans. It is hoped that others may be inspired to undertake model studies of thermocline behaviour, in which he had such an enthusiastic interest.

GORDON W. GROVES

Instituto de Geofísica Universidad Nacional Autónoma de Mexico.

ABSTRACT

Experiments here reported show that a vertical density gradient can be concentrated in a small aquarium tank by simple agitation immediately below the fluid surface with a mesh. A pycnocline, which is immediately formed, descends rapidly at first and then more and more slowly as its distance from the source of turbulence increases. An explanation for pycnocline descent is suggested. Fluid particles which move upward from the region of the pycnocline are rapidly deformed and mixed throughout the upper layer whereas fluid particles which move downward into the quiet layer below are buoyed upward intact. Thus the upper layer increases in thickness at the expense of the lower layer, *i.e.*, mixing across the pycnocline is one-way.

The sequence of events in the tank agrees with the hypothesis that pycnoclines in the ocean can be formed as a result of turbulence produced at the sea surface by wind. However, since these experiments were not properly scaled and since the turbulence spectrum in the ocean is undoubtedly dissimilar from that in the aquarium tank, our results are only suggestive and do not incontestably verify this hypothesis.

Introduction. Thermoclines are among the most striking features of the ocean's thermal structure. Since the effect of salt on density in the open ocean is generally small, the thermocline is a layer through which the vertical density gradient is large relative to overlying and underlying gradients; *i. e.*, the thermocline is also a "pycnocline".

Knowledge of pycnocline formation and maintenance is summarized in a report of the Chesapeake Bay Institute of the Johns Hopkins University (Pollak, 1954). Qualitative explanations of the phenomenon appear in a number of publications (Sverdrup, *et al.* 1942; Schule, *et al.*, 1952; Anonymous, 1946). Presumably wind stress on the sea surface produces stirring and mixing downward

to a limited depth. The layer affected is rendered nearly homogeneous, but below the region of effective mixing the vertical density gradient remains essentially unaffected. In between is a thin layer of sharp transition. In this way an initial vertical gradient, perhaps established by warming near the sea surface, is modified only by redistribution of mass in a vertical column, thereby "creating" a pycnocline.

Purposes of Experiment. Experiments were performed in a small tank to ascertain whether or not a pycnocline could be formed by introducing turbulent energy near the surface and possibly to gain insight into the mechanism of pycnocline formation and maintenance. Although the results were affirmative, it will be pointed out below that there are objections to drawing an analogy to events as they occur in the ocean.

Equipment and Experimental Procedure. A small rectangular aquarium tank, 27×17 cm and 19 cm deep, was used. A rectangular one-quarter inch galvanized iron mesh (hardware cloth) was cut to fit snugly into the tank. The mesh, with appropriate linkages to an electric motor, was driven up and down in regular oscillatory motion near the surface. This equipment is illustrated in Fig. 1.

The density structure desired initially was a linear increase with depth from top to bottom of tank. A clear mixture of roughly half sea water and half distilled water was diluted with dyed sea water in four proportions. It was found most practical to introduce the lightest (least colored) mixture into the tank first. Successively denser (more deeply colored) mixtures were then introduced near the bottom through a siphon. Sharp interfaces, visible because of the dye and because of refraction of light from a source behind the tank, tended to develop between successive mixtures. However, sharp gradients could be smoothed out by waving the nozzle up and down across the interfaces during siphoning. It was impossible to avoid all sharp vertical density gradients, but those which remained after siphoning could be "mixed away" by means of a small piece of hardware cloth on the end of a pencil. Establishing the initial gradient in the tank was the most difficult part of the whole experimental procedure, but by these crude methods a gradual increase in density with depth could be obtained (Fig. 2, curve A; Fig. 4).

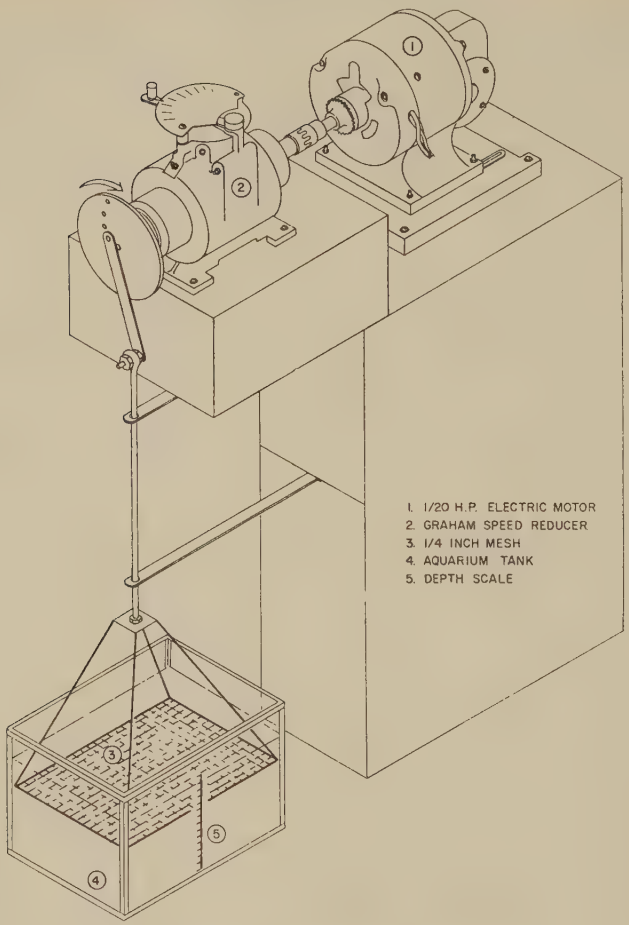

Figure 1. Experimental apparatus.

The experimental procedure was to agitate the fluid near it surface, the mesh describing simple harmonic motion over a 2.5 cr range of depth. From time to time the motor was stopped and, afte all visible movement of the fluid had ceased, samples were draw with a volumetric syringe and titrated. Titration and temperatur measurements in the tank were to an accuracy allowing the deter mination of density to 0.1 in σ_t.

Sampling depth was read from a scale pasted to the tank an zeroed at the water surface before any samples were drawn. "Adjuste

depth" enters because withdrawal of the samples lowered the fluid surface appreciably during the experiments. Adjustments were made according to the formula, $z_a = [z_s - (h_i - h_n)]\,[h_i/h_n]$, where z_a is "adjusted depth", h_i is water depth at start of the experiment, h_n is water depth at start of sampling run, and z_s is reading from depth scale.

During agitation by the mesh, the tank was checked visually to see that no "large scale" circulation was set up, *i.e.*, that there were no circulation cells which seemed to be bounded by the walls of the tank. When this happened, as it sometimes did, the fluid to a considerable depth would overturn, producing a homogeneous layer very quickly. However, when a mesh was obtained that was manufactured with reasonable precision, when it filled the tank snugly, and when it was nearly level, the motion appeared to result only from the irregular "turbulent" elements produced by the mesh grid, free of the influence of lateral boundaries.

Results. Results of a typical experiment appear in Fig. 2. A homogeneous surface layer is created by the stirring and mixing produced by the mesh. Immediately below, a sharp pycnocline appears. The vertical gradient in this pycnocline is greater than that which existed anywhere in the tank before agitation was begun. With the passage of time the pycnocline descends, rapidly at first but then more and more slowly as the distance from the mesh increases.

There are some further qualitative observations of tank experiments that can be mentioned. If the mesh is oscillated close to the bottom of the tank, a pycnocline forms above the mesh and gradually ascends. If the mesh is oscillated through an intermediate depth, pycnoclines form both above and below, rising and descending respectively. Thus, the position at which turbulent energy is introduced is important in determining the modification of the density structure that will occur.

Pycnoclines can be destroyed, or at least diminished in intensity, as well as created by the mixing. If, during an experiment, the frequency of mesh oscillation is increased suddenly, then turbulent elements penetrate into the lower stratum. As a result the gradient in the pycnocline becomes diminished. If the mesh is allowed to continue oscillating at this new, higher frequency, a new sharp pycnocline will form at some greater depth in the tank.

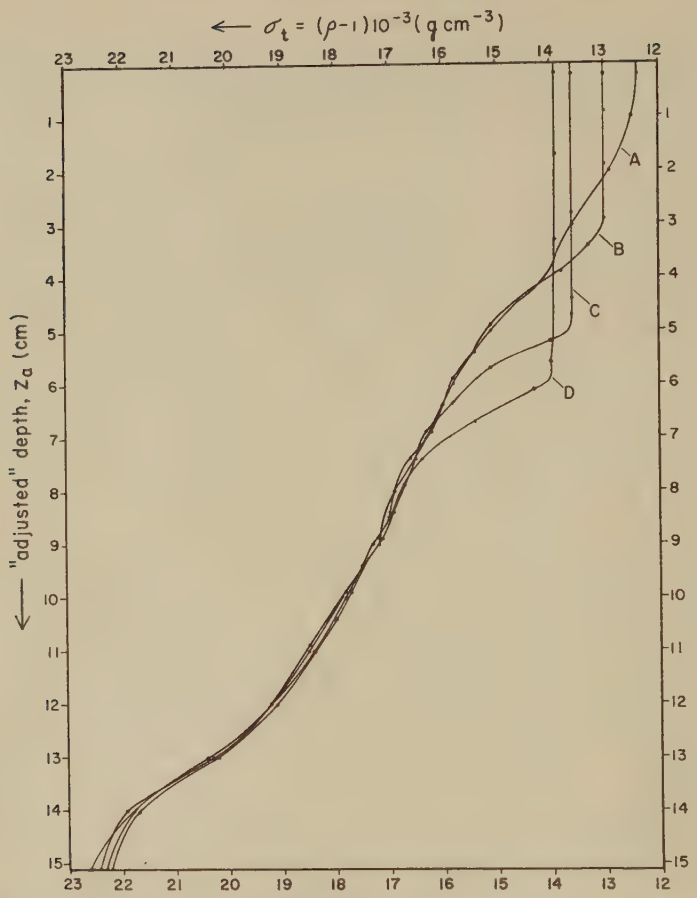

Figure 2. Successive density profiles in tank during an experiment; Curve A represen initial profile, curves B, C, and D occurring at later times.

Pycnocline Formation. Turbulence over the range of the mes is so extreme that a mixed layer, bounded below by an interfac is formed with the first thrust. This occurrence defies any usef interpretation. At the same time, however, fluid elements are in pelled downward by the mesh, interspersed by upward elemen (Fig. 3a). Their spacing is uniform and equal to the grid size the agitating mesh. Across the interfaces separating these elemen of differing density, molecular diffusion is favored. Those dow

ward elements which penetrate most deeply into the undisturbed fluid below are buoyed upward, intact, before any appreciable mixing takes place. At an intermediate level, somewhat above the level to which extreme downward elements penetrate, an interface gradually appears. The quantitative aspects of these events, *e.g.*, the depth and rapidity of pycnocline formation, depend on the original density structure, on the fundamental dimensions of the mesh, and on the frequency; but qualitatively it seems that the development of a mixed surface layer and a subjacent stable layer may occur when stirring is induced by any means whatever. For example, when the surface of the tank is cooled by suspending a sheet of dry ice just above it, roughly the same series of events takes place. But in this case other factors determine the size and spacing of the fluid filaments.

Once formed, the pycnocline maintains its identity and progresses downward. The interface is in irregular wave-like motion, and it separates the turbulent surface layer from the stable fluid below, which is quiet (Fig. 3b). This abrupt change in the state of motion across the interface can be seen during the experiment by sprinkling ashes from above, which, as they sink, describe irregular and varied paths downward until they pass the interface. Thereafter the particles sink slowly, straight downward. The predominant wave length of the wavy interface is now greater than it was just after the first few thrusts of the mesh, and apparently it is unrelated to the grid

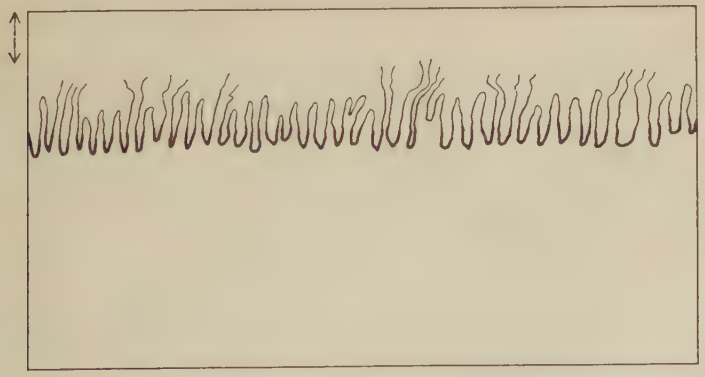

a.

Figure 3a. Initial appearance of interface after first thrust of mesh.

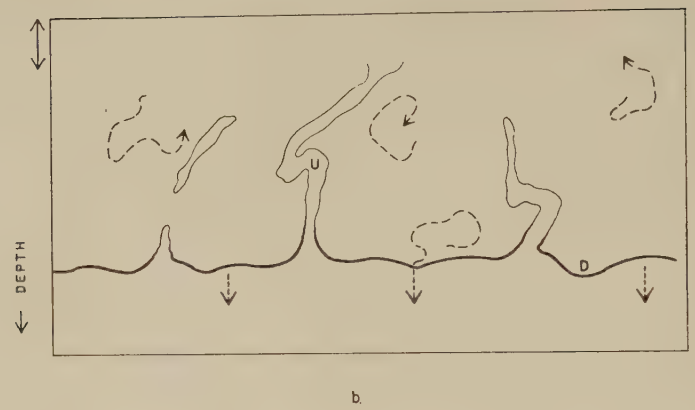

b.

Figure 3b. Subsequent appearance of interface.

size. Segments of typical paths are illustrated in Fig. 3b by dashed arrows.

The explanation for descent of the pycnocline is as follows Downward directed fluid elements at the interface (*e.g.*, at D) enter a quiet environment and are buoyed upward, intact. Upward directed elements (*e.g.*, at *U*) enter a turbulent environment where they are deformed and mixed quickly throughout the surface layer Thus the mixing, or entrainment, is one way, and the surface layer thickens at the expense of the lower layer, so that the pycnocline must gradually descend. Fig. 4 illustrates the varying rate of descent of the pycnocline.

Rouse and Dodu (1955) performed experiments with equipment basically similar to that described here. They began their experiments with a two-layered system of fresh and saline waters. They found that turbulence induced in the upper layer by a mesh was restricted to the upper layer, with entrainment from the layer below, an occurrence which our experiments have duplicated.

Analogy to Events in the Ocean. There is a striking similarity between events in the tank and those occurring in the ocean during increased winds. Francis and Stommel (1953), using data from weather ships, have shown that the oceanic thermocline descended during a gale. The author analyzed these same data in greater detail and found that (1) the surface layer becomes more nearly

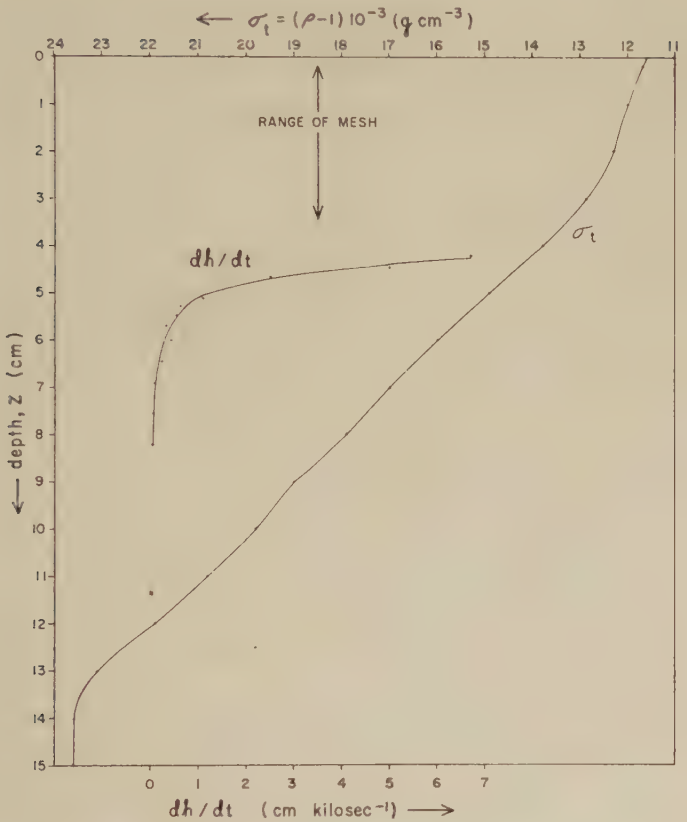

Figure 4. Diagram showing initial density profile and region of agitation ("range of mesh") as a function of distance from surface as well as the rate of pycnocline descent as a function of pycnocline depth, for a particular experiment.

isothermal (as measured by the BT), (2) the temperature gradient in the upper part of the thermocline becomes more intense, and (3) the separation between surface layer and thermal layer becomes sharper. An example of this series of events has been shown by Cromwell and Reid (1956: Fig. 6). This series of events can also be seen here in Fig. 2.

It has been suggested (by Carl Eckart) that the turbulence spectra in the tank and in the ocean are dissimilar and that this dissimilarity may be critical. The turbulent energy introduced into the tank by the mesh lies within the dissipative range of the spectrum, whereas

in the ocean there may be relatively little turbulent energy concentrated at such small scale. Thus, even when properly scaled model experiments are performed, results cannot be applied to the ocean with certainty until more is known of the spectrum of ocean turbulence.

Acknowledgements. The author is grateful for the interest and help of Dr. Wilhelm Brandhorst in setting up and carrying out the experiments. The advice and comments of Dr. Ray Montgomery, Dr. Carl Eckart and Dr. Warren Wooster have been very helpful. This work was partially supported through Research Support Shops by the Office of Naval Research.

REFERENCES

Anonymous

1946. The application of oceanography to subsurface warfare. Summ. Tech. Rep NDRC, *6A*, Div. 6.

Cromwell, Townsend and J. L. Reid, Jr.

1956. A study of oceanic fronts. Tellus, *8* (1): 94–101.

Francis, J. R. D. and Henry Stommel

1953. How much does a gale mix the surface layers of the ocean? Quart. J. R met. Soc., *79*: 534–536.

Pollak, M. J.

1954. Notes from the conference on the thermocline of 25–27 May, 1953. Chesa peake Bay Institute, Ref. 54–2.

Rouse, H. and J. Dodu

1955. Diffusion turbulente a travers une discontinuite de densite. Houille blanche Aug.–Sept., No. 4: 522–532.

Schule, J. J., *et al.*

1952. Effects of weather upon the thermal structure of the ocean. U.S. Navy Hydrographic Office, Misc. 15360.

Sverdrup, H. U., M. W. Johnson and R. H. Fleming

1942. The Oceans. Prentice Hall, Inc., New York. 1087 pp.

BOUNDARY LAYER EFFECTS IN ESTUARIES

By

M. R. ABBOTT

Hydraulics Research Station,
Wallingford, Berkshire, England

ABSTRACT

This paper is concerned with the velocity in the boundary layer of an estuary during a tidal cycle; the estuary considered has negligible salinity effect. The problem reduces to solving the usual non-steady boundary layer equations if it is assumed that (a) flow is two-dimensional, with a horizontal bed at any cross-section, and (b) little variation in breadth of the estuary in the boundary layer region. Further, the eddy viscosity is considered constant; thus the boundary layer equations are the same as those for a laminar layer except that they have an enhanced coefficient of viscosity due to turbulence. The surface or main stream velocity is assumed sinusoidal in time, though the amplitude and phase lag at any point can be specified arbitrarily. The boundary layer equations are solved by a method of successive approximation. The first approximation for the longitudinal velocity contributes periodic terms with the frequency of the tidal motion but with attenuated amplitude and phase advance near the bed. The second approximation gives, in addition to periodic terms having twice the frequency of the tidal motion, a steady term which is non-zero even outside the boundary layer. This mean velocity is of importance near the bed due to its influence on the movement of loose bed material. A simple criterion is given for the direction of mean velocity at a point just above the bed; for the Thames this agrees with observation. The theory is applied in detail to the Thames Estuary, and results compare satisfactorily with observation in spite of the assumptions in the theory.

I. INTRODUCTION

In the usual one-dimensional treatment of tidal flow in an estuary, the water velocity is taken to be uniform over a cross-section. The resulting motion is periodic, with amplitude and phase of velocity independent of depth. This simplified model is adequate for determining tidal amplitude and lag up an estuary, since over much of the depth at any point the flow is closely uniform and one-dimensional. However, it is clear that in reality the flow near the bed is considerably modified by boundary layer effects. In particular, the amplitude and phase of the tidal current near the bed will differ

from those at the surface. Thus, in order to obtain a more accurate and detailed description of flow, it is necessary to consider a variation of the velocity with depth. Additional refinements to be considered are the retention of the convective acceleration terms as well as the usual $\partial u/\partial t$ term. These are nonlinear and can be expected to alter radically the details of the theoretical flow; the velocity may cease to be strictly periodic at each depth.

Due to the complexity of the problem it is necessary to introduce several simplifications. First, flow is taken as two-dimensional with no variation in the lateral direction. In particular it is assumed that the bed is horizontal at each cross-section and that any side effects can then be neglected since in practice the width of an estuary is much greater than the depth. Secondly, it is assumed that its breadth, in the boundary layer region, changes little with the longitudinal co-ordinate. Thirdly, it is assumed that the tidal velocity in the main stream is sinusoidal in time, though amplitude and phase lag can vary with longitudinal co-ordinate in any manner. Finally, eddy viscosity is taken constant. In reality, eddy viscosity is certainly a function of the depth co-ordinate and of surface tidal velocity; therefore it depends on both space co-ordinates and time. Due to lack of information on the behaviour of eddy viscosity under these conditions of non-steady boundary layer flow, the present assumption is adopted, though it is very much an over-simplification.

In spite of these rather drastic simplifications it is believed that the theory gives many of the essential features of flow in an estuary as can be seen when results of the theory are compared with observations from the Thames.

The problem reduces to solving the usual non-steady boundary layer equations. The behaviour of the main stream velocity is assumed known; this information can be obtained from observation or can be calculated as a separate problem from one-dimensional theory. The latter would be necessary, unless model results were available, for determining the possible effect of any proposed artificial changes in an estuary. The boundary layer equations, with this periodic main stream velocity, are solved by a method of successive approximation (Schlichting, 1932).

The first approximation for longitudinal velocity contains periodic terms having a frequency which is the same as that of the tidal motion but having also both attenuated amplitude and phase advance near the bed. The exact details depend on the characteristics

of the main stream velocity and therefore ultimately on the geometry of the estuary and the tide at its mouth. The second approximation to the longitudinal velocity component takes account of the non-linear convective acceleration terms and contributes, besides periodic terms with twice the frequency of tidal motion, a nonperiodic term which is in general non-zero at all depths, even outside the boundary layer. Thus there is superimposed on the periodic motion a net motion of water either landward or seaward at each position and depth. This net motion is known as the mass transport when it refers to the net movement of a given particle of water, while the mean velocity, which is used in this paper, refers to conditions at a fixed point.

A knowledge of the magnitude and direction of the mean velocity at a point near the bed is of practical importance due to its influence on the movement of loose bed material. It is found that, if the surface velocity in an estuary is written as

$$U(x,t) = U_0(x) \cos \{ \omega t - \psi(x) \},$$

$U_0(x)$ being the amplitude of the tidal current, $\psi(x)$ the lag, and $2\pi/\omega$ the tidal period, then the mean velocity just above the bed is landward or seaward according as

$$\frac{d}{dx}(U_0 e^{\psi}) \gtrless 0.$$

At a point on an estuary where $U_0 e^{\psi}$ is a maximum, there is a mean velocity at the bed towards this point from both upstream and downstream; it is likely therefore that at such a point there is an accumulation of bed material. In fact, it is shown for the Thames that a maximum of $U_0 e^{\psi}$ actually occurs in the Mud Reaches, which is well known as a region of heavy silting.

The method employed in this paper follows that of Schlichting (1932). The main mathematical results can also be deduced from Longuet-Higgins (1953), who treats in detail the general problem of mass transport in water waves; however, in the present less general application it is felt that the simple derivation from Schlichting's work is of interest.

II. GENERAL THEORY

Boundary layer equations are now derived for an estuary with a known periodic surface velocity due to the tide at its mouth. The

simplifications given in § I are adopted: flow is taken to be two-dimensional, with no variation in the lateral direction; the bed of the estuary at any cross-section is assumed horizontal; and eddy viscosity is considered constant. Due to turbulence, the kinematic eddy viscosity (ν) is much greater than the molecular kinematic viscosity for laminar motion; ν, which occurs as a parameter in the theory, is estimated for the Thames from experimental data.

The x-axis is taken along the bed, the positive direction upstream, while the y-axis is directed upwards. The equation of motion in the x-direction is then

$$\frac{\partial u}{\partial t}+u\frac{\partial u}{\partial x}+v\frac{\partial u}{\partial y}+\frac{1}{\varrho}\frac{\partial p}{\partial x}=\nu\left(\frac{\partial^2 u}{\partial x^2}+\frac{\partial^2 u}{\partial y^2}\right), \tag{1}$$

where (u, v) is the water velocity, ϱ water density, and p pressure. In the main stream, outside the boundary layer, we have Bernoulli's equation

$$\frac{\partial U}{\partial t}+U\frac{\partial U}{\partial x}+\frac{1}{\varrho}\frac{\partial p}{\partial x}=0, \tag{2}$$

where $U(x, t)$ is the main stream velocity, or, in particular, the surface velocity. The usual boundary layer approximations are made by neglecting $\partial^2 u/\partial x^2$ in comparison with $\partial^2 u/\partial y^2$ and by taking $\partial p/\partial x$ as a function of x only: from (1) and (2) therefore

$$\frac{\partial u}{\partial t}+u\frac{\partial u}{\partial x}+v\frac{\partial u}{\partial y}=\frac{\partial U}{\partial t}+U\frac{\partial U}{\partial x}+\nu\frac{\partial^2 u}{\partial y^2}. \tag{3}$$

If it is assumed that changes in the breadth of the estuary in the boundary layer region are effectively small [requiring $\frac{1}{u}\frac{\partial u}{\partial x}\gg\frac{1}{b}\frac{\partial}{\partial}$ and $\frac{1}{v}\frac{\partial v}{\partial y}\gg\frac{1}{b}\frac{\partial b}{\partial y}$ say, where $b(x, y)$ is the local breadth of the estuary], then the continuity equation is simply

$$\frac{\partial u}{\partial x}+\frac{\partial v}{\partial y}=0. \tag{4}$$

The surface velocity is assumed known and is expressed as

$$U(x,t)=U_1(x)\cos\omega t+U_2(x)\sin\omega t=(U_1-iU_2)e^{i\omega t}, \tag{5}$$

where "the real part of" is implied. Eqs. (1) to (4) are those used by Schlichting (1932), with the simpler oscillation $U=U_1\cos\omega$

replacing (5). This applies only in the present application to an estuary in which the tide can be represented by a standing oscillation. The more general expression (5) permits amplitude and phase of the tidal current to be specified at each point of an estuary, and in § III and IV Schlichting's analysis is extended to cover this case.

III. FIRST APPROXIMATION

The boundary layer eqs. (3) and (4), with the main stream velocity given by (5), are solved by successive approximation. We write

$$u = u_1 + u_2 + \ldots, \quad v = v_1 + v_2 + \ldots;$$

the first approximation is obtained from (3) with the convective acceleration terms neglected; eqs. (3) and (4) are then linear and can be readily solved for u_1 and v_1. The second approximation then involves the convective acceleration terms evaluated according to the first approximation with $u = u_1$, $v = v_1$. It is seen that neglect of the convective terms is a valid first approximation if

$$\left| U \frac{\partial U}{\partial x} \right| \ll \left| \frac{\partial U}{\partial t} \right|,$$

or roughly

$$U \ll \sqrt{gh},$$

where h is the mean depth of the estuary. In general this is satisfied and we can proceed as indicated.

Neglecting the convective terms in (3), the following is obtained for u_1

$$\frac{\partial u_1}{\partial t} - \nu \frac{\partial^2 u_1}{\partial y^2} = \frac{\partial U}{\partial t}. \tag{6}$$

Put

$$\eta = y \sqrt{\frac{\omega}{2\nu}} \tag{7}$$

and introduce a stream function

$$\psi_1 = \sqrt{\frac{2\nu}{\omega}} (U_1 - i\, U_2)\, e^{i\omega t}\, \zeta_1(\eta); \tag{8}$$

we then have

$$u_1 = (U_1 - i\, U_2)\, e^{i\omega t}\, \zeta_1', \qquad v_1 = -\sqrt{\frac{2\nu}{\omega}} (U_1' - i\, U_2')\, e^{i\omega t}\, \zeta_1, \tag{9), (10}$$

and substituting (9) into (6) gives

$$i\,\zeta_1^{\mathrm{I}} - \tfrac{1}{2}\,\zeta_1^{\mathrm{III}} = i. \tag{11}$$

On the bed, both components of velocity are zero, and as the surface is approached, $u_1 \to U$, the main stream velocity. In general, the depth is many times greater than the boundary layer thickness and the boundary layer effect is therefore insensible before the surface is reached; thus, so far as the effect on u_1 is concerned, the surface can be taken as $\eta = \infty$. The boundary conditions are then

$$\zeta_1 = 0,\ \zeta_1^{\mathrm{I}} = 0 \text{ for } \eta = 0$$

and

$$\zeta_1^{\mathrm{I}} \to 1 \text{ as } \eta \to \infty.$$

The solution of (11) is therefore

$$\zeta_1^{\mathrm{I}} = 1 - e^{-(1+i)\eta}, \tag{12}$$

or

$$\zeta_1 = -\tfrac{1}{2}(1-i) + \eta + \tfrac{1}{2}(1-i)\,e^{-(1+i)\eta}. \tag{13}$$

The real and imaginary parts of (12) and (13) give

$$\zeta_{1r} = -\tfrac{1}{2} + \eta + \tfrac{1}{2}e^{-\eta}(\cos\eta - \sin\eta) \tag{14}$$

$$\zeta_{1i} = \tfrac{1}{2} - \tfrac{1}{2}e^{-\eta}(\cos\eta + \sin\eta) \tag{15}$$

$$\zeta_{1r}^{\mathrm{I}} = 1 - e^{-\eta}\cos\eta, \quad \zeta_{1i}^{\mathrm{I}} = e^{-\eta}\sin\eta. \tag{16), (17}$$

Hence, from (9) and (10) the first approximation to the velocity is given by

$$u_1 = (U_1\zeta_{1r}^{\mathrm{I}} + U_2\zeta_{1i}^{\mathrm{I}})\cos\omega t + (U_2\zeta_{1r}^{\mathrm{I}} - U_1\zeta_{1i}^{\mathrm{I}})\sin\omega t \tag{18}$$

$$v_1 = -\sqrt{\frac{2\nu}{\omega}}\left\{(U_1^{\mathrm{I}}\zeta_{1r} + U_2^{\mathrm{I}}\zeta_{1i})\cos\omega t + (U_2^{\mathrm{I}}\zeta_{1r} - U_1^{\mathrm{I}}\zeta_{1i})\sin\omega t\right\}. \tag{19}$$

It can be seen from (19) that for large η

$$v_1 \to -\sqrt{\frac{2\nu}{\omega}}\,\eta\,(U_1^{\mathrm{I}}\cos\omega t + U_2^{\mathrm{I}}\sin\omega t) = -y\frac{\partial U}{\partial x};$$

this is consistent at the surface with the one-dimensional continuity equation for motion in an estuary, the latter being $h\dfrac{\partial U}{\partial x} + \dfrac{\partial H}{\partial t} = 0$ where h is depth and $\partial H/\partial t$ is the vertical water velocity at the surface.

The shear on the bed is given by

$$\tau = \varrho\nu\left(\frac{\partial u_1}{\partial y}\right)_0 = \varrho\sqrt{\tfrac{1}{2}\omega\nu}\left(\frac{\partial u_1}{\partial \eta}\right)_0$$

$$= \varrho\sqrt{\tfrac{1}{2}\omega\nu}\left[(U_1\zeta_{1r}^{II} + U_2\zeta_{1i}^{II})\cos\omega t + (U_2\zeta_{1r}^{II} - U_1\zeta_{1i}^{II})\sin\omega t\right]_0. \quad (20)$$

From (16) and (17)

$$(\zeta_{1r}^{II})_0 = (\zeta_{1i}^{II})_0 = 1,$$

hence from (20)

$$\tau = \varrho\sqrt{\tfrac{1}{2}\omega\nu}\left\{(U_1+U_2)\cos\omega t + (U_2-U_1)\sin\omega t\right\}. \quad (21)$$

The functions ζ_{1r}, ζ_{1i}, ζ_{1r}^{I}, ζ_{1i}^{I} in (18) and (19) can be obtained numerically from similar functions given by Schlichting (1932). Our $\zeta_{1r}(\eta)$, $\zeta_{1i}(\eta)$, $\zeta_{1r}^{I}(\eta)$, $\zeta_{1i}^{I}(\eta)$ are respectively Schlichting's $\frac{1}{\sqrt{2}}\zeta_{1r}\left(\sqrt{2}\,\eta\right)$, $\frac{1}{\sqrt{2}}\zeta_{1i}\left(\sqrt{2}\,\eta\right)$, $\zeta_{1r}^{I}\left(\sqrt{2}\,\eta\right)$, $\zeta_{1i}^{I}\left(\sqrt{2}\,\eta\right)$. The difference results from the factor $\sqrt{2}$ in (7), which was introduced, following the advice of a referee, in order to simplify some of the equations of this and the following section.

IV. SECOND APPROXIMATION

In the second approximation the nonlinear convective acceleration terms are retained, but they are evaluated according to the first approximation determined above. In fact, u_2 is given by

$$\frac{\partial u_2}{\partial t} - \nu\frac{\partial^2 u_2}{\partial y^2} = U\frac{\partial U}{\partial x} - u_1\frac{\partial u_1}{\partial x} - v_1\frac{\partial u_1}{\partial y}, \quad (22)$$

after putting $u = u_1 + u_2$, $v = v_1 + v_2$ in (3) and taking account of (6). The convective terms on the right of (22) can be written in terms of U_1, U_2 and ζ_1 by means of (5), (18) and (19). The final result is obtained as

$$2\frac{\partial u_2}{\partial t} - \omega\frac{\partial^2 u_2}{\partial \eta^2} = (U_1U_1^{I} + U_2U_2^{I})(1 - \zeta_1^{I}\overline{\zeta_1^{I}} + \tfrac{1}{2}\zeta_1\overline{\zeta_1^{II}} + \tfrac{1}{2}\overline{\zeta_1}\,\zeta_1^{II}) - \tfrac{1}{2}i(U_1U_2^{I} - U_1^{I}U_2)(\zeta_1\overline{\zeta_1^{II}} - \overline{\zeta_1}\,\zeta_1^{II}) + (U_1 - iU_2)(U_1^{I} - iU_2^{I})(1 - \zeta_1^{I2} + \zeta_1\zeta_1^{II})\,e^{2i\omega t}, \quad (23)$$

where a bar is used to denote a complex conjugate. The algebraic details of this step are omitted for brevity.

The solution of (23) is of the form

$$u_2 = G_1(\eta) + G_2(\eta)\, e^{2i\omega t}; \tag{24}$$

here G_1 is the steady contribution and represents mean velocity at a point, and G_2 is the amplitude of the second harmonic part of velocity; G_1 and G_2 vary with x as well as η, but x is merely a parameter in this context. Eq. (24) is substituted into (23) and coefficients of 1 and $e^{2i\omega t}$ are equated. This gives respectively

$$\omega G_1^{II} = -(U_1 U_1^I + U_2 U_2^I)\,(1 - \zeta_1^I \overline{\zeta_1^I} + \tfrac{1}{2}\zeta_1 \overline{\zeta_1^{II}} + \tfrac{1}{2}\overline{\zeta_1}\zeta_1^{II}) + \tfrac{1}{2}\, i\,(U_1 U_2^I - U_1^I U_2)\,(\zeta_1 \overline{\zeta_1^{II}} - \overline{\zeta_1}\zeta_1^{II}) \tag{25}$$

and

$$4\, i\, \omega\, G_2 - \omega\, G_2^{II} = (U_1 - i\, U_2)\,(U_1^I - i\, U_2^I)\,(1 - \zeta_1^{I^2} + \zeta_1 \zeta_1^{II}). \tag{26}$$

From (25), with the aid of (12) and (13), we obtain

$$\omega\, G_1 = (U_1 U_1^I + U_2 U_2^I)\,\zeta_{2b}^I + (U_1 U_2^I - U_1^I U_2)\,\zeta_{2c}^I + c_1 \eta + c_2, \tag{27}$$

where

$$\zeta_{2b}^I = \tfrac{1}{4}\, e^{-2\eta} + 2\, e^{-\eta} \sin\eta + \tfrac{1}{2} e^{-\eta} \cos\eta - \tfrac{1}{2}\, \eta\, e^{-\eta}\,(\cos\eta - \sin\eta) - \tfrac{3}{4} \tag{28}$$

$$\zeta_{2c}^I = \tfrac{1}{4} e^{-2\eta} + \tfrac{1}{2} e^{-\eta} \sin\eta - e^{-\eta} \cos\eta - \tfrac{1}{2}\, \eta e^{-\eta}\,(\sin\eta + \cos\eta) + \tfrac{3}{4}, \tag{29}$$

and c_1 and c_2 are constants of integration. On the bed, mean velocity is zero, therefore $c_2 = 0$. Also, mean velocity must remain finite as $\eta \longrightarrow \infty$, hence $c_1 = 0$. In the vicinity of the bed, which so far as the movement of sediment is concerned is the region of greatest interest, the mean velocity can therefore be written as

$$G_1 = \frac{1}{\omega}(U_1 U_1^I + U_2 U_2^I)\,\zeta_{2b}^I + \frac{1}{\omega}\,(U_1 U_2^I - U_1^I U_2)\,\zeta_{2c}^I\,. \tag{30}$$

Outside the boundary layer,

$$G_1 \longrightarrow \frac{3}{4\omega}(U_1 U_2^I - U_1^I U_2 - U_1 U_1^I - U_2 U_2^I); \tag{31}$$

for $U_2 = 0$ this agrees with Schlichting (1932). Eq. (31) is not valid right to the surface, since no account has been taken of the boundary condition at the free surface.

From (30), together with (28) and (29), it can be shown that

$$G_1^{\mathrm{I}}(0) = \frac{1}{2\omega}\left\{(U_1 - U_2)\, U_1^{\mathrm{I}} + (U_1 + U_2)\, U_2^{\mathrm{I}}\right\}, \tag{32}$$

while $G_1(0) = 0$. Therefore, mean velocity just above the bed is landward or seaward according as

$$(U_1 - U_2)\, U_1^{\mathrm{I}} + (U_1 + U_2)\, U_2^{\mathrm{I}} \gtrless 0. \tag{33}$$

This is a simple criterion to apply since it depends only on the behaviour of surface currents. Some further discussion of (33) is given in § VI.

Mean velocity, considered above, refers to conditions at a fixed point while the net movement of water particles over a tidal cycle is determined from the mass transport velocity. It is shown by Longuet-Higgins in an appendix to Russell and Osorio (1957) that $(\partial M/\partial \eta)_0 = (\partial G_1/\partial \eta)_0$, where M denotes mass transport velocity, which is of course, with the mean velocity, zero on the bed. Therefore, just above the bed, mass transport and mean velocity are in the same direction and consequently (33) also applies as a criterion for the mass transport direction at a point just above the bed. The movement of suspended sediment is controlled mainly by mass transport, that of sediment on the bed by mean velocity; it is likely, therefore, that if sediment is in motion near the bed, it also moves in a direction given by (33).

An expression for mass transport can be derived from u_1, v_1, G_1, and it can be shown, after a change of notation, that the expression obtained agrees with Longuet-Higgins (1953: eq. 188). In particular, outside the boundary layer,

$$M \to \frac{1}{4\omega}\left(5\, U_1 U_2^{\mathrm{I}} - 5\, U_1^{\mathrm{I}} U_2 - 3\, U_1 U_1^{\mathrm{I}} + 3\, U_2 U_2^{\mathrm{I}}\right),$$

which is in agreement with his eq. (189).

Now it remains to determine the second harmonic component of velocity from (26). The expressions involved are lengthy and only the final result is given:

$$u_2 = G_1(\eta) + \frac{1}{\omega}\left\{(U_1 U_1^{\mathrm{I}} - U_2 U_2^{\mathrm{I}})\, \zeta_{2ar}^{\mathrm{I}} + (U_1 U_2)^{\mathrm{I}}\, \zeta_{2ai}^{\mathrm{I}}\right\} \cos 2\omega t$$
$$- \frac{1}{\omega}\left\{(U_1 U_1^{\mathrm{I}} - U_2 U_2^{\mathrm{I}})\, \zeta_{2ai}^{\mathrm{I}} - (U_1 U_2)^{\mathrm{I}}\, \zeta_{2ar}^{\mathrm{I}}\right\} \sin 2\omega t, \tag{34}$$

where $\zeta_{2a}^{\mathrm{I}}(\eta)$ is Schlichting's $\zeta_{2a}^{\mathrm{I}}(\sqrt{2}\eta)$.

In the theory of this section we started by assuming a main stream velocity given by $U = U_1 \cos \omega t + U_2 \sin \omega t$, but we obtained from the second approximation a steady term superimposed on this. However, this steady term is small compared with U_1 and U_2, so the dominant part of the main stream velocity can be correctly taken as above.

V. DETAILS FOR THE THAMES ESTUARY

The theory presented in the previous sections is now applied in detail to the Thames. The origin is taken at London Bridge, with the positive x-direction upstream; from now on x is in miles, with Southend, for example, at the seaward or downstream end of this estuary, being given by $x = -43$. The mean depth between London Bridge and Southend is about 30 ft.

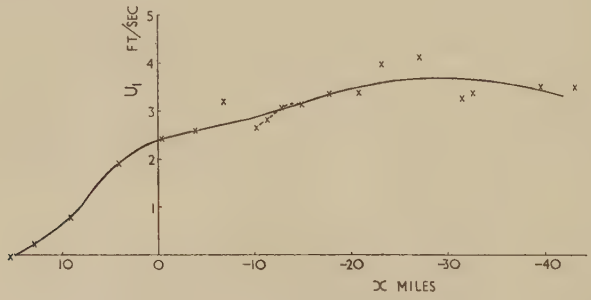

Figure 1. $U_1(x)$ for the Thames Estuary.

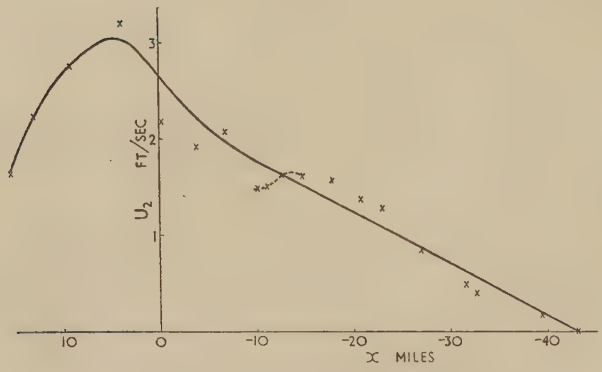

Figure 2. $U_2(x)$ for the Thames Estuary.

Amplitude and lag of the tidal current up the Thames are obtained from Inglis and Allen (1957: table 6) for a tide on 2 November 1948. U_1 and U_2 are obtained from these quantities and are shown in Figs. 1 and 2 along with the smoothed curves which are used from now on. It is necessary to smooth the rather erratic curves since U_1^{I} and U_2^{I} are required in the theory. With U_1^{I} and U_2^{I} calculated from these smoothed curves, with ζ_{1r}, ζ_{1i}, ζ_{1r}^{I}, ζ_{1i}^{I}, ζ_{2ar}^{I}, ζ_{2ai}^{I}, ζ_{2b}^{I} derived from Schlichting (1932), and with the new function ζ_{2c}^{I} shown in Fig. 3, we calculate the following quantities.

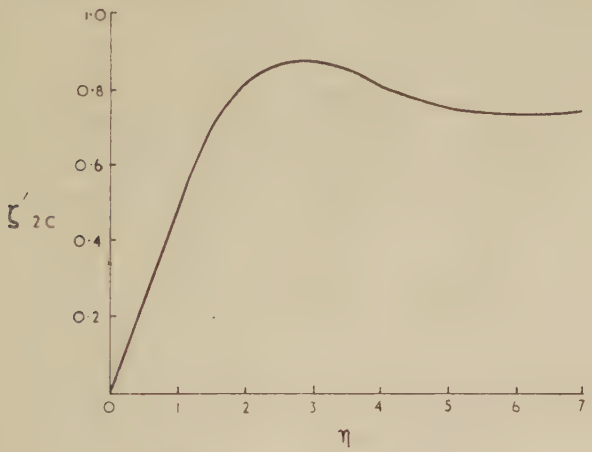

Figure 3. Graph of ζ_{2c}^{I}.

(i) *The Longitudinal Velocity Near the Bed.* The longitudinal velocity component to the second order is calculated from (18), (30) and (34) over a complete tidal cycle. This is shown in Fig. 4 at $x = -40$ and $x = -20$ and at distances up from the bed given by $\eta = 1/(2\sqrt{2})$ and $\eta = 1/\sqrt{2}$. Surface velocity, from (5), is given for comparison.

Experimental results obtained from Long Reach ($x = -20$) are shown in Fig. 5. There is reasonable agreement in the general shape, though detailed comparison is difficult because of the rather random behaviour of the experimental results, particularly at 1 ft from the bed, and because of lack of information about the value of ν. The agreement in amplitude is best if $\eta = 1/(2\sqrt{2})$ is made to correspond

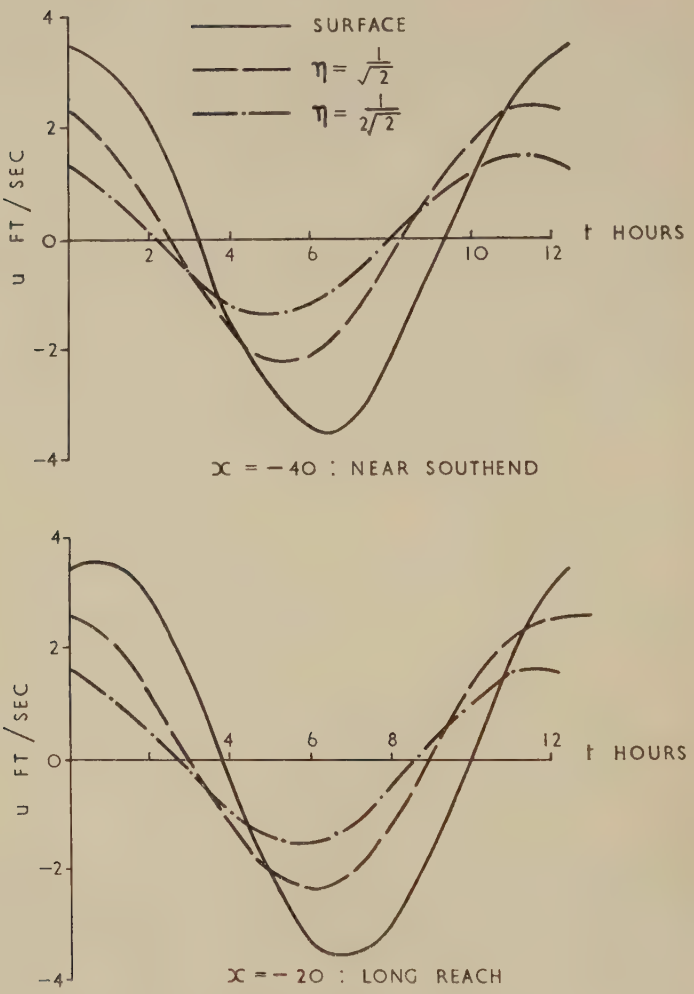

Figure 4. Longitudinal velocity at various depths.

to $y = 1$; this gives for the kinematic eddy viscosity a value o 5.7×10^{-4}ft²/sec, which compares with a purely molecular value o 1.2×10^{-5}ft²/sec at 15°C. Some support for the use of a constan eddy viscosity is obtained from another series of observations i the Thames at $x = -20$; this series included the velocity at 4 f

from the bed and it appears that $\eta = \sqrt{2}$ corresponds roughly to $y = 4$, giving the same value of ν as above.

The theoretical phase lead of the velocity near the bed, shown in Fig. 4, has some confirmation from experimental results. For instance, at $x = -20$ the theory gives the current 1 ft above the bed as 60 minutes in advance of the surface current; on the other hand, in Fig. 5, the current 1 ft up is slack, on the average, about 45 minutes before the surface current becomes slack.

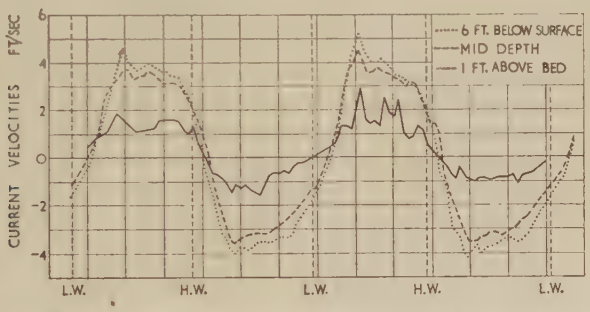

Figure 5. Measured longitudinal velocity throughout two tidal cycles in Long Reach. From Inglis and Allen (1957).

(ii) *Mean Velocity Near the Bed.* The mean velocity near the bed, calculated from (30), is shown in Fig. 6 at various x. The theory indicates a landward mean velocity up the bed of the estuary to a point between $x = 0$ and $x = 10$, where it reverses to seaward just above the bed. At 1 ft above the bed, between $x = -20$ and $x = -30$, the order of the theoretical mass transport velocity is 0.086 ft/sec, which represents a net excursion of 3,800 ft in a tidal period; this is smaller than the values given by Inglis and Allen (1957): about 8,000 ft at positions 1 ft above the bed. The theory gives 8,000 ft at 2 ft above the bed.

According to Inglis and Allen, the first reversal point of the mean velocity just above the bed, reckoning from the seaward end of the estuary, occurred in the Mud Reaches between $x = -11$ and $x = -15$; present calculations place the reversal point between $x = 0$ and $x = 10$. This difference is not due to failure of the theory; rather, it results from the extreme sensitivity to U_1 and U_2 of several of the formulae and from a lack of experimental points, in particular between $x = -5$ and $x = -10$, $x = -20$ and $x = -40$ (Fig. 1) and

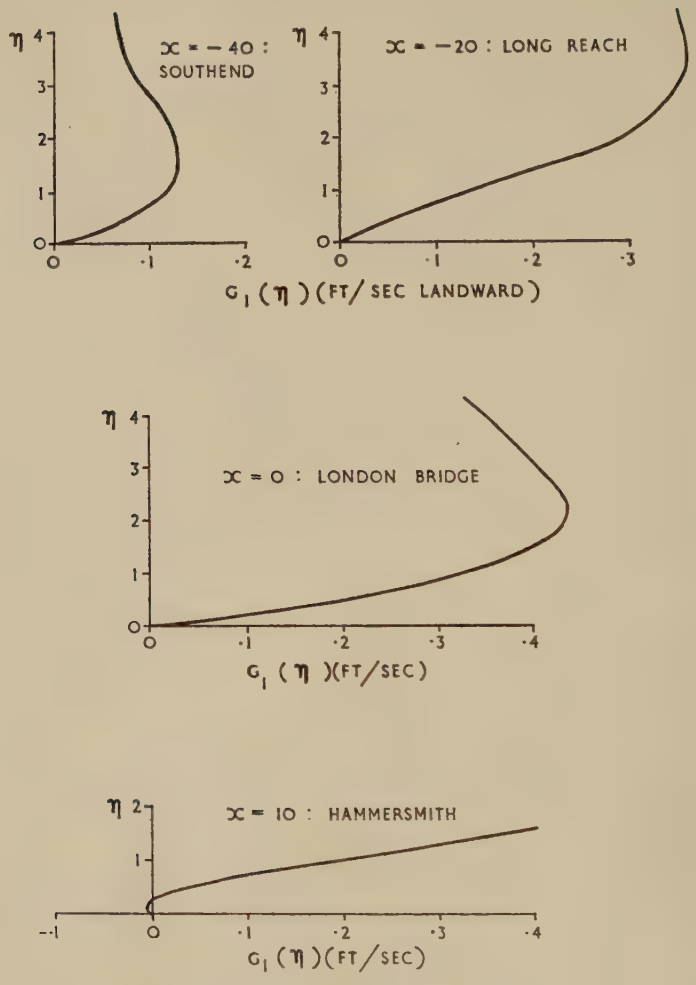

Figure 6. Mean velocity near the bed.

between $x = 5$ and $x = -10$ (Fig. 2), where smoothed curves had to be drawn to obtain the derivatives. It can be shown from (33) that if the dotted curves are taken in Figs. 1 and 2 between $x = -10$ and $x = -15$, the theoretical reversal point occurs in the vicinity of $x = -13$, which is in good agreement with the experimental evidence. The points between $x = -10$ and $x = -15$ fall on a smooth

curve; due to the scatter in the rest of the range, it would not be satisfactory to apply the theory by following more exactly the individual points.

(iii) *The Shear on the Bed and the Vertical Velocity Component Near the Bed.* The shear on the bed and the vertical component of velocity are given to the first order by (19) and (21) respectively. At $x = -20$, the shear leads the surface velocity by about $1^1/_2$ hours, and at 1 ft above the bed the vertical component of velocity has a corresponding lead of over $3^1/_2$ hours. The maximum shear, with ν as in (i), is 2.1×10^{-3} lb wt/ft^2 and the maximum vertical velocity, 1 ft up, is 3.4×10^{-6} ft/sec. This latter figure is so small compared to the settling velocity that it can have no direct effect on the suspension of solids in an estuary.

The value of maximum shear given above is too small by a factor of about 30 when compared with the value given by Chezy's formula, using the known value of Chezy's constant for the Thames. Also, it can be shown from (18) that the energy dissipation in one tidal cycle is too small according to the present theory by a factor of about 40. Therefore, ν, as given in (i), is too small either on a shear or on an energy basis by about 10^3, since both maximum shear [from (21)] and energy dissipation are proportional to $\nu^{1/2}$ in the present theory. Due to the flow being turbulent, such a discrepancy is to be expected, since the constant value of ν used above was estimated in (i) solely on velocity considerations; and it is unlikely that the particular constant value chosen reproduces the turbulent shear correctly.

VI. FURTHER REMARKS ON THE DIRECTION OF MEAN VELOCITY JUST ABOVE THE BED

The criterion $(U_1 - U_2)\, U_1^{\mathrm{I}} + (U_1 + U_2)\, U_2^{\mathrm{I}} \gtrless 0$, derived in § IV for landward or seaward mean velocity just above the bed, is applicable when the surface velocity is expressed as

$$U(x, t) = U_1(x) \cos \omega t + U_2(x) \sin \omega t.$$

If instead we use the more natural form

$$U(x, t) = U_0(x) \cos \{ \omega t - \psi(x) \}, \tag{35}$$

where $U_0(x)$ is the amplitude of the surface current and $\psi(x)$ th lag[1], the criterion becomes simply

$$U_0^{\mathrm{I}} + U_0 \psi^{\mathrm{I}} \gtrless 0$$

or

$$\frac{d}{dx}\left(U_0 e^{\psi}\right) \gtrless 0 \qquad (36$$

for landward or seaward mean velocity respectively. Reversal point of the mean velocity are given by $U_0^{\mathrm{I}} + U_0 \psi^{\mathrm{I}} = 0$. If we plot graph of $U_0 e^{\psi}$ against x (positive direction of x upstream), the mea

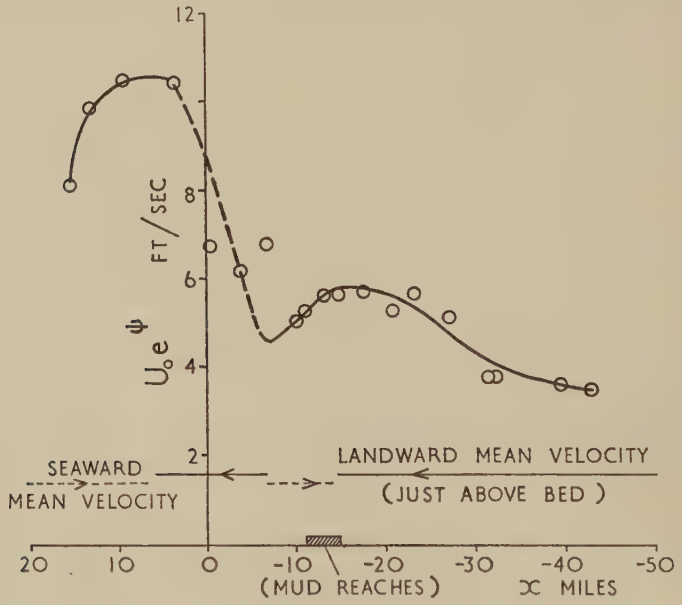

Figure 7. Graph of $U_0 e^{\psi}$ against x for the Thames.

velocity is landward or seaward, depending on whether the slope this graph is positive or negative and the reversal points correspon to the stationary points of $U_0 e^{\psi}$. This is shown for the Thames i Fig. 7; as noted in § V, there is a mean velocity into the Mud Reache

[1] In this notation: $G_1 \longrightarrow \frac{3U_0}{4\omega}\left(U_0 \psi^{\mathrm{I}} - U_0^{\mathrm{I}}\right)$ and $M \longrightarrow \frac{U_0}{4\omega}\left(5U_0 \psi^{\mathrm{I}} - 3U_0^{\mathrm{I}}\right)$ outside the boundary layer.

from both upstream and downstream which could account for the heavy silting in this region.

If the lag is linear with x up an estuary, so that ψ^{I} is constant, then it is seen that the reversal point will be landward of the location of maximum tidal current.

As a simple example, consider an estuary which is such that U_0 is constant and $\psi = \omega x/c$, where $c = \sqrt{gh}$ and h is a constant depth. In this case then the tide is a constant amplitude progressive wave travelling along the estuary with constant speed. Now, with $U_0^{\mathrm{I}} = 0$ and $\psi^{\mathrm{I}} > 0$ in (36), the mean velocity just above the bed is always landward in such an estuary. Of course, in practice the relations U_0 = constant and $\psi \propto x$ apply to part of an estuary only; eventually, as we go landward, the amplitude ceases to be constant and the mean velocity may then change direction at some point given by (36). But, it can be seen that, since the direction of mean velocity just above the bed has a large influence on the net direction of sediment movement, a portion of an estuary with a constant amplitude progressive tide is not in equilibrium since, according to the present theory, there is always this landward mean velocity which will eventually change the shape and characteristics of the estuary; and in doing so, it will change the pattern of the tides. The new direction of the mean velocity up the estuary could then be calculated from (36), once the new tidal behaviour is known.

Consider an estuary which has no mean velocity just above the bed throughout its length. If this is so, apart from transport by turbulent diffusion, there is little net movement of sediment; thus the estuary remains constant in shape and might be said to have attained a stationary state. From (36), the condition for this is

$$U_0^{\mathrm{I}} + U_0 \psi^{\mathrm{I}} = 0$$

or

$$U_0(x) = U_0(0) e^{-\psi}, \tag{37}$$

if $\psi = 0$ at $x = 0$. Since ψ is an increasing function of x, we have, on the assumptions of the present theory, that an estuary which is stationary has the amplitude of the tidal current *decreasing* in the landward direction in accord with (37). This differs from the usual idea that an estuary is in a stationary condition if the amplitude of the tidal current is constant along it. It is believed that the present condition is more realistic, since it is related more closely to the mechanism by which an estuary adjusts its shape.

My thanks are due Mr. G. H. Lean of the Hydraulics Researc Station, Wallingford, for first suggesting the application of Schlich ting's work to this problem. The work described in this paper wa carried out as part of the research programme of the Hydraulic Research Board of the Department of Scientific and Industria Research and is published with the permission of the Director o Hydraulics Research.

REFERENCES

Inglis, C. C. and F. H. Allen

1957. The regimen of the Thames Estuary as affected by currents, salinities an river flow. Min. Proc. Instn. civ. Engrs., *7*: 827–878.

Longuet-Higgins, M. S.

1953. Mass transport in water waves. Phil. Trans., (A) *245*: 535–581.

Russell, R. C. H. and J. D. C. Osorio

1957. An experimental investigation of drift profiles in a closed channel. Pro 6th. Conf. on Coastal Engng., Florida: 171–193.

Schlichting, Hermann

1932. Berechnung ebener periodischer Grenzschichtströmungen. Phys. Z., *3* 327–335.

SALINITY EFFECTS IN ESTUARIES

By

M. R. ABBOTT

Hydraulics Research Station,
Wallingford, Berkshire, England

ABSTRACT

This paper examines the relative importance, in the equation of motion, of the convective acceleration terms and of the extra pressure gradient due to a longitudinal gradient of salinity up an estuary. For estuaries in which the latter is the most important, a criterion is given for the direction of mean water velocity just above the bed.

I. INTRODUCTION

A previous investigation (Abbott, 1960) of an estuary examined the effect of the bed's boundary layer on the tidal velocity; the density gradient, due to varying salinity, was neglected. However, in spite of this and other simplifications which were made to keep the problem tractable, the theory gave results for the Thames that were in reasonable agreement with observation; these results included the effect of the boundary layer on amplitude and phase of the tidal current near the bed, the drift velocity (*i.e.*, the mean velocity at a fixed point) near the bed, and the direction of this drift along the estuary.

Neglect of the density gradient will not give realistic results in every case; in some estuaries this effect may be all important in determining the character of the flow. In § II this paper attempts to assess the effect on the flow of a given density gradient in a given estuary.

Theoretically the basic one-dimensional motion in an estuary is governed by a balance of the time acceleration term $\partial u/\partial t$, the instantaneous surface slope term, and the frictional resistance. To this level of approximation the motion is periodic; however, when convective acceleration terms are taken into account, then the motion is no longer strictly periodic, there being in general a drift velocity at all depths at each point along an estuary in a direction depending on the behaviour of the surface current.

In some estuaries the most important secondary effect may b the salinity gradient rather than the convective effect, and in thi case drifts are again likely to occur, since the salinity gradient i constant in sign and does not reverse with the tide; this introduce a preferred direction and a resultant drift at each depth. Even i an estuary in which the salinity gradient is relatively small, ther may still be movements of water due to it; this applies particularl to secondary flow in a lateral direction.

Knowledge of the magnitude and direction of the drift in a estuary is of practical importance because of the influence it ha on the movement of sediment. The problem of evaluating the drif theoretically is probably intractable when it is due to both densit and convective effects and when neither predominate. Howeve when density differences are more important, a criterion is obtained in § III, for the direction of drift just above the bed of an estuary In § IV this is applied to the Mersey, and it is shown that the drif just above the bed reverses to seawards in the vicinity of Eastham

II. DENSITY EFFECTS IN TIDAL ESTUARIES

First consider a general estuary where the x-axis is taken horizonta in the upstream direction, the y-axis vertically upwards, and th z-axis in a lateral direction. The longitudinal momentum equatio may be written

$$\varrho\left(\frac{\partial u}{\partial t}+u\frac{\partial u}{\partial x}+v\frac{\partial u}{\partial y}+w\frac{\partial u}{\partial z}\right)+\frac{\partial p}{\partial x}=\frac{\partial \tau_{xx}}{\partial x}+\frac{\partial \tau_{xy}}{\partial y}+\frac{\partial \tau_{xz}}{\partial z}\ , \qquad (1$$

where (u, v, w) is the water velocity referred to these axes, τ_{xy} et the components of stress (turbulent plus viscous), p the pressure and ϱ the water density. The bed is given by $y = B(x, z)$, the mea tide level up the estuary by $y = s(x)$. The water surface at an time is taken as $y = \eta(x, t)$, where $s = \overline{\eta}$, the mean value of η ove a tidal period at a fixed point.

The pressure term in (1) may be evaluated as follows, assumin that the pressure is hydrostatic:

$$p = g\int_y^\eta \varrho\, dy\ ; \qquad (2$$

therefore

$$\frac{\partial p}{\partial x}=g\varrho\frac{\partial \eta}{\partial x}+g\int_y^\eta \frac{\partial \varrho}{\partial x}\,dy, \qquad (3$$

$$= g\varrho \frac{\partial \eta}{\partial x} + g(\eta - y)\frac{\partial \varrho}{\partial x} \tag{4}$$

f it is assumed that $\partial\varrho/\partial x$ is independent of y. Pritchard (1954) as observed that this horizontal gradient does not change appreciably with depth in the James River. In general $\partial\varrho/\partial x$ is negative. The first term of (4) is the usual surface slope term; the second term, which is zero on the surface, is the pressure gradient due to the density gradient in an estuary which is related to the known salinity gradient; in fact, neglecting differences of temperature, we may take $\partial\varrho/\partial x$ as proportional to the salinity gradient. The right-hand side of (1) is approximately $\partial\tau_{xy}/\partial y$, since the other two terms are in general small, and they are hereafter neglected. Hence, from (1) and (4) we have

$$\varrho\left(\frac{\partial u}{\partial t} + u\frac{\partial u}{\partial x} + v\frac{\partial u}{\partial y} + w\frac{\partial u}{\partial z}\right) + g\varrho\frac{\partial \eta}{\partial x} + g(\eta - y)\frac{\partial \varrho}{\partial x} = \frac{\partial \tau_{xy}}{\partial y}\ . \tag{5}$$

Consider the various terms of (5). For the Thames their rough maximum orders of magnitude are given in lb-ft-sec units by:

$$\varrho\frac{\partial u}{\partial t} \sim \varrho\,\omega U_0 \ :\ 4\times 10^{-2},$$

$$\varrho u\frac{\partial u}{\partial x} \sim \frac{\varrho\,\omega U_0^2}{2c} \doteq 3\times 10^{-3},$$

$$\varrho v\frac{\partial u}{\partial y} \sim \frac{\varrho\omega U_0 H}{h} \doteq 10^{-2},$$

$$\varrho w\frac{\partial u}{\partial z} \text{ is neglected,}$$

$$g\varrho\frac{\partial \eta}{\partial x} \sim \frac{g\varrho\,\omega\, H}{c} \doteq 8\times 10^{-2},$$

$$g(\eta - y)\frac{\partial \varrho}{\partial x} \sim c^2\left|\frac{\partial \varrho}{\partial x}\right| \doteq 5\times 10^{-3},$$

$$\frac{\partial \tau_{xy}}{\partial y} \sim \frac{\tau_{bed}}{h} \sim \frac{g\varrho U_0^2}{h\bar{C}^2} \doteq 9\times 10^{-2}.$$

Here U_0 is the current amplitude, H the tidal amplitude, $2\pi/\omega$ the tidal period, $c = \sqrt{g\bar{h}}$, h the mean depth, and C Chezy's constant. In

deriving the above it is assumed that the tide can be represented b a progressive wave

$$u = U_0 \cos\left\{\omega\left(t - \frac{x}{c}\right)\right\}, \quad \eta = H \sin\left\{\omega\left(t - \frac{x}{c}\right)\right\}; \qquad (1$$

this is not strictly accurate but will suffice for the present purpos In estimating $\varrho v \partial u/\partial y$ it is assumed that v varies linearly fro zero at the bed to $\partial\eta/\partial t$ at the surface and that $\partial u/\partial y$ is roughl u/y in the boundary layer region where $\varrho v \partial u/\partial y$ has its maximu value. The values for the Thames which are used are: $U_0 = 4$ ft/se $H = 8$ ft, $h = 26$ ft, $C = 120$ ft$^{\frac{1}{2}}$/sec, $\partial\varrho/\partial x = -6 \times 10^{-6}$ lb/ft^4.

The dominant terms are therefore the time acceleration term, th surface slope term and the shear term—the three terms which a retained in the usual approximate theory of motion in an estuar Next in order of magnitude are the sum of the convective accelera tion terms (irrespective of any phase difference between them) an the density gradient term, which is the smallest of those considere

Thus, for tidal motion in the Thames, a second approximatio which takes account of the convective acceleration but whic neglects variations of salinity is valid in general, though the reserva tions given in § I apply with regard to lateral effects and secondar flow.

A rough measure of the relative importance of density (salinit effects in a general estuary may be obtained from the dimensionle number

$$D = \frac{c^3 \left|\frac{\partial \varrho}{\partial x}\right|}{\omega U_0^2 \varrho}.$$

D is proportional to the ratio of the density gradient term to th sum of the convective acceleration terms in the longitudinal equatio of motion. In summing the convective terms it is assumed tha $\frac{U_0}{c} \propto \frac{H}{h}$; for a progressive wave in a frictionless uniform chann there is the exact relation $\frac{U_0}{c} = \frac{H}{h}$.

Small values of D indicate that the most important second ord effects are the nonlinear convective terms in the equation of motio these giving rise to sizable drift currents in an estuary as shown b Abbott (1960). On the other hand, large values of D indicate tha

ny drifts are due primarily to salinity differences. Examples are: Thames, $D = 0.8$; Mersey, $D = 7$; James, $D = 12$. Thus in the latter wo estuaries, salinity effects predominate; this is confirmed numerically by Pritchard (1956), who has shown from observations in the James River (a tributary estuary of Chesapeake Bay) that the convective terms of mean motion are insignificant compared to the erms dependent on density gradient, surface slope and shear force.

In calculating values of D above, the steepest salinity gradient n an estuary is used; though the values given are only rough, they give an indication of the relative importance of salinity effects in he three estuaries.

III. MEAN MOTION

In this section we examine the drifts in an estuary which result vhen the motion is meaned over a tidal cycle. The components of vater velocity in an estuary may be written

$$u = \bar{u} + U_0 \cos(\omega t - \varepsilon) + u', \quad v = \bar{v} + v', \quad w = w', \tag{7}$$

s in Pritchard (1956), where $(\bar{u}, \bar{v}, o)$ is the steady drift velocity at point, $U_0 \cos(\omega t - \varepsilon)$ the tidal motion, and (u', v', w') the turbuent fluctuations. Both U_0 and ε are functions of x and y.

Following Pritchard, eqs. (7) are inserted into (1) and the mean s taken over a tidal cycle. First we observe from (4) that

$$\overline{\frac{\partial p}{\partial x}} = g\varrho \frac{dS}{dx} + g(S-y)\frac{\partial \varrho}{\partial x}, \tag{8}$$

vhere $S(x)$ is the mean tide level of the water surface in an estuary. t is assumed in deriving (8) that ϱ and $\partial\varrho/\partial x$ vary little over a tidal ycle compared to the variation of $\partial\eta/\partial x$ and η. This is reasonable ince a relatively large change in salinity produces only a small hange in density. In (8), $\partial\varrho/\partial x$ can be taken, for example, as a nean of values occurring at high slack water and low slack water; or convenience a bar is omitted.

From (7), (1) and (8) we obtain

$$\bar{u}\frac{\partial \bar{u}}{\partial x} + \bar{v}\frac{\partial \bar{u}}{\partial y} + U_0 \frac{\partial U_0}{\partial x} + g\frac{dS}{dx} + \frac{g(S-y)}{\varrho}\frac{\partial \varrho}{\partial x} = \frac{1}{\varrho}\frac{\partial \bar{\tau}_{xy}}{\partial y}. \tag{9}$$

When taking the mean of (1) it is assumed that the time scale of the urbulent fluctuations in (7) is much smaller than the time scale of

the tidal motion. An equivalent equation to (9) occurs in Pritcha
(1956).

A criterion for the direction of drift just above the bed will
derived for estuaries which have a high value of D. In this ca
the convective terms of mean motion can be neglected in (9)
comparison with the density gradient term; this has been confirm
by comprehensive observations in the James River (Pritchard, 195
Pritchard and Kent (1956) calculated from theory and observati
the drift profile over the whole depth of a section; however, f
practical considerations of sediment movement we are chiefly inte
ested in the direction of drift just above the bed, and a simple a
easily applied theoretical criterion can be obtained for this.

The term $U_0 \partial U_0/\partial x$ in (9) will, as a first approximation,
neglected, since in many cases the amplitude of the tidal current
nearly constant along an estuary. However, the result will later
quoted when this term is retained but assumed independent of

With these assumptions (9) becomes

$$\frac{1}{\varrho}\frac{\partial \overline{\tau}_{xy}}{\partial y} = g\frac{dS}{dx} + g\frac{(S-y)}{\varrho}\frac{\partial \varrho}{\partial x}; \qquad (1$$

integrating this with respect to y gives

$$\overline{\tau}_{xy} = g\varrho y\frac{dS}{dx} + g(Sy - \tfrac{1}{2}y^2)\frac{\partial \varrho}{\partial x} + f(x), \qquad (1$$

since the variation of ϱ with y is small. On the surface $\overline{\tau}_{xy} =$
hence

$$f(x) = -g\varrho S\frac{dS}{dx} - \tfrac{1}{2}gS^2\frac{\partial \varrho}{\partial x}. \qquad (1$$

From (11) and (12) we have

$$\overline{\tau}_{xy} = -g\varrho(S-y)\frac{dS}{dx} - \tfrac{1}{2}g(S-y)^2\frac{\partial \varrho}{\partial x}; \qquad (1$$

on the bed, therefore,

$$\overline{\tau}_{xy} = gh\left\{\tfrac{1}{2}h\left(-\frac{\partial \varrho}{\partial x}\right) - \varrho\frac{dS}{dx}\right\}, \qquad (1$$

where $h(x, z) = S(x) - B(x, z)$ is the local depth at mean tide lev

In general the flow in an estuary is "rough turbulent", so that the shear on the bed is given by

$$\tau_{xy} = k\varrho u|u|, \tag{15}$$

where k is a positive quantity. We now show that the sign of the mean shear is the same as that of the drift so that we can deduce the direction of the latter from (14).

Neglecting turbulent fluctuations, we can write the velocity just above the bed as

$$u = \overline{u} + U_0 \cos\varphi, \tag{16}$$

where $\overline{u} < U_0$ and φ varies from 0 to 2π over a tidal cycle. Let the first zero of u occur at $\varphi = \alpha\ (0<\alpha<\pi)$; then

$$\overline{u} + U_0 \cos\alpha = 0$$

and

$$\begin{aligned}\tau_{xy} &= k\varrho u^2 \text{ in } 0<\varphi<\alpha \text{ and } 2\pi-\alpha<\varphi<2\pi,\\ &= -k\varrho u^2 \text{ in } \alpha<\varphi<2\pi-\alpha.\end{aligned}$$

Taking the mean of (15) over a tidal cycle gives

$$\begin{aligned}\overline{\tau}_{xy} &= \frac{k\varrho}{2\pi}\left\{\int_0^{\alpha} u^2 d\varphi - \int_{\alpha}^{2\pi-\alpha} u^2 d\varphi + \int_{2\pi-\alpha}^{2\pi} u^2 d\varphi\right\}\\ &= \frac{k\varrho}{\pi}\left\{\int_0^{\alpha} u^2 d\varphi - \int_{\alpha}^{\pi} u^2 d\varphi\right\}.\end{aligned}$$

This reduces to

$$\begin{aligned}\overline{\tau}_{xy} = \frac{k\varrho}{\pi}\Big\{&2\overline{u}^2\alpha + 4\overline{u}U_0 \sin\alpha + U_0^2 \sin\alpha\cos\alpha\\ &+ U_0^2\alpha - \pi\overline{u}^2 - \tfrac{1}{2}\pi U_0^2\Big\},\end{aligned} \tag{17}$$

after substituting (16) and evaluating the integrals. Now,

$$\cos\alpha = -\frac{\overline{u}}{U_0}, \quad \sin\alpha = \frac{\sqrt{U_0^2-\overline{u}^2}}{U_0} \quad \text{as} \quad 0<\alpha<\pi;$$

therefore, from (17)

$$\overline{\tau}_{xy} = \frac{k\varrho}{\pi}\left\{3\overline{u}\sqrt{U_0^2-\overline{u}^2} + \left(U_0^2 + 2\overline{u}^2\right)\left(\cos^{-1}\left(-\frac{\overline{u}}{U_0}\right) - \frac{\pi}{2}\right)\right\}. \tag{18}$$

It is easily seen that

$$\cos^{-1}\left(-\frac{\overline{u}}{U_0}\right) - \frac{\pi}{2} = \overline{u}P, \qquad (1$$

where P is always positive. From (18) and (19), therefore, we obta

$$\overline{\tau}_{xy} = A\overline{u}, \qquad (2$$

where A is always positive. Thus the drift and the mean shear ha
the same sign.

Therefore, from (14), the drift just above the bed will be lan
wards or seawards according as

$$\tfrac{1}{2}h\left(-\frac{\partial \varrho}{\partial x}\right) \gtrless \varrho\frac{dS}{dx}. \qquad (2$$

This expresses the balance between density gradient and slope of t
mean tide level. It can be seen from (21) that, if the density gradie
is independent of lateral position in an estuary, any landward dri
will reverse near the sides of the estuary first, where $h(x, z)$ will
smaller than the value in the centre of the estuary. However, (2
does not apply right up to the banks, since stresses other than
will be important there.

Eq. (21) also applies when flow near the bed is "smooth turb
lent"; there is now a viscous layer, and at the bed we have

$$\overline{\tau}_{xy} = \mu\frac{\partial \overline{u}}{\partial y}, \qquad (2$$

where μ is positive, and on the bed $\overline{u} = 0$. Therefore the sign of
just above the bed is the same as that of $\partial\overline{u}/\partial y$ at the bed, whi
by (22) has the same sign as $\overline{\tau}_{xy}$. Again we have shown that the dri
and the mean shear have the same sign.

If account is taken of the $U_0\partial U_0/\partial x$ term occurring in (9),
obtain in place of (21)

$$\tfrac{1}{2}h\left(-\frac{\partial \varrho}{\partial x}\right) \gtrless \varrho\left(\frac{dS}{dx} + \frac{U_0}{g}\frac{\partial U_0}{\partial x}\right) \qquad (2$$

for landward or seaward drift respectively. It is assumed in derivi
(23) that U_0 is independent of y.

In the case of the Thames it can be shown from (21) that the density gradient alone (as determined from the measured values of salinity), without the convective effect, cannot sustain a landward drift near the bed. Table I gives results of these calculations.

TABLE I

x	$\frac{1}{2}h\left(-\frac{\partial \varrho}{\partial x}\right)$	$\varrho \frac{dS}{dx}$
Miles from London Bridge	lb/ft^3 × 10^4	lb/ft^3 × 10^4
− 40	0.3	1.3
− 35	0.6	1.3
− 30	0.9	1.3
− 25	1.4	3.0
− 20	1.2	3.0
− 15	1.0	3.0
− 10	1.2	3.0
− 5	0.8	3.0

The values of h, $\partial \varrho/\partial x$ and dS/dx are from Inglis and Allen (1957). Thus, throughout the range of x considered, $\frac{1}{2}h(-\partial \varrho/\partial x) < \varrho(dS/dx)$, indicating a *seaward* drift near the bed; but both observation and theory (Abbott, 1960) indicate a *landward* drift up to $x = -15$.

IV. APPLICATION TO THE MERSEY ESTUARY

It has been shown in § II that the effects of salinity differences are important in the Mersey Estuary. The direction of drift just above the bed will now be investigated from (21). The derivation of this criterion assumed that the convective acceleration terms may be neglected in comparison with the contribution of the longitudinal salinity gradient to the equation of motion and that the term $U_0 \partial U_0/\partial x$ is negligible. With these assumptions we can proceed as follows.

The longitudinal salinity up this estuary has been obtained from a survey carried out at both low and high water on 14 December 1957; the mean of the low water and high water salinity gradient was then taken. The mean tide level used corresponds to the tide on the above day. Finally the channel depth has been taken from a recent survey of this estuary. Results of these calculations are given in Table II.

TABLE II

Place	*Distance from Gladstone Dock* (*miles*)	$\frac{1}{2}h\left(-\frac{\partial\varrho}{\partial x}\right)$ (lb/ft³ × 10⁵)	$\varrho\frac{dS}{dx}$ (lb/ft³ × 10⁵)
Gladstone Dock	0	7.6	0
Prince's Pier	3	8.8	0
Eastham	9	71	77
Hale Head	16	4.4	920

The slope of the mean tide level at Hale Head is only approxima since the tide gauge dries out before low water is reached. Howev the main conclusion which can be drawn is independent of t approximation.

Table II shows that, according to the present theory, the dr just above the bed reverses from landward to seaward in the vicini of Eastham. The tidal curves up to this point are still fairly sinu oidal in form. Though the ebb is rather longer than the flood, the is still symmetry about the mean tide level. Also, the variation $\partial\varrho/\partial x$ over a tidal cycle is not yet excessive, as it is beyond c 11 12 miles from Gladstone Dock. For these reasons the use of criteri (21) is probably justified in the case of the Mersey. The theory extremely sensitive to the mean tide level, and when (21) is appli the tidal information used should correspond to the tide occurri during the salinity sampling.

A model of the Mersey Estuary is in operation at the Hydrauli Research Station, Wallingford, and, when salinity is correct represented, the position of zero drift just above the bed occu slightly seaward of Eastham, which is in satisfactory agreement wi the theoretical prediction. Further, across the section from Camm Laird to Brunswick Dock, the model indicates a mean landwa drift velocity just above the bed of about 0.4 ft/sec in the prototyp A rough theoretical value for comparison can be obtained as follow From (14) and (18) we have approximately

$$\frac{k\varrho}{\pi}\left\{3U_0\bar{u}+U_0^2\left(\cos^{-1}\left(-\frac{\bar{u}}{U_0}\right)-\frac{\pi}{2}\right)\right\}=gh\left\{\tfrac{1}{2}h\left(-\frac{\partial\varrho}{\partial x}\right)-\varrho\frac{dS}{dx}\right\},\quad(2$$

since $\bar{u} \langle\langle U_0$ in general. Also, k can be replaced by g/C^2, where C Chezy's constant and

$$\cos^{-1}\left(-\frac{\overline{u}}{U_0}\right) = \frac{\pi}{2} + \frac{\overline{u}}{U_0} + 0\left(\frac{\overline{u}}{U_0}\right)^3 ; \tag{25}$$

ience, from (24), the drift is given by

$$\overline{u} = \frac{\pi C^2 h}{4 U_0 \varrho}\left\{\frac{1}{2} h\left(-\frac{\partial \varrho}{\partial x}\right) - \varrho \frac{dS}{dx}\right\} . \tag{26}$$

When approximate values of the various quantities are inserted, (26) gives $\overline{u} = 0.3$ ft/sec, in reasonable agreement with the model results.

The work described in this paper was carried out as part of the research programme of the Hydraulics Research Board of the Department of Scientific and Industrial Research and is published with the permission of the Director of Hydraulics Research.

REFERENCES

ABBOTT, M. R.
1960. Boundary layer effects in estuaries. J. Mar. Res., *18*: 83–100.

INGLIS, C. C. AND F. H. ALLEN
1957. The regimen of the Thames Estuary as affected by currents, salinities and river flow. Min. Proc. Instn. civ. Engrs., *7*: 827–878.

PRITCHARD, D. W.
1954. A study of the salt balance in a coastal plain estuary. J. Mar. Res., *13* (1): 133–144.
1956. The dynamic structure of a coastal plain estuary. J. Mar. Res., *15* (1): 33–42.

PRITCHARD, D. W. AND R. E. KENT
1956. A method for determining mean longitudinal velocities in a coastal plain estuary. J. Mar. Res., *15* (1): 81–91.

ON THE USE OF TIME SERIES CONCEPTS AND SPECTRAL AND CROSS-SPECTRAL ANALYSES IN THE STUDY OF LONG-RANGE FORECASTING PROBLEMS

By

WILLARD J. PIERSON, JR.

New York University

ABSTRACT

Monthly values of sea surface temperature anomalies and wind anomalies for area of the North Atlantic Ocean are studied as a vector Gaussian process. covariances and the spectra and cross-spectra provide information on the nature the interaction of ocean and atmosphere. The long period fluctuations are found be fairly coherent. Indications are that the sea surface temperature can be predic for one month into the future on the basis of past values with a 50 % reduction variance. Prediction problems are discussed.

1. *Introduction.* The concepts of stationary time series metho of power spectral analysis of time series, and of techniques for p diction of time series are playing an increasingly important role numerous fields. One field of interest to the writer is that of wav and ship motions (Pierson, 1955, 1957; Putz, 1955).

In meteorological studies, spectra have been studied in connecti with numerous problems (see, for example, Cramer and Reco 1955; Griffith, *et al.*, 1956), and regression methods have been us in attempting to derive prediction schemes (see Lorenz, 195 Malone, 1956; Miller, 1956; and Wadsworth, 1951). It is the purpo of this paper to suggest briefly, by means of studying an interesti stationary Gaussian vector process, a way in which spectral a cross-spectral analyses and regression schemes might be combin to develop prediction procedures and to obtain some fairly accura long-range prediction methods. The study of spectra and cro spectra provides information on how the prediction works and how to improve the planning of further investigations.

The theory used in this paper is that of stationary random vect processes, already well described in the literature. Useful references a Bartlett (1949), Lévy (1948), Grenander and Rosenblatt (1957), Pre and Tukey (1956), Blackman and Tukey (1958), and Goodman (195

Time series methods require lengthy sample records for analysis. Thus the obvious instability of attempts to extrapolate four or eight rear apparent cycles far into the future on the basis of only about 60 years of data is emphasized by such methods.

2. *The Problem for Analysis.* The system considered here consists of three series of data, two of which consist of the mean monthly ea surface temperature anomalies for individual months from 1880 o 1940 for area E and area N of the North Atlantic as published by Smed (1946, 1949). The location of these fields is given in Fig. 1. The third series is the mean monthly pressure gradient anomaly in he form of a Δp measured over a fixed horizontal distance over areas E and N at sea level as defined by Neumann and Pandolfo n Neumann, *et al.* (1958). The average pressure gradient for the month was computed from the gradient of the average pressure for hat month. The wind anomaly near the surface over these two ocean areas is of course directly proportional to the pressure gradient anomaly.

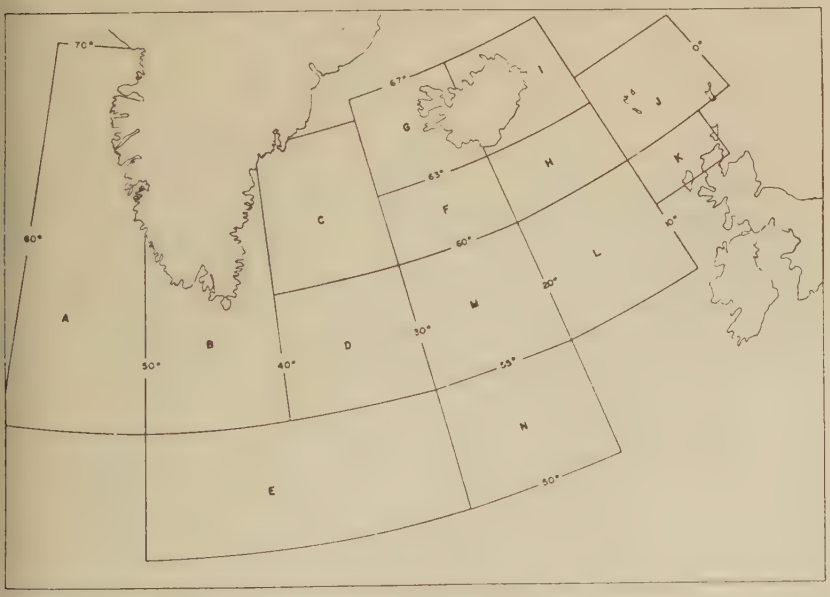

Figure 1. Location of fields for which temperature data are given by Smed.

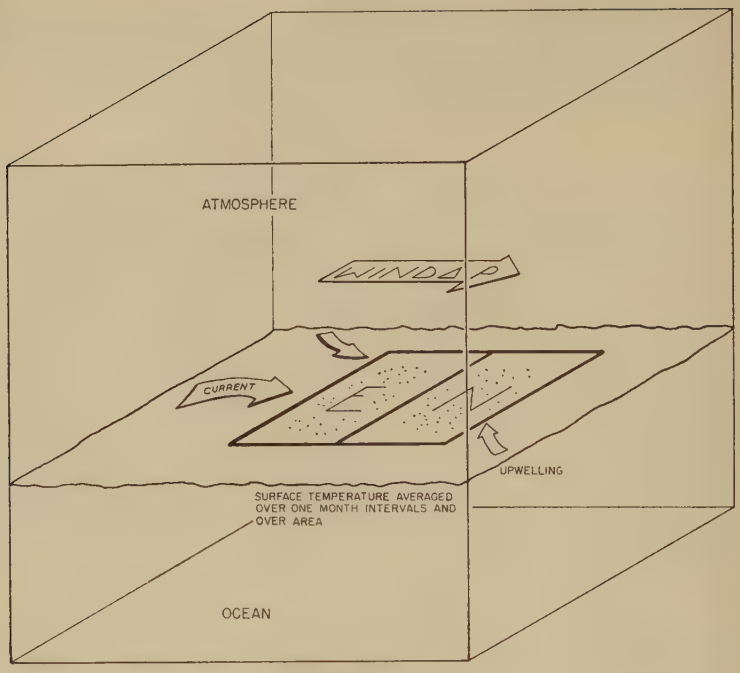

Figure 2. Model.

The anomalies refer to departures from the mean for the particula month given, and thus both the mean value over the whole perio and the annual cycle have been removed. Somewhere between 40 and 500 values were available—one for each month from abou 1880 to 1940 for each of the three series. There were portions o each series missing, and this fact complicated the analysis.

A schematic model of the inter-related time series to be studied shown in Fig. 2.

3. *Definitions.* Let the mean monthly temperature anomalies fo area E be given by $X_0, X_1, X_2, \ldots, X_N$, those for area N b $Y_0, Y_1, Y_2, \ldots, Y_M$; let the anomalies for the pressure gradient b given by $Z_0, Z_1, Z_2, \ldots, Z_S$ where, in the cases studied, sho portions of the individual series did not overlap and some of th data were missing. The formulas to be discussed were modified t take missing data into account.

A mathematical model for the vector time series defined by X_n, Y_n, Z_n) can be formulated on the assumption, which appears be justifiable from various tests of the data, that the data are mples from a stationary vector Gaussian process.

$$\left.\begin{aligned} X_n &= \sum_{j=0}^{\infty} a_j \cos(\mu_j n \Delta t) + b_j \sin(\mu_j n \Delta t) \\ Y_n &= \sum_{j=0}^{\infty} c_j \cos(\mu_j n \Delta t) + d_j \sin(\mu_j n \Delta t) \\ Z_n &= \sum_{j=0}^{\infty} e_j \cos(\mu_j n \Delta t) + f_j \sin(\mu_j n \Delta t). \end{aligned}\right\} \tag{1}$$

n (1), $\Delta t = 1$ month and μ_j has the units of radians/month.

Eqs. (1) are to be considered as a very large sum of terms (in the mit infinite) with very small individual amplitudes (in the limit finitesimal). The numbers, a_j, b_j, c_j, d_j, e_j, and f_j, are considered be numbers to be drawn at random from a multivariate normal istribution with zero means and with variances and covariances hat are a function of μ_j and that as yet have not been determined. he notation has been chosen to show that X_n, Y_n and Z_n are known nly at discrete points and to show how the quantities, a_j, b_j, etc. ropagate through the computations.

4. *Lag Relationships.* Consider the expected value given by

$$R_x(p) = E(X_n, X_{n+p}) = E\left[\sum_{j=0}^{\infty} \tfrac{1}{2}(a_j^2 + b_j^2) \cos(\mu_j p \Delta t)\right], \tag{2}$$

here $E(X_n, X_{n+p}) = R_x(p)$ would be estimated from the data by

$$R_x(p) = \frac{1}{N-p} \sum_{n=0}^{N-p} (X_n)(X_{n+p}). \tag{3}$$

he covariances, $R_y(p)$ and $R_z(p)$, would be found in a similar way. The relationship between X_n and Y_n would be found from

$$R_{xy}(p) = E(X_p, Y_{n+p}) = E\left[\tfrac{1}{2}\sum_{j=0}^{\infty} (a_j c_j + b_j d_j) \cos(\mu_j p \Delta t) + \tfrac{1}{2}\sum_{j=0}^{\infty} (-b_j c_j + a_j d_j) \sin(\mu_j p \Delta t)\right]. \tag{4}$$

imilar results for $R_{xz}(p)$ and $R_{yz}(p)$ would come from interchanging ppropriate symbols.

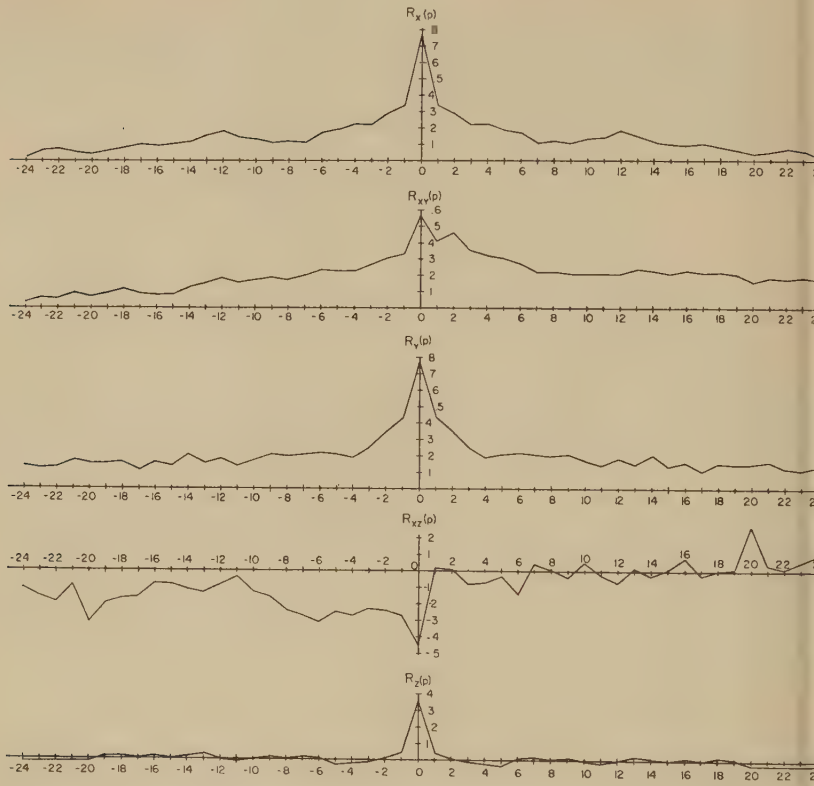

Figure 3. Graphs of $R_x(p)$, $R_y(p)$, $R_z(p)$, $R_{xy}(p)$ and $R_{xz}(p)$.

The curves for $R_x(p)$, $R_y(p)$, $R_z(p)$, $R_{xy}(p)$, and $R_{xz}(p)$ are graph in Fig. 3 where one should note, for example, that $R_x(p) = R_x(-$ and that $R_{xy}(p) \neq R_{yx}(p)$. $R_x(p)$ and $R_y(p)$ and $R_{xy}(p)$ have t dimensions of $(°C)^2$, $R_x(p)$ those of $(mb)^2$, and $R_{xz}(p)$ those of °C-m The values for these lag relationships are given in Table I.

5. *Discussion of Lag Relationships.* The graphs in Fig. 3 yie interesting information about the system under study as they star Some general statements about the predictability of a given co ponent of the vector process from just its own past or from the pa of some other component can be made.

For example, about 25 % of the variance of X_n can be predict one month into the future on the basis of only its current valu

TABLE I. VALUES OF $R_x(p)$, $R_y(p)$, $R_z(p)$, $R_{xy}(p)$ AND $R_{xz}(p)$.

R_x	$R_{xy}(+p)$	$R_{xy}(-p)$	R_y	$R_{xz}(+p)$	$R_{xz}(-p)$	R_z
0.775	0.552	0.552	0.778	–0.450	–0.450	0.369
.336	.412	.332	.434	.016	– .270	.044
.290	.460	.308	.348	.010	– .238	.011
.221	.356	.268	.249	– .082	– .230	– .012
.225	.322	.226	.193	– .072	– .274	– .020
.188	.310	.230	.210	– .030	– .248	– .026
.169	.276	.236	.219	– .140	– .308	.011
.106	.222	.202	.211	.044	– .274	.014
.121	.224	.178	.197	.010	– .238	.005
.109	.213	.191	.211	– .042	– .156	.012
.134	.210	.174	.171	.048	– .130	– .003
.142	.208	.158	.138	– .026	– .038	– .014
.179	.208	.186	.185	– .070	– .088	.004
.148	.240	.152	.153	.014	– .136	.028
.114	.227	.129	.205	– .026	– .116	.008
.097	.206	.086	.138	.008	– .084	– .001
.091	.227	.083	.158	.076	– .078	.014
.098	.217	.093	.108	– .028	– .160	.000
.077	.222	.114	.158	– .002	– .168	.014
.062	.212	.088	.148	.010	– .200	.012
.037	.166	.070	.152	.266	– .318	– .021
.050	.187	.093	.173	.040	– .092	– .020
.068	.178	.062	.131	.020	– .196	– .021
.058	.188	.066	.122	.060	– .160	– .022
.019	.181	.035	.124	.098	– .112	– .018

nly 4 % of the variance could perhaps be predicted 12 months to the future on the basis of only its current value. The graphs of oth $R_x(p)$ and $R_y(p)$ show that X_n and Y_n depend to some extent n what has happened as much as two years ago and that the prediction of, say, the next monthly temperature anomaly value might se past observations extending back as much as two years.

In contrast, a value of Z_n is virtually independent of all past or ture values. Perhaps 1 % of the variance of Z_n could be predicted ne month into the future on the basis of its present value. Lack of rrelation of the pressure anomaly with its past is probably explained by the fact that frequencies of the pressure gradient variability are associated with the passage of cyclones and anticyclones nd hence are associated with much shorter periods—of the order

of three to ten days. The averaging process essentially filters out considerable part of these high frequencies.

The curve for $R_{xy}(p)$ is also interesting. The dependance of t temperature anomaly at area N, Y_n on the anomaly at area E, one or two months ago is greater than the dependence of the temp ature anomaly at E on the anomaly at N one or two months ag Stated another way, prediction of Y_n one or two months into t future on the basis of the present value of X_n would be about twi as good as a prediction of X_n one or two months into the future the basis of the present value of Y_n. Thus the ocean currents flowi from E to N appear to transport part of the anomaly at E to N wi a time delay. The effect is evident even out to a two year lag, sin the right side of the curve is consistently higher than the left sic

The curve for $R_{xz}(p)$ is perhaps the most striking of all. Althou Z_n is unpredictable from its own past, the future values of X_n a predictable from present and past values of Z_n. Positive values Z_n tend to be followed by negative values of X_n; negative values Z_n, by positive values of X_n. (Or, as actually depicted by the grap negative values of X_n tend to be preceded by positive values of Z positive values of X_n, by negative values of Z_n.) Perhaps 9 % of t variance of X_n would be predictable six months into the future the present value of Z_n. The process is not reversible. Knowledge past and present values of X_n provides no help in predicting Z

The persistent covariances out to two years in all but the win are subject to sampling variability, as are estimates of any par meters. Unfortunately sampling variability in covariance estimat from time series is not well understood (Blackman and Tukey, 195 preface), and precise statements about the reliability of the estimates cannot be made on the basis of information given so f From physical properties of the atmosphere and oceans, results a not contradictory to what one might expect.

The curve for $R_{yz}(p)$ would also be needed to complete an analy of the problem, but it has not been computed.

6. *Spectra, Cross-spectra and Coherencies.* The lag relationshi graphed above can be used to compute the spectra and cross-spect of the vector Gaussian process under study by using the formul from Tukey (1949) for spectra and from Goodman (1957) for cro spectra. This provides important information on the frequenc involved and on the reality of results obtained. The curves defin

$R_x(p)$, $R_y(p)$, . . . , $R_{xz}(p)$ are made periodic by repetition beyond $= +24$. The 24 coefficients of the Fourier series that define exactly e even functions and the 48 coefficients that define the even and d parts of the other functions are then found. If $L_x(h)$, $h = 0$, . . . , 24 are these numbers for the series X_n, then finally they e smoothed by computing $U_x(h) = 0.23\,L_x(h-1) + 0.54\,L_x(h) + 23\,L_x(h+1)$ to obtain an estimate of the spectrum of X_n.

For the spectra, $U_x(h)$ $(h = 0, 1, \ldots, 24)$, is an estimate of that rt of the total variance of X_n contributed by those components (1) that have frequencies between approximately $2\pi(h-\frac{1}{2})/48$ nd $2\pi(h+\frac{1}{2})/48$ radians/month (in the absence of aliasing). Or stated nother way, $U_x(h)$ estimates approximately

$$\sum_{j=j_a}^{j=j_b} E(a^2+b^2), \tag{5}$$

here

$$\mu_{j_a} = 2\pi(h-\tfrac{1}{2})/48$$

$$\mu_{j_b} = 2\pi(h+\tfrac{1}{2})/48.^1$$

The cospectrum, say $C_{xy}(h)$, is the smoothed form of the cosine rms in the Fourier series representation of $R_{xy}(p)$. The cospectrum alues are thus approximately an estimate of

$$\sum_{j=j_a}^{j=j_b} E(a_j c_j + b_j d_j), \tag{6}$$

here, since a_j and c_j and b_j and d_j may be uncorrelated, the sum ould be zero and where j_a and j_b have the same significance as bove.

The quadrature spectrum, say $Q_{xz}(j)$, is an estimate of

$$\sum_{j=j_a}^{j=j_b} E(-b_j e_j + a_j f_j) \tag{7}$$

nder the same conditions.

[1] More precisely, the a_j^2 and b_j^2 are weighted by a triangularly shaped filter xtending from about $2\pi(h-2)/48$ to $2\pi(h+2)/48$ instead of by a square filter etween $2\pi(h-\frac{1}{2})/48$ and $2\pi(h+\frac{1}{2})/48$.

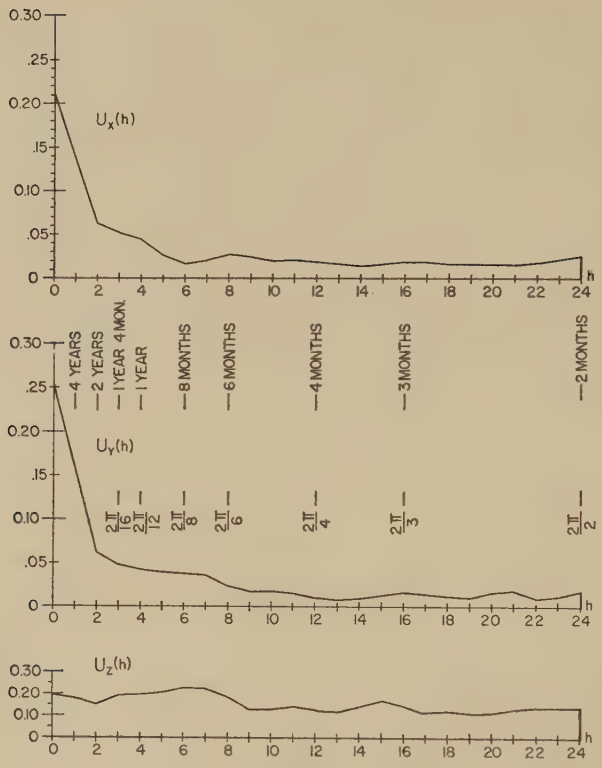

Figure 4. Graphs of $U_x(h)$, $U_y(h)$ and $U_z(h)$; $\mu = 2\pi h/48$.

Finally a quantity called the coherency, whose distribution h
been studied by Goodman (1957), can be computed. It is defined

$$K_{xy}(h) = \frac{[C_{xy}(h)]^2 + [Q_{xy}(h)]^2}{U_x(h) \cdot U_y(h)}$$

for the components X_n and Y_n, and by a similar equation for
and Z_n. The coherency is one provided the component of the vect
process can be generated by the effect of a linear operator on t
other component. In general, in geophysical problems it will
expected to be less than one.

The values of $U_x(h)$, $U_y(h)$, $U_z(h)$, $C_{xy}(h)$, $Q_{xy}(h)$, $K_{xy}(h)$, $C_{xz}($
$Q_{xz}(h)$, and $K_{xz}(h)$ are graphed in Figs. 4 and 5 and tabulated
Table II. $C_{xy}(h) = C_{yx}(h)$ and $Q_{xy}(h) = -Q_{yx}(h)$, for example.

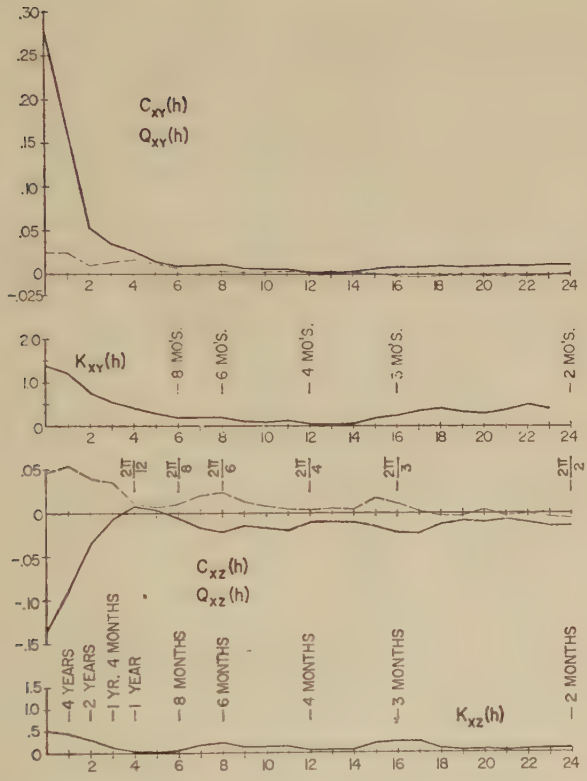

Figure 5. Graphs of $C_{xy}(h)$, $Q_{xy}(h)$, $K_{xy}(h)$, $C_{xz}(h)$, $Q_{xz}(h)$, and $K_{xz}(h)$; $\mu = 2\pi h/48$

7. *Interpretation of the Spectra.* The spectrum given by $U_x(h)$ can interpreted as follows, except for the possibility of aliasing which ll be discussed in § 9. The contribution to the total variance of the ne series for area E made by frequencies between zero and $2\pi/96$ dians/month (half the distance from 0 to $2\pi/48$) is about 0.105 C)²; since the frequency interval is half of the range for other h, e plotted value is halved. These frequencies correspond to periods nging from eight years to infinity. The contribution from fre-ıencies ranging from $2\pi/96$ to $2\pi/36$ is 0.139 (°C)². These frequencies rrespond to periods of from eight to three years, and the point ıere the estimate is plotted corresponds to a period of four years. The spectrum is quite flat for frequencies corresponding to periods

TABLE II. VALUES OF $U_x(h)$, $U_y(h)$, $U_z(h)$, $C_{xy}(h)$, $Q_{xy}(h)$, $K_{xy}(h)$, $C_{xz}(h)$, $Q_{xz}(h)$ AND $K_{xz}(h)$.

h	U_x	U_y	U_z	C_{xy}	Q_{xy}	K_{xy}	C_{xz}	Q_{xz}	K
0	.2112	.2625	.189	.2746	.0228	1.37	−.1362	.0471	.
1	.1391	.1574	.176	.1619	.0229	1.22	−.0893	.0544	.
2	.0619	.0626	.154	.0535	.0088	0.76	−.0352	.0392	.
3	.0517	.0472	.193	.0334	.0141	0.54	−.0071	.0358	.
4	.0452	.0419	.196	.0227	.0161	0.41	.0077	.0109	.
5	.0271	.0388	.209	.0139	.0101	0.28	.0037	.0061	.
6	.0169	.0369	.230	.0087	.0066	0.19	−.0054	.0104	.
7	.0202	.0355	.225	.0096	.0070	0.20	−.0170	.0202	.
8	.0272	.0238	.187	.0109	.0037	0.20	−.0224	.0241	.
9	.0250	.0167	.126	.0065	.0019	0.11	−.0151	.0127	.
10	.0202	.0172	.128	.0052	.0019	0.09	−.0171	.0080	.
11	.0219	.0148	.142	.0057	.0030	0.13	−.0203	.0048	.
12	.0193	.0100	.125	.0012	.0019	0.03	−.0110	.0040	.
13	.0158	.0082	.118	.0001	.0020	0.03	−.0101	.0054	.
14	.0138	.0094	.139	.0025	.0008	0.05	−.0106	.0043	.
15	.0158	.0127	.169	.0058	.0005	0.17	−.0159	.0175	.
16	.0169	.0160	.146	.0076	−.0020	0.23	−.0216	.0111	.
17	.0167	.0139	.116	.0076	−.0044	0.33	−.0215	.0011	.
18	.0158	.0118	.122	.0085	−.0025	0.42	−.0120	−.0057	.
19	.0163	.0109	.111	.0078	−.0004	0.34	−.0088	−.0028	.
20	.0160	.0157	.113	.0083	−.0014	0.28	−.0107	.0031	.
21	.0148	.0171	.130	.0094	−.0026	0.38	−.0077	−.0033	.
22	.0170	.0090	.135	.0085	−.0021	0.50	−.0109	−.0006	.
23	.0224	.0108	.136	.0100	−.0003	0.41	−.0156	−.0039	.
24	.0244	.0164	.136	.0106	.0003	0.28	−.0157	−.0057	.

of less than four months, and all frequencies above $2\pi/4$ contribu a total variance of about 0.21 (°C)². A similar interpretation cou be given to the power spectrum for area N.

The spectrum for the pressure gradient anomaly is strikingly d ferent from the other two spectra. It shows that contribution the total variance is nearly the same for all frequencies from ze to $2\pi/2$ radians/month and suggests that aliasing may be a proble Thus frequencies in the data corresponding to periods of from t years (or greater) to two months are all of nearly equal importan

8. *Interpretation of the Cross-spectra.* Several different thin could have happened when $R_{xy}(p)$ and $R_{xz}(p)$ were estimated. Fir

ıe three series could have been completely independent, and $R_{xy}(p)$ ıd $R_{xz}(p)$ at all lags would have been zero. Second, two of the ries could have been completely dependent in such a way that the ectrum of one series could have been completely determined from ıe other. Third, as was the case here, the series could have been rtly dependent and partly independent.

An example from another field will perhaps make this point earer. Consider the heaving motion of a ship hove to in a long ested Gaussian seaway such as those studied by Lewis (1955) and escribed by Pierson (1957).

For the time being, let X_n, as above, be the waves and Z_n the eaving motion of the ship. Under the assumption of linearity, and eglecting some of the finer aspects of the problem, the response of ıe ship to one of the sinusoidal waves in the sum can be described y (9), where a continuous variable has been used for simplicity. he frequencies involved are quite different, of course:

$$A\ddot{Z} + B\dot{Z} + CZ = a \cos \mu t + b \sin \mu t. \tag{9}$$

On solving for what Z would have to be and by computing the pectrum of Z and appropriate cross-spectra, the spectrum of Z ould simply be the spectrum of X times a certain function af A, , C and μ. The cross-spectra also would be functions of A, B, C, nd μ times the spectrum of X. The coherency would have to be lentically equal to one, as there is a completely deterministic linear rocess connecting X and Z.

One of the important results from Goodman (1957) is that, if 9) is replaced by any linear operator on X_n, then the coherency ould still be one for sufficiently great resolution in the absence of eading error in the two series.

The situation in the atmosphere-ocean system under study in this aper is much less well defined. The dynamics of the system con- ecting the two temperature fields is not well understood. It depends n the currents (both transient and quasi-steady) in that section of he ocean and on upwelling on the northern portion of the areas tudied, as was shown by Neumann, *et al.* (1958). There is doubt as o whether or not these effects could even be described in part by linear transformation on X_n to get Y_n, especially since the atmos- here-ocean complex appears to exhibit certain characteristics of a onlinear rectifying filtering and feedback network.

Also, the terms a_j, b_j, c_j, d_j, e_j, and f_j in (1) should more probab be considered as being of the form

$$a_j = a_{D1j} + a_{D2j} + \ldots a_{R1j} + a_{R2j} + \ldots \text{ (and so on)},$$

where a_{D1j} is an actual effect acting on c_{D1j} and d_{D1j} due to one set causes such as currents; a_{D2j} is another effect due to, say, upwellin a_{R1j} is a random component due to, say, errors in the data, and on. The problem of setting up a physical model for the process under study is thus quite complex.

However, despite these difficulties, the cross-spectra and cohere cies shown in Fig. 5 can be interpreted in a useful way. Some i formation on the time scale of the effects of anomalous temperatu and winds over the area of interest can be deduced.

The graphs of $C_{xy}(h)$ and $Q_{xy}(h)$ show some of the features of t temperature anomalies at areas E and N. The curve for $C_{xy}(h)$ quite similar in appearance to $U_x(h)$ and $U_y(h)$ except for the fa that it is near zero at $2\pi/4$. The quadrature spectrum is positiv and this shows that a maximum in the temperature anomaly area E tends to be followed at a later time by a maximum in t temperature anomaly in area N. For example, the value of C_{xy} (is about 0.16, the value of $Q_{xy}(1)$ is about 0.02 corresponding to phase lag of $\tan^{-1}(1/8)$, or about 7°. Since the frequency involv corresponds to a period of four years, this means that a peak in a oscillation with about a four year period for area E tends to followed about one month later by a peak in the correspondi oscillation at area N. The lag of Y_n behind X_n (N behind E) between one month and two months for frequencies less than $2\pi/$

The graph of $K_{xy}(h)$ shows that the low frequency oscillations a closely related in the two areas. A value greater than one for $h =$ and $h = 1$ is possibly explained by sampling variation and by t fact that the missing data in the two series did not occur at t same times. For frequencies corresponding to periods between eig and three months, the coherency is less than 0.25, and this can interpreted to mean that what occurs in one area for these frequenci has little to do with what occurs in the other area.

The graph of $C_{xz}(h)$ is a modified upside down version of $C_{xy}(h$ The quadrature spectrum, $Q_{xz}(h)$, is relatively stronger, and at fo years the cross-spectra correspond to a phase difference of fo months when interpreted in the way that follows. For low frequenci

e cospectrum implies that an above-average pressure gradient
nomaly produces a below-average temperature anomaly, and con-
rsely. The positive quadrature spectrum at frequencies of $2\pi/48$
$2\pi/12$ shows that a minimum in the long-period fluctuation of
e pressure gradient anomaly tends to be followed several months
ter (at 4 years, it is 4 months) by a maximum in the temperature
nomaly.

The graph of $K_{xz}(h)$ shows that the temperature anomaly is not
o strongly related to the pressure gradient anomaly. Only for
ng period fluctuations of three years or more does the coherency
qual 1/2. For the higher frequency fluctuations it is quite small.
his does not mean that the study of a more complex system will
ot lead to significant results inter-relating the wind field and the
mperature anomalies at the higher frequencies.

In summary, the spectral analyses yield valuable information in
ie interpretation of the lag relationships discussed earlier in this
aper. The part of the system containing predictable fluctuations is
the longer periods, *i.e.*, greater than about a year; the shorter
eriod fluctuations are only weakly connected from one part of the
stem to the other. There is some connection between the temper-
ure anomaly fluctuations in the areas at the shorter periods of two
three months.

9. *Aliasing.* Spectra computed from time series that are read at
qually spaced points are subject to the phenomenon called aliasing,
explained by Blackman and Tukey (1958). A mean monthly value
essentially an average of the daily values of which it is composed,
nd effectively the day to day fluctuations have been smoothed by
ich an operation.

The anomalies could, in principle, have been found for any time
y an average of the reports for the 30 days centered about the time
the computation. If, for example, values of the mean anomaly
r the average of the last half of one month and the first half of
ie next month were found, the series could be made to consist of
vice as many points. With 48 lags in the covariance estimates, the
nal spectra would then have twice the frequency range.

The contributions at these higher frequencies, if any, are, in the
mputations given, folded back on the zero to $2\pi/2$ frequency
ale. Due to aliasing, for example, a spectral component with a true
equency of 2π radians/month could actually show up at the origin.

The process of averaging over the time domain effectively impos a low pass filter in the frequency domain. However, since all of t spectra exhibit a contribution at $2\pi/2$, there is some aliasing in of the spectra.

If the number of points in the series were doubled, as describ above, and if the flat parts of the spectra *were* truly white noise d to a simple random error component at each point, the result the doubled frequency scale would be to halve the given spectr estimates, report the same values over the new range, and th preserve the total variance.

Other factors based on experience in meteorology and ocean graphy must enter to judge these effects in the absence of the abili to extend the frequency range. The aliasing in the spectrum of t pressure gradient anomaly is probably serious, although some of t variance of the pressure gradient anomaly has been assigned to t right frequency since the temperature anomalies have responded it. This presence of aliasing combined with the effect of the low pa filter does not permit one to learn all that could be learned abo the effect of the wind in the system under study.

Aliasing is probably not too serious in the temperature spectr The spike is truly at low frequencies and not at some higher fr quency that has been aliased, as would be evidenced by the fa that other quantities measured over the ocean exhibit true anoma ous behaviour over entire months and years (for example, icebe counts).

10. *Sampling Variability.* The three spectra and the vario cross-spectra of the process are not precisely known. For examp on the basis of 400 points in the series and 24 lags, each spectr estimate has less than 40 degrees of freedom in a χ^2 distributio This means that the values of $U_x(h)$, $U_y(h)$, and $U_z(h)$ can multipled by 3/2 and 2/3 and that the true value of the spectru will be between these bounds with a probability of 0.90. A simil lack of precision also exists for the cross-spectra. In the year 200 the degrees of freedom will be doubled, but this is not of mu help now.

Even with these broad confidence bands, it is evident that t contributions at low frequencies in $U_x(h)$ and $U_y(h)$ are significant higher than the contributions at middle and higher frequenci Within sampling variability, $U_z(h)$ might easily be the mean ho

ontal line through the indicated values. Similarly the cross-spectra nd coherencies indicate a structure at low frequencies that cannot e explained on the basis of sampling variability.

It must therefore be concluded at a fairly high confidence level nat some part of the structure of the spectra and cross-spectra is eal. This in turn implies that the general shapes but not the details f the graphs of the covariance functions given in Fig. 3 are correct.

11. *Prediction.* The above results have shown that temperature nomalies in some sense propagate from E to N (X to Y) and that arge long-period pressure gradient anomalies are followed by emperature anomalies of an opposite sign. To complete the study, would be necessary to study $R_{yz}(p)$ and the appropriate spectra nd cross-spectra, but on the basis of the above partial analysis, esults suggest that the temperature anomalies at area N could be redicted from their own past and present values and from the past nd present values of X_n and Z_n. Although the theory would work ust as well in principle, the direction of the phase shifts and the oherencies involved suggest quite strongly that a prediction of Z_n rom its own past and present and from the past and present of X_n nd Y_n would not be very successful.

A complete study of the prediction problem has not been carried ut. A one-month prediction of the temperature anomaly for area E was made on the basis of the least squares regression equation omputed from the inverse of the determinant of $R_x(p)$ (see, for xample, Cramer, 1946). The prediction is thus a simple weighted near combination of 24 past values of the X_n series. As pointed out arlier, the one month lag would permit an explanation of 25 % of he variance of the record. The full utilization of $R_x(p)$ permits an xplanation of 50 % of the variance of the fluctuations. (This sug- ests that certain of the regression schemes that use just one or two 4 hour lags to predict future temperatures and pressures might e improved by going back several weeks into the past.)

Fig. 6 shows a portion of the graph of the temperature anomalies, he predicted anomalies, and the residual error. The longer period luctuations are quite successfully predicted. The short period luctuations are only partially predicted. The error graph, quite listinctly different from the original anomaly graph, appears to mphasize the higher frequencies more than the original series.

The prediction has not been made on independent data. This un-

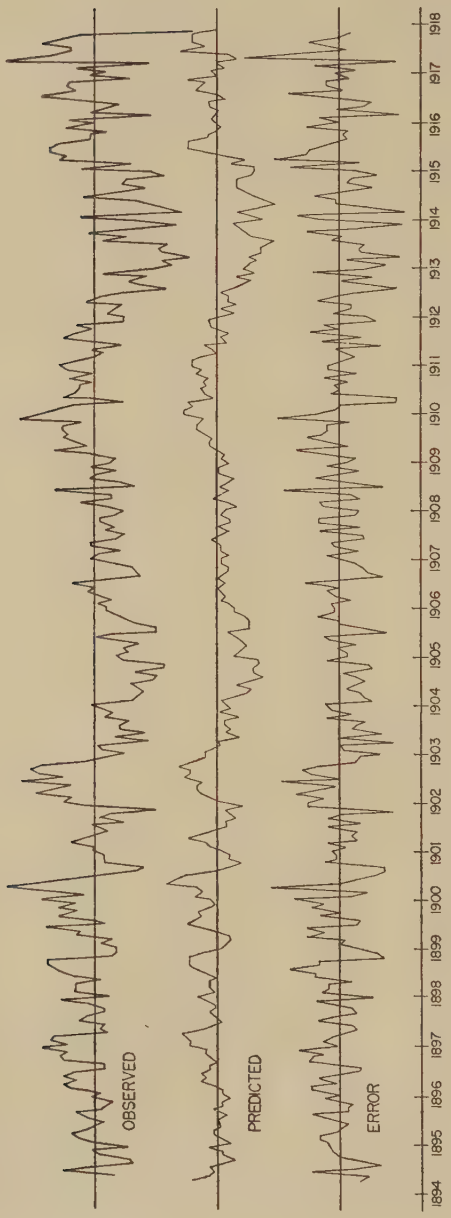

Figure 6. Selected portion of predictions for area E.

rtunate situation was forced on the writer because the data avail-
ble to him consisted only of the period of years given at the start
this paper. If a big enough portion of it had been set aside as
dependent data, the sampling variability of the spectral and cross-
ectral estimates would have suffered to the detriment of the study
their interesting features. The value of the 50 % reduction in
ariance might thus be questioned both on the basis of the lack of
independent check and also on the basis of what good it might
e, even if real.

It is believed, however, that the interesting features of the graphs
own in Fig. 3, 4, and 5 are an important result of this study.
nce the structure shown in these figures is real, results of the pre-
ction are quite likely to be not entirely accidental.

12. *Paths for Further Investigation.* There are many ways in
hich the investigation described above could be extended. The
ediction of the Y_n series could be carried out by a least squares
gression and by inverting a 96×96 determinant of the values of
(p), $R_y(p)$, $R_z(p)$, $R_{xy}(p)$, $R_{xz}(p)$, and $R_{yz}(p)$ so as to determine
e coefficients in the following equation:

$$\begin{aligned} Y_{+1} = {} & a_0 Y_0 + a_{-1} Y_{-1} + \ldots + a_{-24} Y_{-24} \\ & + b_0 X_0 + b_{-1} X_{-1} + \ldots + b_{-24} X_{-24} \\ & + c_0 Z_0 + c_{-1} Z_{-1} + \ldots + c_{-24} Z_{-24} \end{aligned} \tag{10}$$

Or perhaps the spectra and cross-spectra given above could be
noothed, described analytically in a simpler way, reinverted, and
ed to find a simpler predictor.

A point to note is that the structure of the wind system has been
mpletely suppressed to the level of white noise by using monthly
omaly values. (But the wind still affected the temperature.)
owever, the wind does have a definite spectral shape at shorter
riods. If other areas of the ocean were included and if five day
ean anomalies or weekly anomalies were studied instead of monthly
lues, the role of the atmosphere could be followed better because
e effects of aliasing and filtering would be greatly reduced. This
ght result in improved monthly anomaly predictions, since the
orter period fluctuations of from two to four months are missed
the predictions shown.

13. *Conclusions.* The system studied in this report is an inte esting one from both a meteorological and an oceanographic poi of view. The analysis of its properties was far from complete in th study. Results show that predictability lies in the continuous spe trum of the long period components, that temperature anomali downstream follow upstream fluctuations, and that the long perio part of the wind fluctuation is followed by a temperature fluctuatio but not conversely. The short period wind fluctuations that ha been aliased in part and that have been filtered out in part by usi monthly values may explain the two to four month variations in t temperature anomalies.

With the advent of larger, faster electronic computers, studies more complex systems similar to this can be carried out mo easily, and they should yield results of considerable importanc The results of this study can serve as a practical guide in planni such a program.

14. *Acknowledgments.* This work was sponsored by the Geophysi Research Directorate of the Air Force Cambridge Research Cent Air Research and Development Command. This paper is a revisi under the same title of Chapter 3 of the final report for this proje on Contract No. AF19(604)–1284, prepared by G. Neumann, *et* (1958). The help of Raymond Stevens in discussing the problem a in carrying out the computations is gratefully acknowledged. T author is indebted to Professor Gerhard Neumann and Dr. Eberha Wahl for their helpful suggestions and discussions.

REFERENCES

Bartlett, M. S.

1949. An introduction to stochastic processes. Cambridge University Pr England. 312 pp.

Blackman, R. B. and J. W. Tukey

1958. The measurement of power spectra from the point of view of commun tions engineering. Dover Publications, Inc., New York. 190 pp.

Cramer, Harald

1946. Mathematical methods of statistics. Princeton University Press. 575

Cramer, H. E. and F. A. Record

1955. Power spectra of the eddy-velocity components. J. Met., *12* (2): 146–

Goodman, N. R.

1957. On the joint estimation of the spectra, co-spectrum and quadrature s

trum of a two-dimensional stationary Gaussian process. Sci. Pap. Engng. Statist. Lab., N.Y. Univ. No. 10. 169 pp.

RENANDER, ULF AND MURRAY ROSENBLATT
1957. Statistical analysis of stationary time series. John Wiley and Sons, Inc., New York. 300 pp.

RIFFITH, H. L., H. A. PANOFSKY AND I. VAN DER HOVEN
1956. Power spectrum analysis over long ranges of frequency. J. Met., *13* (37): 279–282.

ÉVY, P.
1948. Processes stochastiques et mouvement brownien. Gauthier-Villars, Paris.

EWIS, E. V.
1955. Irregular waves in model tanks, *in*, Ships and waves. Coun. on Wave Res. and Soc. of Naval Architects and Marine Engineers. J. W. Johnson, Ed. Pp. 324–331.

ORENZ, E. N.
1956. Empirical orthogonal functions and statistical weather prediction. Sci. Rep. Statist. Forecast. Proj., M.I.T., No. 1; 49 pp.

ALONE, T. F.
1956. Application of synoptic climatology to weather prediction, *in*, Petterssen's Weather Analysis and Forecasting. McGraw-Hill Book Co., New York; Chap. 28: 238–255.

ILLER, R. G.
1956. Statistics and the predictability of weather. Bull. Amer. meteor. Soc., *35*: 495–496 (Abstr.).

EUMANN, GERHARD, EDWIN L. FISCHER, J. P. PANDOLFO AND W. J. PIERSON, JR.
1958. Studies on the interaction between ocean and atmosphere with application to long range weather forecasting. Final Rep. Engng. Res. Div., N.Y. Univ. Contract AF19(604)–1284. 100 pp.

ERSON, W. J., JR.
1955. Wind generated gravity waves, *in*, Advances in Geophysics. Vol. 2, Academic Press, Inc., New York. Pp. 92–178.
1957. On the phases of the motions of ships in confused seas. Tech. Coll. Engng. Res. Div., N.Y. Univ., Contract NONR 284(17). 37 pp.

KEY, HARRY AND J. W. TUKEY
1956. Power spectral methods of analysis and their application to problems in airplane dynamics, *in*, Flight Test Manual, NATO, Advisory Group for Aeronautical Research and Development, IV-C, pp. 1–41. (Reprinted as Monogr. Bell System No. 2606.)

UTZ, R. R.
1955. Prediction of wave motion, *in*, Ships and waves. Counc. on Wave Res. and Soc. of Naval Architects and Marine Engineers. J. W. Johnson, Ed. Pp. 33–54.

Smed, Jens

1946. Monthly anomalies of the surface temperature in some areas of the nort western North Atlantic in 1876–1939 and 1945–1946. Ann. biol. Cope hague, *3*: 12–13.

1949. Monthly anomalies of the surface temperature in areas of the northe North Atlantic during the years 1876–1939 and 1945–1949. Anal. bi Copenhague, *6*: 18–27.

Tukey, J. W.

1949. The sampling theory of power spectrum estimates. Symposium on applic tions of autocorrelation analysis to physical problems, Woods Hole, Ju 13, 1949, Navexos-P-735. Office of Naval Research.

Wadsworth, G. P.

1951. Application of statistical methods to weather forecasting. Compendium Meteorology. Amer. Met. Soc., Boston. Pp. 849–858.

MAGNESIUM, STRONTIUM, AND BARIUM CONCENTRATIONS AND CALCITE-ARAGONITE RATIOS OF SOME RECENT MOLLUSCAN SHELLS

By

KARL K. TUREKIAN AND RICHARD L. ARMSTRONG

Department of Geology, Yale University

ABSTRACT

Approximately 100 recent molluscan shells have been analyzed spectrographically r Mg, Sr and Ba; their calcite-aragonite ratios were determined by X-ray diffrac- on. The methods are described in detail. The most important parameter controlling ie concentration of these trace elements in calcium carbonate shells appears to be eneric association rather than water temperature or calcite-aragonite ratio of the ell. As a group, snails are higher in Mg and lower in Sr and Ba than clams. The fractionation ratio" of the trace alkaline-earths [*e.g.*, $f = (Sr/Ca)_{shell}/(Sr/Ca)_{sea}$] creases from 0.00041 for Mg to 0.18 for Sr to 1.6 for Ba, indicating other than a mple ionic size control in trace element incorporation into the shells.

INTRODUCTION

The relationship of chemical composition and crystal structure f calcareous tests to environment and phylogeny of an organism as been a subject of recent study, particularly by geologists seeking possible additional clue to the nature of ancient environments see Chave (3, 4), Lowenstam (9, 10); Turekian (14); Turekian and Vaagé (16); Odum (11)].

It is evident from these studies that the trace element composition f a calcium carbonate shell will be a function, to a greater or lesser egree, of: (a) trace element content relative to calcium in the nvironment from which the shell is deposited; (b) temperature of he water in which the animal lives; (c) a "species" effect perhaps elated to the microenvironment of the living organism, its feeding abits, and mode of shell construction; (d) the particular polymorph r ratio of polymorphs of calcium carbonate deposited, *viz.*, calcite nd aragonite; and (e) salinity.

A fossil shell incorporated in a sediment-water matrix is also ubject to the vicissitudes of the subsequent local diagenetic history

of that region, hence it may not bear an exact chemical record
the original environment.

In this paper the general spectrographic techniques used in d
termining the concentration of Mg, Sr and Ba in calcium carbona
materials and the X-ray techniques used to determine the calcit
aragonite ratios are described and applied to a cursory study of so
contemporary marine molluscan tests. We will report later on oth
modern marine fauna as well as fossil materials.

EXPERIMENTAL

Magnesium, strontium, and barium (trace alkaline-earths) we
determined by using a Jarrell-Ash 3.4 m Ebert mount plane gratin
spectrograph and a DC arc source. For high values of Sr encountere
in modern shells, a flame photometric or X-ray fluorescence tec
nique might be more convenient. On the other hand, the low B
and Mg values are probably ascertained better with the emissio
spectrograph. The alternate chemical methods appear to require
larger amount of time than the emission spectrographic procedur
with an additional disadvantage of doubtful accuracy at the leve
of concentration encountered in this work.

The calcite-aragonite ratios have been determined with a Norel
Diffractometer, using radiation from a copper target. Our X-ra
diffraction method has given results similar to those obtained b
Lowenstam (9) and others.

Spectrographic Procedure for Magnesium. Each sample was mixe
with two parts of spectrographically pure graphite (National Carbo
SP-2 grade). Five mg of this mixture were weighed to 3% in
Roller-Smith torsion balance and placed in a $^3/_{32}''$ deep, necke
$^3/_{16}''$ diameter electrode (National Carbon Co. L4006) and arced
completion at 10 amp (DC arc). Kodak SA-2 plates were used an
processed in D-19 developer at 20°C for 3 minutes with continuou
agitation.

There is option in the choice of Mg lines that can be used f
analysis. At low concentrations a set of five lines around 2800 Å
satisfactory. In this study we have used the Mg 2779.834; this li
is usable when the Mn concentration is low, as is the case for mode
molluscan shells (7); otherwise the less sensitive neighboring M
2781.417 is preferred because no interferences from Mn are presen

ne Mn content of modern gastropods, about 5 ppm, will not be a gnificant error in our present work.

Ca 3009.21 was used as an internal standard.

Fig. 1 is a working curve constructed from standards listed in able II. The coefficient of variation is approximately 12% so that uplicate analyses will give an error at the 95% confidence level of 17% of the average value reported.

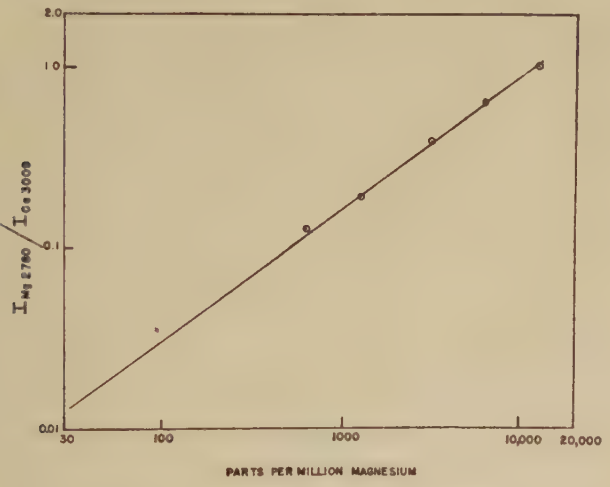

Figure 1. Working curve for magnesium.

The range of values for which the Mg 2780 line is useful is from) ppm to at least 13,000 ppm (our highest standard). For higher alues of Mg, as may be encountered in nonmolluscan tests such as ose of echinoderms, corals, some foraminifera, algae or in mag-esium-rich limestones, the Mg 3329.93 line may be used. This line also compared to the Ca 3009 line as the internal standard, and ackground correction is essential. Since the Kodak SA-2 emulsion as a constant gamma over the range of wavelengths used, only a ngle film calibration curve is necessary.

Spectrographic Procedure for Strontium and Barium. A procedure eviously developed for Sr in carbonate rocks and fossils (Kulp, *al.*, 8) was improved for modern shells and was modified to include multaneous determination of Ba.

For standards and dilution purposes it was necessary to obt calcium carbonate with low concentrations of Sr and Ba. At f this was obtained by purifying the best analytical grade calci carbonate (Mallinkrodt "Primary Standard" calcium carbon which contained about 400 ppm Sr and less than 10 ppm Ba) an ion-exchange procedure described previously (Turekian, *et al.*, Depending on the method employed in ion-exchange separation was usually possible to obtain purified calcium carbonate rang in contamination from 5 to 50 ppm Sr. This material then useful both for preparing the spectrographic standards and dilution of the normally high-Sr modern shells to bring them in correct concentration range (due to self-absorption in the hig concentration ranges), to be discussed later.

The low Ba content of most reagent grade calcium carbon eliminates the purification step for the preparation of Ba standa In addition, the modern shells were so low in Ba that no dilut by Ba-free calcium carbonate was necessary for their analysis.

Wray and Daniels (17) reported that the analytical grade calci nitrate used by them contained less than 50 ppm Sr. Our experie generally confirms this; consequently, where such concentrations tolerable in dilution procedures, as in the present case, it is necessary to prepare ion-exchange purified material. However, an analysis of silicates for Sr (and Ba) by the procedure of Tureki *et al.* (15), the highest possible purity of calcium carbonate is quired for accurate determinations.

Sr standards were prepared by mixing known amounts of str tium carbonate with ion-exchange purified calcium carbonate. standards were made by mixing known amounts of barium carbon with analytical grade calcium carbonate.

Concentrations of Sr and Ba in the calcium carbonate bases u in preparing standards were determined by a common correct procedure described by Ahrens (1: 142).

The spectrographic parameters in determining Sr and Ba listed in Table I. Since Ca is the dominant component, no difficu with regard to a matrix effect was anticipated (15). The Ca 4 line was used as an internal standard for both Sr and Ba; the li used for these elements are Sr 4607 and Ba 4554. For the Koc SA-1 emulsion these wavelengths are in the region of a rapi changing gamma, but the three utilized lines of Sr, Ca, and Ba close enough to allow the use of a common film calibration cur

TABLE I. Spectrographic Parameters*

	Magnesium	*Strontium*	*Barium*
ecial Sample eparation	1:2 with graphite	1:4 with purified (50 ppm Sr) calcium carbonate for modern shells	None for modern shells
ectrodes	5 mg sample-graphite mixture in $^3/_{32}$″ deep, necked electrodes ($^3/_{16}$″ diam.) (National Carbon #4006)	5 mg in $^3/_{16}$″ deep, necked electrode ($^3/_{16}$″ diam.) (National Carbon #4000)	Same as Sr
ectrode gap	4 mm	4 mm	4 mm
cing (D.C. arc ode excitation)	10 amps to completion	16.5 amps to completion	16.5 amps to completion
t width (μ)	10	50	50
ansmission	100%	3%	3%
lter	None	Glass	Glass
nulsion	Kodak SA #2	Kodak SA #1	Kodak SA #1
velopment	3 min. Kodak D-19, 20° C	3 min. Kodak D-19, 20° C	3 min. Kodak D-19, 20° C
alysis line (Å)	2779.83 or 2781.42 or 3329.93	4607.33	4554.04
mparison calcium e (Å)	3009.21	4578.56	4578.56

* Spectrograph: Jarrell-Ash 15,000 lines/inch grating. 3.4 meter Ebert mount, 5 Å/mm dispersion.
Microphotometer: Jarrell-Ash Model 2100.

ne Sr 4607 line in a step sector image was used for construction this calibration curve.

Use of a glass filter is desirable to eliminate any important interring second order lines, but this was not done in the work of Kulp, *al.* (8). The importance of such a precaution becomes evident for mples high in iron (15). In the case of most calcareous materials is may not be a fundamental difficulty. However, the second order ckground may affect the accuracy, since background correction is

important in determining the true relative intensities of lines in region of the spectrum.

Data for Sr standards are given in Table II and are used for working curve in Fig. 2. From these and previous results (8) estimate of error can be made. This corresponds to a coefficien variation of about 9%, hence the figures are valid for single de minations on the 95% probability level, to ±18%; for dupli

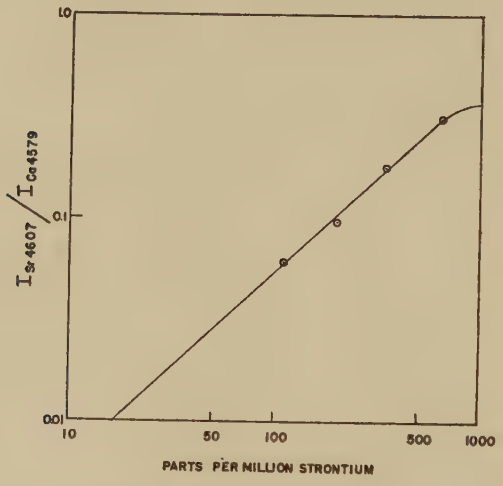

Figure 2. Working curve for strontium.

determinations the precision is ±13% of the value listed. Most of values for Sr are single analyses.

Note in Fig. 2 that self-absorption becomes prominent for Sr 4607 line when the concentration of Sr exceeds about 650 p Since most modern shells fall above this value it was necessary dilute each shell sample in a ratio of 4 to 1 with the purified calci carbonate containing 50 ppm Sr in order to get proper results.

Data for the Ba standards and the working curve are presen in Table II and Fig. 3. The coefficient of variation is about 15 so that at the 95% confidence level a duplicate analysis will h an error of about ±20%. The Ba content of modern shells is low that no dilution was necessary. However, in some fossil sh high Ba concentrations were encountered (16); in such a c

TABLE II. Replicate Determinations of Intensity Ratios Used in the Construction of Working Curves for Magnesium, Strontium, and Barium (ppm in standard)

AGNESIUM						
	Run	680	1330	3280	6530	13000
Ig 2780	1	0.128	0.219	0.384	0.726	0.818
a 3009	2	0.136	0.242	0.405	0.523	1.094
	3	0.108	0.159	0.388	0.658	1.000
	4	0.138	0.162	0.379	0.741	1.084
	5	0.135	0.184	0.412	0.601	1.145
	Av.	0.129	0.193	0.394	0.650	1.028
oeff. of Var. (%)		9.6	18.8	3.6	13.9	12.5
TRONTIUM						
	Run	110	199	347	644	1237
r 4607	1	0.066	0.088	0.193	0.300	0.376
a 4579	2	0.056	0.088	0.163	0.327	0.392
	3	0.058	0.094	0.164	0.298	0.388
	4	0.063	0.113	0.198	0.316	0.378
	5		0.101	0.182	0.362	0.362
	Av.	0.061	0.097	0.180	0.315	0.379
oeff. of Var. (%)		9.1	10.8	8.8	8.5	2.6
ARIUM						
	Run	12	40	75	183	
a 4554	1	.095	.240	.555	1.10	
a 4579	2	.155	.320	.495	0.99	
	3	.110	.258		1.18	
	Av.	.120	.273	.525	1.09	
oeff. of Var. (%)		26	15.3		8.7	

ilution may be necessary. The Ba 4554 line becomes too dark for se, with the exposure conditions employed, before self-absorption noticed.

Procedure for Determination of Calcite-aragonite Ratios. To determine shell mineralogy, a quantitative X-ray analysis was employed. This method is simple, reasonably precise, and can be pplied to a powdered specimen of almost any size down to a few illigrams; moreover, it is nondestructive as well as noncontaminative. The same powdered shell which was used for the spectrographic nalyses was used for X-ray analysis without further preparation.

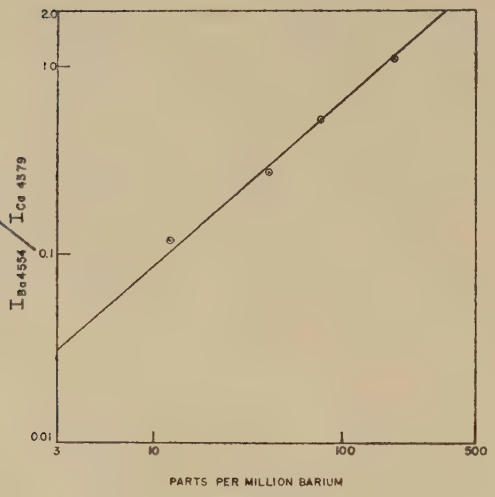

Figure 3. Working curve for barium.

Two methods were used for mounting samples, the choice method depending on the quantity of material available. No syste atic deviation between the two types of mounts could be detect If the sample was of sufficient size it was poured into brass hold with a circular central depression approximately 1 mm deep a 22 mm in diameter. The top of the loosely packed sample w gently flattened with a spatula to the top level of the holder. Jiggli and tapping of the holder and excessive packing or scraping w the spatula was avoided. No special attempt was made to insu that the sample evenly filled the depression in the holder, sin only the central portion was exposed to the X-ray beam. So long the central portion was reasonably flat and gently packed, excessive deviations due to preferred orientation were found. It necessary that the sample be finely ground in order to obtain go reproducibility.

For samples which were too small for the brass holders, circu cover glasses were used. The sample was thinly spread out in t center of the glass disk and flattened gently with a spatula. Samp of as little as 5 mg could be satisfactorily prepared in this mann If the spinning sample in the goniometer head occasionally bro apart and shifted the edges of the glass disk during peak measu ments, then the sample had to be remounted and rerun.

The apparatus was a North American Philips Company X-ray fraction unit on which was mounted a goniometer spectrometer ıipped with a geiger counter. Working conditions were: copper liation, source operated at 30 kv and 20 ma, nickel filter, 1 degree verging and .006 inch receiving slits, multiplier setting 1, time ıstant 8 sec, scale factor variable, scanning manual. The {111} ıgonite peak at ~26.2° 2θ and the {104} calcite peak at ~29.4° were used for analysis. Maximum peak intensities were read from e ratemeter dial, using manual scanning. A background measurent was made between 28.5° and 29° 2θ.

After correction for background, peak intensities were converted a function:

$$R = \frac{\text{Intensity of Calcite Peak}}{\text{Intensity of Calcite Peak} + \text{Intensity of Aragonite Peak}}.$$

e calcite percentage corresponding to the resulting ratio was read ɔm the standard curve shown in Fig. 4.

Two types of standards were used in preparing the curve. Specimens of pure calcite and aragonite crystals were ground and mixed various proportions. Using these standards, an original curve was epared. Comparison with the curve published by Lowenstam (9) ɔwed a moderate discrepancy, so new standards were prepared

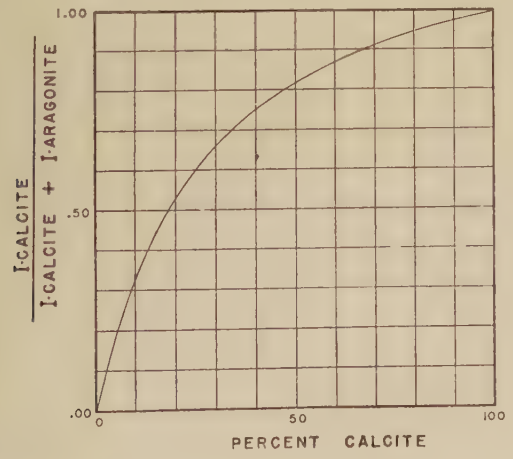

Figure 4. Working curve for calcite-aragonite ratio.

with shell calcite from *Ostrea lurida* and aragonite from *Stromb gigas*. In addition some of the original standards were reground a fresh mineral standards were prepared. Careful measurement wi the new standards established the curve shown in Fig. 4. The mine and shell standards gave identical results which have been fitted the theoretical curve drawn from $\alpha X/[\alpha X+(1-X)]=R$, where X the mole fraction calcite, α = intensity ratio, and I-calcite/I-a gonite for a 1:1 mixture. Our α value for the standard curve is 4 which is slightly larger than the α of Lowenstam's curve (about 4. Thus calcite percentages determined from the two curves will dif by a maximum of 2%; usually the difference will be less, since o values near the center of the curve are greatly affected.

Runs of several shell samples and standards were repeated und varying conditions at different times in order to obtain an estima of the precision of the method (see Table III). It is apparent that t coefficient of variation is a function of the calcite content of t sample. For intermediate concentrations (20 to 60% calcite), t coefficient of variation is approximately 5%, decreasing at high concentrations and increasing with lower concentrations. A standa containing 1.1% calcite in aragonite showed a coefficient of var tion of 38%.

TABLE III. Precision Test of Calcite-Aragonite Ratio Determination

Sample	*AF 128*	*1.1 % Calcite Stand.*
Brass sample mount	24.0	1.9
	21.5	1.1
	23.0	0.5
	22.5	1.3
Glass sample mount	21.5	1.5
	24.5	–
	23.0	–
		–
Average (% calcite)	22.9	1.3
Standard deviation	1.2	0.5
Coefficient of Variation (%)	5.2	38

In the region of low calcite concentrations there is an added certainty because of variations in background intensity. Thus re aragonite may appear at times to have 0.5% calcite when mpared to the theoretical curve constructed with an $\alpha = 4.5$. nsequently, where values of 0.5% calcite were encountered during e routine gathering of data, these were assumed to be pure aranite.

RESULTS

Results obtained on approximately 100 modern marine molluscan ells are presented in Table IV. The Ba and Mg figures are an erage of two determinations while most of the Sr numbers are om single determinations; exceptions are the *Macoma* series (AF-34 AF-43) which were run in duplicate. The appropriate error estiate for each element is given under the description of analytical ocedures.

Since concentrations were determined from working curves in hich parts per million of the element sought was plotted as a nction of the intensity ratio of the analysis line to the appropriate lcium standard line, the values are to be interpreted on the basis a pure calcium carbonate base. The ratios of the trace alkaline-rths to calcium can be determined by normalization based on this sumption. Modern shells contain about 3% organic matter (13), t this will not seriously affect our results even though they are esented on a pure calcium carbonate basis.

The shells are from the collection at Peabody Museum, Yale niversity. The locality data were limited.

DISCUSSION

Concentration of Magnesium, Strontium and Barium. The most portant parameter controlling the concentration of these trace ements in modern molluscan tests appears to be the generic associaon, although even this is often obscured by individual differences.

Magnesium. In Table IV it is seen that *Lucina* and *Chione* (clams) well as *Trivia* and possibly *Oliva* (snails) are generally lower in g than the mean for all aragonitic shells. On the other hand, *ycymeris* (clam) *Cerithium* and *Columbella* (snails) generally show gher Mg than this mean.

TABLE IV. Composition and Calcite-Aragonite Ratios of Recent Molluscan Shells, in ppm.

PELECYPODA (clams)

Number	*Species*	*General Location*	% *Calc.*	*Mg*	*Sr*
Macoma					
AF 34	*M. balthica*	L.I. Sound, Conn., U.S.A.	0	155	1700
AF 35	*M. balthica*	Halifax, N.S., Canada	0	280	1400
AF 36	*M. sabulosa*	Gulf of Maine, U.S.A.	0	150	1700
AF 37	*M. balthica*	Gulf of Maine, U.S.A.	0	125	1400
AF 38	*M. fragilis*	L.I. Sound, Conn., U.S.A.	0	185	1600
AF 39	*M. fragilis*	Labrador, Newfoundland	0	185	1600
AF 40	*M. constricta* Brug	Sanibel, Fla., U.S.A.	0	135	1800
AF 41	*M. balthica*	Wood's Hole, Mass., U.S.A.	0	320	1700
AF 42	*M. constricta*	Jamaica, B.W.I.	0	210	1500
AF 43	*M. sabulosa*	off Martha's Vineyard, Mass., U.S.A.	0	175	1700
Cardium					
AF 44	*C. costatum*	Zanzibar	0	190	1600
AF 45	*C. vathelute*	Suez	0	130	1200
AF 46	*C. negosum*	Ceylon	0	90	1500
AF 47	*C. edule*	England	0	110	1800
AF 48	*C. aculeatum*	Mediterranean	0	88	1300
Hemicardium, Laevicardium					
AF 49	*H. unedo*	Philippines	0	140	1000
AF 50	*H. obvalis*	Bay of Panama	0	130	1400
AF 51	*L. lyratum*	Philippines	0	120	1100
AF 52	*L. elenese*	Gulf of California	0	220	1500
Chione					
AF 53	*C. gnidia*	Guaymas, Gulf of Calif.	0	89	1100
AF 54	*C. histrionica*	Perlas Islands, Panama	0	95	1400
AF 55	*C. fluctifraga*	California, U.S.A.	0	98	1400
AF 56	*C. amathusia*	Zanitos, Peru	0	81	1600
AF 57	*C. lamarcki*	China	0	65	1100
AF 58	*C. stutchburi*	Aukland, New Zealand	0	72	1300
Lucina					
AF 59	*L. borealis*	Bantry, Great Britain	0	53	1500
AF 60	*L. nutthalli*	San Diego, Calif., U.S.A.	0	89	1300
AF 61	*L. filosa*	Martha's Vineyard, Mass., U.S.A.	0	58	1000

(con

TABLE IV. (cont.)

mber	*Species*	*General Location*	% *Calc.*	*Mg*	*Sr*	*Ba*
lina						
62	*T. venulosa*	Philippines	0	120	2100	14
63	*T. crucigera*	Japan	0	100	2200	7
64	*T. modesta*	California, U.S.A.	0	59	–	17
65	*T. staurella*	Fiji Islands	0	180	2000	8
66	*T. cumingi*	Gulf of California	0	99	1600	6
67	*T. incarinata*	Mediterranean	0	100	2300	7
68	*T. dispar*	Vaneole Bay, Oahu, Hawaii	0	160	>5000	9
69	*T. elizabethae*	Guam	0	140	2100	6
ca						
70	*A. senelis*	W. Africa	0	69	1300	8
71	*A. granosa*	East Indies	0	69	1200	6
72	*A. kraussi*	Shantung, China	0	99	2500	41
74	*A. ovalis*	New Haven, Conn., U.S.A.	0	140	1300	8
ycymeris						
75	*G. diomedea*	Hawaii	0	220	1800	29
76	*G. gigans*	Gulf of Mexico	0	140	1600	17
77	*G. scriptus*	W. Africa	0	190	1900	6
dakia						
78	*C. nigifera*	Fiji Islands	0	105	1300	4
79	*C. thaanumi*	Hawaii	0	200	1500	7
cten						
80	*P. ventricosa*	Guaymas, Gulf of Calif.	100	1400	860	8
81	*P. magellicanus*	Eastport, Maine, U.S.A.	100	440	1100	6
82	*P. hericius*	Puget Sound, Wash., U.S.A.	95	610	–	–
83	*P. albolineatus*	Oahu, Hawaii	80	3400	660	12
84	*P. celator*	Stewart Island, New Zealand	95	1400	1100	7
85	*P. pallium*	New Caledonia	100	4700	1200	9
ASTROPODA (snails)						
ctarius						
86	*T. Echivella/cumingi*	India	0	99	1500	14
87	T. *pagodus*	Australia	0	310	1300	8
nna, Malea						
88	*T. maculata*	Philippines	0	81	1400	7
89	*M. pomum*	Indian Ocean	0	130	1000	5

(cont.)

TABLE IV. (cont.)

Number	*Species*	*General Location*	% *Calc.*	*Mg*	*Sr*
Conus					
AF 90	*C. eburneus*	Ceylon	0	120	2100
AF 91	*C. princeps*	Gulf of California	0	76	1100
AF 92	*C. pulicarius*	Tutuila, Samoa	0	220	1100
AF 93	*C. dactyloeus*	New Zealand	0	430	1000
AF 94	*C. hebraeus*	Hawaii	0	120	1000
AF 95	*C. papilionacens*	W. Africa	0	51	1100
AF 96	*C. marmoreus*	Moluccas	0	84	1300
AF 97	*C. striatus*	Red Sea	0	75	1000
Littorina					
AF 98	*L. tenebrosa*	France	75	1400	1500
AF 99	*L. scabra*	Philippines	0	180	1700
AF 100	*L. melanostoma*	Ceylon	0	800	1800
AF 101	*L. pulchra*	Panama	0	180	1600
AF 102	*L. fasciata*	Panama	0	170	1600
AF 103	*L. basteroti*	Dalmatia	0	1450	1100
Astraea					
AF 104	*A. sulcata*	Australia	33	1900	1700
AF 105	*A. petrosum*	Fiji Islands	0	1200	1900
AF 106	*A. calcer*	New Caledonia	2	1600	2500
Cerithium					
AF 107	*C. ruprestre*	Mediterranean	0	510	1100
AF 108	*C. vertagus*	East Indies	0	490	1300
AF 109	*C. stercus muscarum*	Panama	0	170	1100
AF 110	*C. columna*	Hawaii	1	430	860
AF 111	*C. morus*	Ceylon	0	290	1100
Oliva					
AF 112	*O. guttata*	Society Islands	0	150	1800
AF 113	*O. elegans*	New Guinea	0	72	1400
AF 114	*O. erythrostoma*	Philippines	0	99	1800
AF 115	*O. peruvana*	Peru	0	58	1300
AF 116	*O. venulata*	Gulf of California	0	64	1200
Trivia					
AF 117	*T. europaea*	Guernsey	0	84	1300
AF 118	*T. sanguinea*	Panama	0	72	1700
AF 119	*T. solandri*	Peru	0	38	1400

(con

TABLE IV. (cont.)

ıber	Species	General Location	°/₀ Calc.	Mg	Sr	Ba
mbella						
120	*C. pardalina*	Bay of Yeddo, Japan	0	460	1200	9
121	*C. flavida*	Ceylon	0	73	1500	5
122	*C. major*	Panama	0	480	1400	5
123	*C. ovulata*	Philippines	0	1100	2700	7
urella, Diodora						
124	*F. volcano*	California, U.S.A.	37	270	900	5
125	*F. lineata*	Australia	1	480	1100	9
126	*D. aspersa*	California, U.S.A.	38	140	1000	8
ita						
127	*N. fuviculatum*	Ceylon	27	3000	1200	7
128	*N. scrabricosta*	Panama	22	3000	1100	–
129	*N. polita*	Philippines	52	4300	1200	5
130	*N. costata*	Nicobar	26	3400	1700	7
131	*N. albicella*	Red Sea	44	3800	1200	7
132	*N. plicata*	Micronesia	3	460	1500	7

Those genera which have species with some calcite in the shell ıcture are generally high in Mg, and this obtains even when a cies of such a genus has no calcite in it at all. Compare, for ex- ple, *Littorina tenebrosa* (75°/₀ calcite, 1400 ppm Mg) with *L. mela- toma* (0°/₀ calcite, 800 ppm Mg), or *Astraea sulcata* (33°/₀ calcite, 0 ppm Mg) with *A. petrosum* (0°/₀ calcite, 1200 ppm Mg). Note t the snail genus *Nerita*, whose species show ranges from 3–52°/₀ cite, has a mean value of 3200 ppm Mg, while the clam genus *ten*, with 80–100°/₀ calcite, has an average of only 2000 ppm. s elicits the fundamental importance of generic control of the Mg tent of the organism rather than the aragonite-calcite ratio, as gested by Chave (3).

n our sampling, the snails as a group are higher in Mg than the ms (Table IV). For Chave's smaller sampling (11 clams, 7 snails) reverse appears to be the case; his average of individual shells lyzed for Mg is different from the values he determined from arated calcareous sediments (4). The following are his values in n Mg for the molluscan fraction of carbonate sediments: Caesar ek, Florida – 580; Angelfish Key, Florida – 580; Great Isaac nk, B.W.I. – 12,000; average of separate molluscan shells – 2,700. two Florida samples agree well with our average for individual

molluscan shells (533 ppm), but on the basis of either of our sets analyses his Great Isaac Bank sample seems to have some constitue other than a molluscan component.

STRONTIUM. A similar story can be told for this element, althou the range of variation is not as great as that for Mg. The aragoni clam genus *Tellina* is fundamentally high in its Sr concentrat relative to other molluscan genera, as was shown also by Thomps and Chow (13) and Odum (11). At the other end, the aragoni snail genera *Conus*, *Cerithium*, and the mixed *Fissurella* and *Diod* contain only half as much Sr as *Tellina*. The other aragonitic for and mixed aragonite-calcite forms (excepting *Pecten*) show ab the same mean value, with some variation within genera. T mainly calcitic *Pecten* species are low in Sr, but not much more than the totally aragonitic *Conus* and *Cerithium*. Hence we again the importance of generic control on the trace-element c centration of molluscan tests.

Clams as a group are higher in Sr than snails (Table V), as c cluded previously by Thompson and Chow (13) from their la sampling. Our values for clams and snails show remarkably g agreement considering the fact that we used different techniq and a different sampling of shells.

TABLE V. AVERAGE Mg, Sr AND Ba CONCENTRATIONS IN MOLLUSCAN SHEL OBTAINED IN THIS STUDY, INCLUDING COMPARISON of Mg AND Sr WITH DATA F CHAVE (3) AND THOMPSON AND CHOW (13) RESPECTIVELY

	Magnesium				*Strontium*				*Bariu*	
	T. and A.		Chave		T. and A.		T. and C.		T. and	
	No. obs.	Mg (ppm)	No. obs.	Mg (ppm)	No. obs.	Sr (ppm)	No. obs.	Sr (ppm)	No. obs.	(p
Clams	51	354	11	3080	49	1570	44	1620	49	
Snails	47	727	7	2160	47	1390	46	1470	45	
Clams and snails	98	533	18	2700	96	1480	90	1540	94	

BARIUM. The low amount of Ba in contemporary molluscan sh is a consequence of the low Ba concentration in the ocean. Howe of the three elements here considered, the greatest variability concentration was observed for this trace alkaline-earth. Clams the whole have a higher Ba concentration than snails; this may

plained in terms of the environment in which these two groups are st often associated. Snails to a large extent are epifauna while ms have a large component of infauna. The low content of Ba in e sea contrasted with its high content in marine muds and shales ay provide the difference in environment of shell growth of clams d snails which leads to our results.

We have noted not only a marked enrichment in the Ba content relatively recent (<10,000 years old) fossil clam shells but also a ich greater increase in older fossil shells with original shell struc-re (16). Presently we are studying the problem of its incorporation shells before and after burial.

MOLLUSCAN SHELL COMPOSITION RELATIVE TO SEA WATER COMSITION. Table VI lists the ratio of each trace alkaline-earth to Ca both molluscan shells and sea water; it also gives the degree of ctionation of these three elements during shell growth. The Sr d Mg values for sea water are from the compilation of Richards 2) and the Ba value is from Bowen (2).

TABLE VI. SHELL COMPOSITION COMPARED TO SEA WATER

	$(\%\ Mg/\%\ Ca) \times 10^3$	$(\%\ Sr/\%\ Ca) \times 10^3$	$(\%\ Ba/\%\ Ca) \times 10^3$
Molluscan shells	1.33	3.70	0.025
Sea water	3180.0	20.2	0.0155
"actionation" A/B	0.00041	0.18	1.6

Note that Ba is slightly enriched in shells relative to Ca when mpared to sea water. On the other hand, Mg is markedly disminated against by molluscan shells. Sr is also discriminated ainst, but not as much as Mg.

The observed relationship suggests that the adsorption properties ions on the surface of the growing shell front or during complexing the blood of the organism has a strong effect on the ultimate ace element content of a molluscan test. If it were a matter of mple substitution in the lattice, then Goldschmidt's (5) commonly oted rules would be operative and Ba should be excluded relative both Ca and Sr because of its much larger ionic radius. However, adsorption and complexing are important controls, one might pect a greater enrichment of Ba than Sr in a growing shell.

ACKNOWLEDGMENTS

The shells analyzed in this study were supplied through t courtesy of Mr. Percy Morris from the collection of Peabody Museu Yale University. We have received financial support for the g chemical paleoecology program from several generous benefact including: The Shell Grant for Fundamental Research; The Perm nent Science Fund of the American Academy of Arts and Scienc and The Penrose Bequest of The Geological Society of America.

REFERENCES

1. Ahrens, L. H.
   1950. Spectrochemical analysis. Addison-Wesley. 267 pp.
2. Bowen, H. J. M.
   1956. Strontium and barium in sea water and marine organisms. J. Mar. b Ass. U. K., *35*: 451–460.
3. Chave, K. E.
   1954. Aspects of the biogeochemistry of magnesium: (1) Calcareous ma organisms. J. Geol., *62*: 266.
4. 1954. Aspects of the biogeochemistry of magnesium: (2) Calcareous sedime and rocks. J. Geol., *62*: 587.
5. Goldschmidt, V. M.
   1954. Geochemistry. Oxford University Press, Oxford. 730 pp.
6. Klug, H. P. and L. E. Alexander
   1954. X-ray diffraction procedures. John Wiley and Sons, Inc., New Y 716 pp.
7. Krinsley, D.
   1959. Manganese in modern and fossil gastropod shells. Nature, London, 770.
8. Kulp, J. L., K. K. Turekian and D. W. Boyd
   1952. Strontium content of limestones and fossils. Bull. geol. Soc. Amer., *63*:
9. Lowenstam, H. A.
   1954. Factors affecting the aragonite-calcite ratios in carbonate-secreting ma organisms. J. Geol., *62*: 284.
10. 1954. Systematic, Paleoecologic and evolutionary aspects of skeletal build materials. Bull. Mus. comp. Zool. Harv., *112*: 287.
11. Odum, H. T.
   1957. Biogeochemical deposition of strontium. Publ. Inst. Mar. Sci. Univ. T *4*: 39.
12. Richard, F. A.
   1957. Some current aspects of chemical oceanography, *in* Physics and Chemi of the Earth. Vol. 2: 77–118.

Thompson, T. G. and T. J. Chow
955. The strontium-calcium atom ratio in carbonate-secreting marine organisms. Deep-Sea Res., *3* (Suppl.): 20.
Turekian, K. K.
955. Paleoecological significance of the strontium-calcium ratio in fossils and sediments. Bull. geol. Soc. Amer., *66*: 155.
Turekian, K. K., P. W. Gast and J. L. Kulp
957. Emission-spectrographic method for the determination of strontium in silicate materials. Spectrochim. Acta, *9*: 40.
Turekian, K. K. and K. M. Waagé
958. Geochemistry of the Fox Hills formation, South Dakota. Bull. geol. Soc. Amer., *69*: 1655.
Wray, J. L. and F. Daniels
957. Precipitation of calcite and aragonite. J. Amer. Chem. Soc., *79*: 2031.

TRIPYRIDYLTRIAZINE, A REAGENT FOR THE DETERMINATION OF IRON IN SEA WATER

By

PETER COLLINS AND HARVEY DIEHL

Department of Chemistry,
Iowa State University, Ames, Iowa

ABSTRACT

Iron, in the parts per billion range in which it occurs in sea water, can be de mined spectro-photometrically with 2,4,6-tripyridyl-s-triazine (TPTZ). The inte violet compound formed by TPTZ and the ferrous ion is extractable into ni benzene if sodium perchlorate be added to the solution. The extraction afford means of concentrating the iron from a large sample into a small volume of ni benzene for spectrophotometric measurement. The extraction also provides a me of removing the iron impurities from the solutions of the various reagents requi reducing agent and buffer, and thus of reducing the blank essentially to zero certain precautions are observed during analysis, particularly with respect to cleaning of glassware, the absolute error is less than 0.1 μg Fe/l.

INTRODUCTION

In an excellent paper published in this Journal in 1954, Le and Goldberg reviewed the problem of determining the min amounts of iron in sea water and advanced the art by adapting the determination the exceptionally sensitive reagent of Smi *et al.* (1952): 4,7-diphenyl-1,10-phenanthroline (bathophenanth line). In the present paper a new reagent, 2,4,6-tripyridyl-s-triaz (Collins, *et al.*, 1959), equal in sensitivity to bathophenanthroline proposed for this determination. 2,4,6-tripyridyl-s-triazine (TP is easy to prepare (Case and Koft, 1959) and is much less expens than bathophenanthroline. The violet ferrous derivative can extracted into nitrobenzene; thus the reagent preserves the adv tages of effecting a concentration of the iron and provides at same time a means of removing any iron impurity from the vari reagents.

The combining ratio of TPTZ and iron is two to one. The extr tion of the violet ferrous derivate into nitrobenzene requires presence of an excess of perchlorate; the extracted materials

$(TPTZ)_2(ClO_4)_2$. The colorimetric measurements can be made ıer on the aqueous solution or on a nitrobenzene extract, the lar extinction coefficients being 22,600 at 593 mμ in aqueous ution and 24,100 at 595 mμ in nitrobenzene. The color conforms Beer's Law in both solvents and is formed completely over the range 3.4 to 5.8; if nitrobenzene extraction is used, the permisle pH range is 2.7 to 7.0. TPTZ is slightly more sensitive than hophenanthroline, for which the corresponding molar extinction fficient is 22,400 is isoamyl alcohol. The solutions are completely ble for 12 hours and probably for an indefinite period. None of common anions, including sulfate, chloride, nitrate, fluoride and chlorate, cause interference in the determination of iron with rz. The only metals which interfere are copper, cobalt and kel, and these interfere only in concentrations a hundred-fold ater than those present in sea water; thus 2.5 ppm of copper, ppm of cobalt, or 5.3 ppm of nickel are needed to produce an preciable color with the reagent.

RECOMMENDED PROCEDURE

Reagents. 2,4,6-tripyridyl-s-triazine; 0.001 M. Dissolve 0.312 g of tan, crystalline solid, with melting point 242–243.5° (G. Frederick ith Chemical Company, Columbus, Ohio), in a few drops of hydroloric acid and dilute to one liter with deionized water.

Hydroxylammonium chloride-sodium perchlorate solution. Dissve 100 g of hydroxylammonium chloride and 100 g of sodium chlorate in distilled water, mix, and dilute to one liter with tilled water. Transfer this solution to a large separatory funnel, d 10 ml of 0.001 M TPTZ and 25 ml of nitrobenzene, shake, and ow the layers to separate. Withdraw and discard the nitrobenzene er. Repeat the extraction with nitrobenzene to make certain that iron has been completely removed from the solution.

Sodium acetate-acetic acid buffer. Dissolve 82 g of sodium acetate d 58 ml of glacial acetic acid in distilled water, mix, and dilute one liter with distilled water. Transfer the solution to a large paratory funnel, add 10 ml of 0.001 M TPTZ, 10 ml of hydroxylamnium chloride-sodium perchlorate solution and 25 ml of nitronzene, shake, and allow the layers to separate. Withdraw and card the nitrobenzene layer. Repeat the extraction to insure mplete removal of all iron.

Standard iron solution; 50 μg Fe/l. Weigh accurately a quanti of about 0.1 g of electrolytic iron[1], dissolve in 20 ml of hydrochlo acid, transfer the solution to a one-liter volumetric flask, dilute the mark with deionized water, and mix thoroughly. Pipet 25.0 of this solution into a one-liter volumetric flask, add 5 ml of hyd chloric acid, dilute exactly to one liter with distilled water, and m thoroughly; this solution will contain approximately 2.5 mg 2,500 μg Fe/l. Pipet 20.0 ml of this solution into a one-liter volumet flask, add 5 ml of hydrochloric acid, dilute to exactly one liter wi deionized water, and mix thoroughly. From the initial weight the iron, calculate the iron content of this solution, which will about 50 μg Fe/l.

Deionized Water. Pass distilled water through a column of Amb lite MB-3 ion exchange resin.

Procedure. Pipet 100.0 ml of the water to be analyzed (sea wat ground water, finished water or distilled water) into a 125-ml sep ratory funnel. Add 2.0 ml of iron-free hydroxylammonium chlorid sodium perchlorate solution, 5.0 ml of 0.001 M TPTZ, and 5.0 ml iron-free buffer solution. If previous treatment of the sample, su as wet ashing, has introduced much acid, neutralize with ammoniu hydroxide to pH 4 to 5. Add 10 ml of nitrobenzene, shake for o minute, allow the phases to separate, and then gently swirl t funnel to dislodge drops of nitrobenzene clinging to the upper wal Drain the nitrobenzene layer into a 25-ml volumetric flask and repe the extraction with another 10 ml portion of nitrobenzene. Dilu the combined extracts to 25.0 ml with ethanol. Determine t absorbancy of the solution at 595 mμ, using 5-cm cells and a 4 mixture of nitrobenzene and ethanol in the solvent cell. Run reagent blank through the entire operation and subtract its a sorbancy from the absorbancy of the unknown solution.

Preparation of Calibration Curve. Pipet various volumes rangi from 0 to 50 ml of a standard iron solution containing 50.0 μg F into 125-ml separatory funnels, dilute each solution to 100 ml wi deionized water, and carry on the analysis as described in the p ceding paragraph.

[1] The electrolytic iron ignited in moist hydrogen (G. Frederick Smith Chem Co.) comes in pieces 0.5–1 mm in size and the weight taken can be adjusted to wit a few milligrams of 0.1 g; of course each lot must be weighed exactly.

RESULTS AND DISCUSSION

Inasmuch as the iron content of sea water has a tendency to ange on standing by adsorption of iron on the walls of the con-ner and because this work was carried out far inland, synthetic mples containing 10 ppm of fluoride, 3% of sodium chloride and rying amounts of iron were prepared and analyzed by the above ocedure. The results shown in Table I were calculated using the ibration curve shown in Fig. 1.

BLE I. Determination of Iron in Synthetic Sea Water, in micrograms per liter

Iron Added	*Iron Found*	*Absolute Error*
0.70	0.70	0.00
3.49	3.40	0.09
6.89	7.35	0.37
10.47	10.4	0.1
13.96	14.2	0.2

mples of treated water obtained from the Ames Municipal Water orks were also analyzed with the following results: 7.1, 7.3, 7.4 μg Fe/l. Difficulty was encountered in the first few determinations, pre-mably because iron adsorbed on the glassware is only slowly ched away. It is recommended that the separatory funnels and

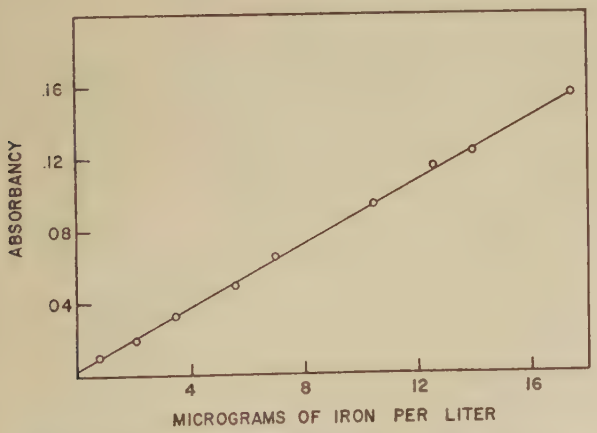

gure 1. Calibration Curve for the Determination of Small Amounts of Iron in Water.

volumetric flasks used be rinsed with only deionized water betwe determinations and that they not be subjected to the usual cleani methods. Pipets may be cleaned in a dichromate-sulfuric acid sol tion prepared from reagent grade chemicals.

As will be seen from the calibration curve (Fig. 1), the absorban values are relatively low, with little scatter; thus, small amounts iron in water can be estimated with fair accuracy using TPTZ. Th success arises from the sensitivity of the reagent, the concentrati effected by the extraction, and the essentially zero blank obtain by cleaning up the reagents. In the recommended procedure, a co centration factor of four is obtained by the extraction; this can increased by using a larger separatory funnel and a larger samp

The main precautions which must be taken in this procedure ar 1) removal of iron from the reagents; and 2) conditioning the glas ware by repeating the procedure several times before carrying o the actual determination.

REFERENCES

CASE, F. H. AND EMIL KOFT

1959. The synthesis of certain substituted 1,3,5-triazines containing the ferro containing the ferroine group. J. Amer. chem. Soc., *81*: 905–906.

COLLINS, P. F., HARVEY DIEHL AND G. F. SMITH

1959. 2,4,6-tripyridyl-s-triazine as a reagent for iron. The determination of ir in limestones, silicates, and refractories. Analyt. Chem., *31*: 1862.

LEWIS, G. J., JR. AND E. D. GOLDBERG

1954. Iron in marine waters. J. Mar. Res., *13*: 183–197.

SMITH, G. F., W. H. MCCURDY, JR. AND HARVEY DIEHL

1952. The colorimetric determination of iron in raw and treated municipal wa supplies by use of 4:7-diphenyl-1:10-phenanthroline. Analyst, *77*: 418–4

OBSERVED AND COMPUTED PATH RADIANCE IN THE UNDERWATER LIGHT FIELD

By

J. E. TYLER

Scripps Institution of Oceanography
University of California
La Jolla, California

ABSTRACT

This paper presents experimental data on changes in underwater radiance in ith and nadir directions as a function of depth for both overcast and clear sunny ting conditions at the surface. The equation developed by Preisendorfer (1957) lescribe path radiance along any path is then used to predict observed changes, predicted results are compared with the observed data.

INTRODUCTION

Recently Preisendorfer (1959) published theoretical proof of the stence of characteristic diffuse light in natural waters. This proof malizes the early conjectures of Jerlov and Liljequist (1938), hitney (1941a, 1941b), *et al.*, which were based on experimental ta obtained by Jerlov in the Baltic and by Whitney in Wisconsin es and in the Atlantic Ocean near Woods Hole, Massachusetts. The concept of characteristic diffuse light, or asymptotic radiance tribution as it has more recently been called, sometimes requires astic changes in the distribution of radiance as a function of pth. Highlights in this distribution must be attenuated and dark as must be filled in with space light. Jerlov (1951) has estimated at these changes are completed at about 300 m in the ocean while ler's (1960) data have shown that the changes are nearly complete 60 m in the water of Lake Pend Oreille. Attempts to study these anges by measuring downward, upward, and horizontal "illumina-n" (Poole, 1945) have apparently not been successful, probably e to the integrating characteristics of the optical collector used. rlov and Liljequist (1938) and Jerlov (1951), however, have given nparative radiance data at 5 m and 15 m which show attenuation the sun's direction as well as an increase in "vertical intensity"

with depth. Whitney's (1941b) radiance data at three depths (3 6 m, 9 m) have also demonstrated attenuation in the direction the sun and a progressive increase in "light intensity" in the verti direction as depth increases; his data are especially interesti because they demonstrate that the rate of change of the zen radiance ("light intensity") with depth is decreasing. More detai measurements with monochromatic light (Tyler, 1958), made depths of 2.5 cm, 3 m and 6 m, demonstrate the complex natu of changes in radiance that are taking place in the upper lay of the ocean.

The theoretical treatment of radiative transfer in hydrosc worked out by Preisendorfer, has contributed greatly to a cl understanding of the physical nature of radiative transfer in multiple scattering and absorbing hydrosol (nonisotropic). T theory can be used to predict changes in radiance along a fix path of sight underwater.

This paper presents monochromatic data for fixed paths of sig illuminated by constant sky conditions, over a depth range fr c. 0.6 to c. 60 m. The equation for path radiance will be given fr Preisendorfer (1957) and the observed radiances will be compar with those obtained by computation.

EXPERIMENTAL

A radiance measuring device (Tyler, *et al.*, 1959) having a so angle of acceptance of 6.6° was oriented vertically and lowered in optically deep homogeneous water. The water involved in this e periment is described in detail by Tyler (1960). For the bandwid under consideration the total attenuation coefficient α was 0.442/ the diffuse attenuation coefficient at 29 m was $K = 0.169$/m, a the absorption coefffcient was $a = 0.117$/m. Since the transfer radiant energy within a hydrosol depends on physical factors on not on chemical or biological considerations, the data presented h can be applied equally well to any hydrosol having physical prop ties which are identical with those of the water used in this resear For example, the water found by Nielsen and Jensen (1957) at th Station 109 in the South Atlantic off Angola is apparently ve similar to the water described here. A Wratten No. 45 filter combi with the sensitivity of the multiplier-phototube itself limited t half-bandwidth to about 64 mμ with peak value at 480 mμ. Radiar

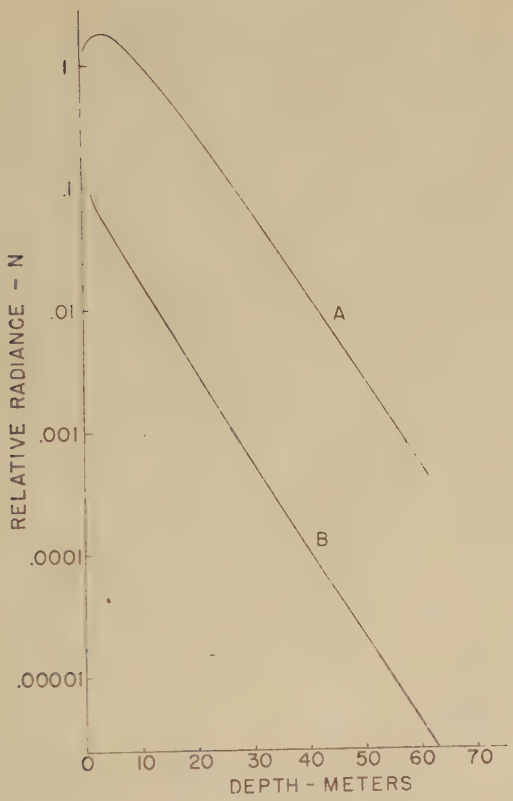

Figure 1. Observed data for zenith (Curve A) and nadir (Curve B) path radiance as unction of depth for a clear sunny day, sun altitude 56.6°.

easurements were obtained in the zenith and nadir directions nultaneously.

Observed data for zenith and nadir directions on a clear sunny y with sun altitude of 56.6° are shown in Fig. 1. Referring to rve A, if the thickness of the water film between the measuring vice and the surface could be made zero, then the instrument uld measure the radiance of the zenith sky. As the instrument is omerged the radiance in the zenith direction increases because e increase in light due to scattering along the path is greater than e decrease in light due to attenuation along the same path. At ' m these two effects just balance each other, with the result that

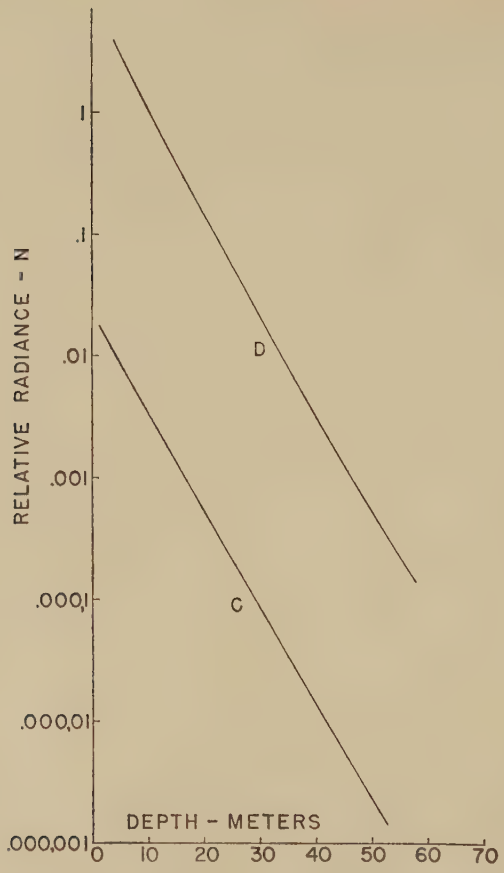

Figure 2. Observed data for zenith (Curve D) and nadir (Curve C) path radiance a function of depth on an overcast day.

the slope of the curve at this depth is zero. Below 3.7 m the negati slope of the curve, which at any point is equal to the instantaneo value of the attenuation coefficient for radiance (radiance k valu is increasing and is in fact approaching the asymptotic value, k discussed by Preisendorfer (1959).

In the nadir direction (Curve B), with the measuring device the surface, the reading is at first influenced by the back scatteri of the sun's rays, which is indicated in Curve B by its initially hi slope. This effect is quickly lost. As depth increases the negati

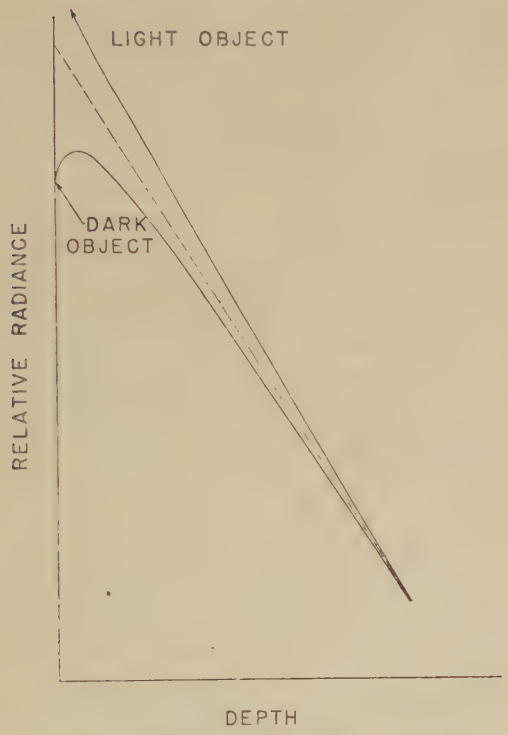

Figure 3. Radiance data adjusted at about 60 m to illustrate the relative radiance enuation of a dark object and a light object by the same water. The intersection of the ned straight line with the ordinate gives the object radiance which would be attenuated arly for all depths.

pe of the nadir curve decreases, again approaching k_{00} as an ymptotic value.

When the slopes of the two curves in Fig. 1 are compared critically 60 m they are found to differ slightly. This means that the region asymptotic distribution (Preisendorfer, 1959) was not reached in s experiment.

Experimental data of this same kind, obtained under an overcast y, are shown in Fig. 2. In this case both nadir (Curve C) and zenith urve D) radiance readings yield relatively high slopes at the sur-ce, with the slopes of both curves decreasing with depth.

In Fig. 3 the zenith readings for the two lighting conditions have en adjusted to have the same radiance value at about 60 m. Thus

Fig. 3 can be used to represent a situation (in homogeneous wa in which a dark object and a light object both appear in the ini radiance distribution for the scene. The directions in which th objects occur are not specified, nor is the initial depth. From Fi the general principle of radiance attenuation can be seen at a glan radiances with magnitudes that are relatively too large to conf with the asymptotic radiance distribution are attenuated rapi whereas those with magnitudes that are relatively too small attenuated slowly, or even enhanced. The net effect of this pro is to inexorably return the distribution to its asymptotic shape follows that there must be a value of radiance which will be att uated lineary over all depths. Its magnitude will depend on the val of α and s for the hydrosol. It is approximated in Fig. 3 by intersection of the dashed line with the ordinate. The slope of dashed straight line is of course equal to k_{00}.

THEORETICAL PREDICTIONS

Preisendorfer (1957) has developed a general equation to desc the path radiance along any path as a function of its length:

$$N_r(Z,\theta,\varphi) = N_0(Z,\theta,\varphi)\, e^{-\alpha r} + \frac{N_*(Z,\theta,\varphi)}{\alpha + K\cos\theta}\left[1 - e^{-(\alpha - K\cos\theta)r}\right].$$

In this equation $N_r(Z, \theta, \varphi)$ is the radiance of a path observed in direction θ, φ, from a depth Z. The first term on the right is transmitted radiance from the source (*e. g.*, a patch of zenith sk The second term represents the space light which accumulates the path by processes of scattering and attenuation.

$N_0(Z_t, \theta, \varphi)$ is the inherent radiance of the source at depth Z_t served in the direction θ, φ;

α is the total attenuation coefficient of the hydrosol;

r is the length of the path;

$N_*(Z, \theta, \varphi)$ is the path function in the direction θ, φ from dept (*i.e.*, the radiance per unit length along the line of sight, whic generated by the scattered light only);

K is the diffuse attenuation function;

θ is the angle between the verticle and the direction of the path;

φ is the azimuth angle.

'or a path of sight directed at the zenith, the angles θ and $\varphi = 0°$ $\cos\theta = 1$. $N_0(Z_t, \theta, \varphi)$ can be interpreted as the radiance of the ith sky (N_0) as seen from just below the water, and the path gth, r, becomes equal to depth Z. Introducing these conditions (1) and dropping the parenthetical notation for θ and φ, we have expression

$$N(Z) = N_0 e^{-\alpha Z} + \frac{N_*(Z)}{\alpha - K}\left(1 - e^{-(\alpha - K)Z}\right), \tag{2}$$

ch should predict Curve A of Fig. 1 and Curve D of Fig. 2.

'or a path of sight directed downward, $\theta = 180°$, $\cos\theta = -1$, $0°$, $N_0 = 0$ (*i.e.*, the bottom is so far away that only space light ds to be considered) and $r = 00$.

Substituting these conditions into (1) and simplyfying yields

$$N(Z) = \frac{N_*(Z)}{\alpha + K}. \tag{3}$$

s equation should predict Curves B and C of Figs. 1 and 2 re-ctively.

During the experiment described here, all of the unknowns of (2) (3) were measured except $N_*(Z)$. In order to compute $N(Z)$ as unction of Z from (2) and (3) it is necessary to first evaluate (Z). The following methods were used.

Method 1. One procedure for evaluating $N_*(Z)$ is based on the t that $N_*(Z)$ is generated by scattering and is thus diffuse light ich will be transmitted exponentially in accordance with

$$N_*(Z) = N_*(0)\, e^{-KZ}. \tag{4}$$

ingle value of $N_*(Z)$ can be computed from experimental data by ans of (2), and from this $N_*(0)$ can be determined by using (4). e resulting value of $N_*(0)$ can now be substituted into (2) to give

$$N(Z) = N_0 e^{-\alpha Z} + \frac{N_*(0)\, e^{-KZ}}{\alpha - K}\left(1 - e^{-(\alpha - K)Z}\right), \tag{5}$$

ich can be used to compute $N(Z)$ as a function of Z over the pth range.

Method 2. Using the form of the equation of transfer for radia given by Preisendorfer (1959), we have

$$\frac{dN(Z,\theta,\varphi)}{dr} = -\alpha N(Z,\theta,\varphi) + N_*(Z,\theta,\varphi);$$

we again apply the conditions for vertical measurements, *i.e.*, r = $\theta = \varphi = 0$ to obtain

$$\frac{dN(Z)}{dr} = -\alpha N(Z) + N_*(Z).$$

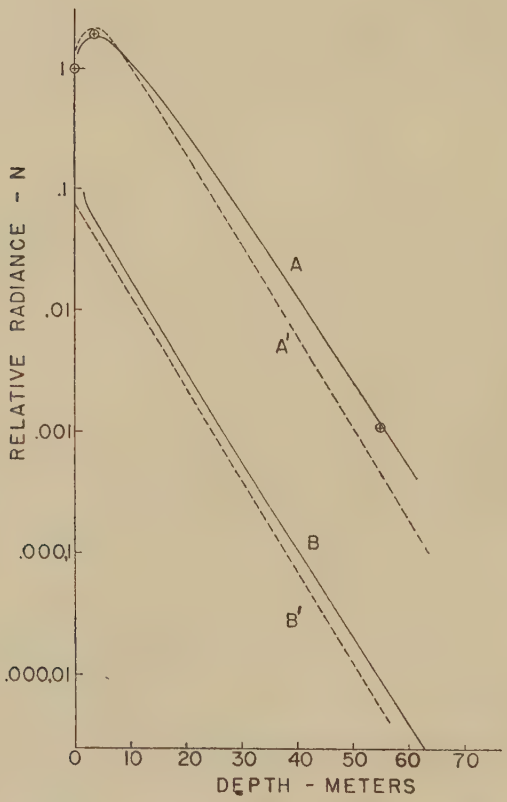

Figure 4. Comparison of observed (A) and computed (A′) values of the zenith radiance and of the observed (B) and computed (B′) values of the nadir path radian clear sunny lighting conditions.

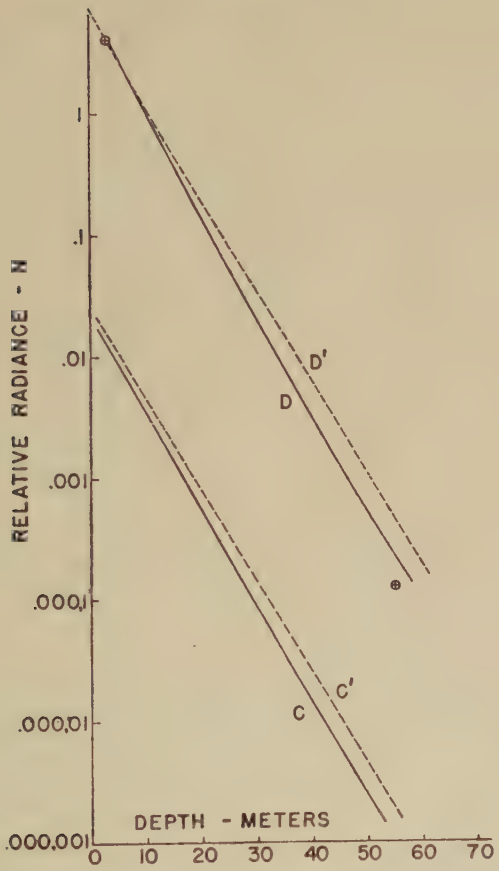

Figure 5. Comparison of observed (D) and computed (D′) values of the zenith path ance and of the observed (C) and computed (C′) values of the nadir path radiance for ·east lighting conditions.

the zenith data for the clear sunny day, $[dN(Z)]/dr$ is 0 at $Z =$ m. Thus N_* can be computed for this depth from

$$N_*(3.7\text{ m}) = \alpha\, N\,(3.7\text{ m}). \tag{8}$$

Using observed values of α, K, Z, N_0, and $N(Z)$, a series of points re computed giving the predicted zenith and nadir radiance as a ıction of depth. These points have been plotted to give curves A′, C′, D′ in Figs. 4 and 5. Fig. 4 compares the results of the com-

putation with observed values obtained on a clear sunny da
Fig. 5 compares the results of computation with observed data
an overcast day.

DISCUSSION

The differences in slope between observed and computed curves
believed to be the result of small inaccuracies in the measureme
of α and K. For example, an average experimental value of K v
used in the computations whereas theory calls for the asympto
value. If a value of K closer to the asymptotic value had been us
then the computed zenith curves would have been much closer
the observed curves. Several points have been computed with
extrapolated value of K for the asymptotic value. These poin
plotted and circled in Figs. 4 and 5, indicate the result that mig
have been obtained if the asymptotic value of K could have be
measured.

The curves shown in Figs. 1, 2, 4 and 5 are on the same relat
basis and can be intercompared. From Curves A and D it can
seen that, although there was generally less light in the water
the overcast day, the radiance from the zenith direction was actua
greater on the overcast day down to a depth of about 10 m.

The approach to asymptotic radiance distribution can be seen
a number of ways. In both Fig. 1 and Fig. 2 the slopes of the zen
and nadir curves are approaching a constant value (k_{00}). Also, t
ratio of zenith to nadir radiance ($\log N_{\text{zenith}} - \log N_{\text{nadir}}$) is approachi
the same constant value for both the clear sunny day and for t
overcast day.

The lack of dependence of the shape of the asymptotic radian
distribution on the surface lighting is seen in the facts that the slo
of the curves for the sunny day are approaching those for the ov
cast day and that the ratio of zenith to nadir radiance approacl
the same value (approx. 30) for both days.

This comparison of observed and computed path radiance is o
of a series of experiments designed to validate the nonisotrop
multiple scattering theory of Preisendorfer and to prove metho
for measuring the specified water properties. In general the resu
of these experiments have consistently demonstrated the validity
this theory and have indicated its usefulness in handling proble
relating to underwater light.

REFERENCES

ov (Johnson), N. G.
51. Optical studies of ocean waters. Rep. Swedish Deep-sea Exped., 1947–1948. 3, Physics and Chemistry No. 1: 1–59.
ov (Johnson), N. G. and Gösta Liljequist
38. On the angular distribution of submarine daylight and on the total submarine illumination. Svenska hydrograf.-biol. Konm. Skr., N.S. Hydrogr., *14*: 3–15.
sen, E. Steemann and E. Aabye Jensen
57. Primary oceanic production. The autotrophic production of organic matter in the oceans. Galathea Rep., Sci. Res. Danish Deep-sea Exped. 1950–52, *1*: 49–136 (see p. 65).
e, H. H.
45. The angular distribution of submarine daylight in deep water. Sci. Proc. R. Dublin Soc., *24*: 29–42.
sendorfer, R. W.
57. Model for radiance distribution in natural hydrosols. Visibility Lab., Scripps Inst. Oceanogr., SIO Ref. 58–42: 1–15.
59. Theoretical proof of the existence of characteristic diffuse light in natural waters. J. Mar. Res., *18*: 1–9.
r, J. E.
58. Comparison of light distribution above and below water, J. Mar. Res., *16*: 96–99.
60. Radiance distribution as a function of depth in an underwater environment. Bull. Scripps Inst. Oceanogr., *7* (5): 363–412.
r, J. E., W. H. Richardson and R. W. Holmes
59. Method of obtaining the optical properties of large bodies of water. J. geophys. Res., *64*: 667–673.
rney, L. V.
41a. The angular distribution of characteristic diffuse light in natural waters. J. Mar. Res., *4*: 122–131.
41b. A general law of diminuation of light intensity in natural waters and the percentage of diffuse light at different depths. J. opt. Soc. Amer., *31*: 714–722.

SEASONAL VARIATION IN SEA LEVEL IN THE PACIFIC OCE DURING THE INTERNATIONAL GEOPHYSICAL YEAR, 1957–1958[1]

By

JUNE G. PATTULLO[2]

Scripps Institution of Oceanography
University of California
La Jolla, California

ABSTRACT

Seasonal variations in sea level derived from IGY measurements are descr and compared with those previously published. These measurements confirm earlier descriptions, which were based on observations from gauges attached mo to continental coastlines. That is, in low latitudes in each hemisphere, sea lev high at the end of summer. There is a zonal band of high sea level from about Equator to 40°N in September while in comparable southern latitudes sea lev low. Furthermore, north of 40°N there is a distinct change of phase; sea level around the Gulf of Alaska and the Aleutians are highest in December.

The following new information has resulted from the improved distributio samples. First, sea level variations in the South Pacific are measurably smaller t those in the North Pacific. Second, the seasonal variation is appreciably larger n the continents than in the central oceanic regions of the northern hemisphere; effect is virtually absent in the southern hemisphere. Finally, the December max found earlier in the Gulf of Alaska are now known to be far more widely distribu than previously thought.

In December, sea level is high from Bering Strait south to the central So Pacific and low nearer the coasts from Mexico to Chile and from southern Japa Australia. Similar contours, but of opposite sign, appear in June.

Introduction. During the recent International Geophysical Y a widespread effort was made to extend and to improve the netw of tide gauges over the oceans, with the primary aim of improv our understanding of seasonal variations in the elevation of the s The necessity for international co-operation and for at least a

[1] Contribution from the Scripps Institution of Oceanography, New Series.

[2] Present address: Department of Oceanography, Oregon State College, C vallis, Oregon.

's observations is obvious. Fortunately, workable instruments e gauges) were readily available. More significant, though, is the that work done just prior to the start of the Year (Lisitzin, 5; Pattullo, *et al.*, 1955) indicated that the seasonal variation in

level is sufficiently coherent over large areas in the ocean so a grid, even of widely separated locations, could be expected yield interpretable results. The principal difficulty in previous stigations had been the vast lack of data in midocean; tide ges, like their human operators, are clustered principally along coastlines of the more scientifically advanced nations of the ld. To remedy this defect, we went to the islands. This paper ribes results of these sea level measurements in the Pacific an.

ocations of Observations. The Pacific Ocean contains several usand islands, but by far the larger number of these are never ted by ships and are only occasionally touched by yachts, fishing ts, or other small craft. Operation of a scientific station in such ot is difficult logistically, and expensive, and it is usually trying he morale of the personnel who man it unless resident observers be found. Therefore, wherever possible, inhabited islands, not ossibly cut off from normal transportation and communication lities, were selected.

n the North Pacific, the U.S. Coast and Geodetic Survey has blished a comprehensive and permanent network of tide gauge ions. There are unfortunate gaps in the grid, principally because e are no suitable islands in the north-central and eastern portions he North Pacific Ocean. South of the Equator, island control is ded among many nations and here new gauges were installed the IGY by Chile, France, Australia and New Zealand. At a few ts installations were made by the Scripps Institution, for the ted States, with the co-operation of the authorities and inhabit-

ata from all gauges used in this paper are listed in Table I, and ion locations are illustrated in Fig. 1.

nstrumentation and Operation of Stations. The difficulties of supply supervision demanded that the instrument be reliable and ple, relatively easy to install and maintain, and operable by a

TABLE I. Station Locations

No.	*Place*	*Latitude*	*Longitude*	*Operator*	I
–	Ugolnyi	63° 02′ N	179° 25′ E	USSR	1
C033	Yuzhno Kurilsk	44° 01′ N	145° 52′ E	UGGI	I
B070	Attu	52° 50′ N	173° 12′ E	USCGS	I
B100	Adak	51° 52′ N	176° 39′ W	USCGS	I
B056	Unalaska	53° 53′ N	166° 32′ W	UGGI	I
B015	Kodiak	57° 43′ N	152° 31′ W	USCGS	I
–	Sitka	57° 03′ N	135° 20′ W	USCGS	I
–	Crescent City	41° 45′ N	124° 12′ W	USCGS	I
–	San Francisco	37° 48′ N	122° 28′ W	USCGS	I
C407	La Jolla	32° 52′ N	117° 15′ W	USCGS	I
C240	Ensenada	31° 51′ N	116° 38′ W	UGGI	I
C271	La Paz	24° 10′ N	110° 21′ W	UGGI	I
C294	Mazatlan	23° 12′ N	106° 25′ W	UGGI	I
C295	Socorro I.	18° 44′ N	110° 01′ W	UGGI	I
C272	Manzanillo	19° 03′ N	104° 20′ W	UGGI	I
C305	Acapulco	16° 50′ N	099° 55′ W	UGGI	I
C307	Salina Cruz	16° 10′ N	095° 12′ W	UGGI	I
46	Balboa	08° 58′ N	79° 34′ W	PMRS	1
47(1)	Talara	04° 35′ S	81° 17′ W	PMRS	1
47(2)	Matarani	17° 00′ S	72° 07′ W	PMRS	1
47(3)	Valparaiso	33° 01′ S	71° 38′ W	PMRS	1
48	Puerto Montt	41° 29′ S	72° 58′ W	PMRS	1
C937	Juan Fernandez	33° 33′ S	78° 47′ W	Chile	I
E712	Easter	27° 09′ S	109° 29′ W	Chile	I
C945	Rurutu	22° 27′ S	151° 20′ W	France	I
E739	Takaroa	14° 40′ S	145° 05′ W	France	I
–	Taiohae	08° 55′ S	140° 06′ W	France	I
52	Samoa	14° 17′ S	170° 41′ W	PMRS	1
E467	Christmas	01° 57′ N	157° 28′ W	USCGS	I
E585	Fanning	03° 54′ N	159° 24′ W	SIO/UK	I
E574	Palmyra	05° 52′ N	162° 06′ W	SIO	I
E728	Arorae	02° 37′ S	176° 50′ E	SIO/UK	I
E620	Ocean	00° 53′ S	169° 35′ E	SIO/UK	I
E569	Kwajalein	08° 44′ N	167° 44′ E	USCGS	I
E563	Eniwetok	11° 22′ N	162° 21′ E	USCGS	I
E605	Moen	07° 27′ N	151° 51′ E	USCGS	I
E606	Koror	07° 20′ N	134° 28′ E	Japan	1
					1
E556	Guam	13° 26′ N	144° 39′ E	USCGS	I
E534	Wake	19° 17′ N	166° 37′ E	USCGS	I
E545	Johnston	16° 45′ N	169° 31′ W	USCGS	I

FROM MEAN SEA LEVEL (cm)

	M	*A*	*M*	*J*	*J*	*A*	*S*	*O*	*N*	*D*
	−10	−12	− 8	−12	− 3	+ 2	+ 5	+11	+17	+12
3	0	− 7	− 2	+ 2	+ 3	+ 4	+ 5	− 1	− 3	− 2
3	+ 2	− 2	0	− 8	− 8	− 2	0	+ 2	+ 6	+ 8
0	− 2	− 5	0	− 9	− 7	− 6	0	− 2	+ 2	+ 2
9	+ 2	− 2	0	+ 2	− 3	− 3	+ 4	+ 1	+ 7	+12
7	− 9	− 6	−10	−14	− 8	− 2	+ 2	+ 2	+ 6	+ 7
1	− 8	− 6	−11	−18	−16	− 6	− 5	+ 2	+ 9	+17
5	+ 2	− 6	−12	− 8	− 8	0	− 4	+ 1	− 4	+ 3
3	+ 3	− 3	− 7	− 5	− 3	− 1	+ 3	+ 2	− 4	+ 1
3	− 5	− 8	− 9	− 7	+ 1	+ 7	+ 8	+ 7	+ 3	+ 5
5	− 8	− 8	− 7	− 2	+ 2	+ 7	+ 8	+ 9	+ 6	+ 3
2	−13	−13	− 5	− 2	+ 8	+13	+16	+11	+ 8	− 1
3	−15	−17	− 3	+ 3	+13	+11	+20	+ 1	− 8	− 1
3	− 3	− 1	+ 5	+ 4	0	− 3	+10	+ 5	0	− 4
0	−12	−15	− 2	+ 2	+11	+ 8	+11	+ 3	+ 3	+ 2
8	−10	−10	0	+ 3	+11	+ 7	+ 7	− 1	+ 2	0
9	− 9	− 1	+ 4	+10	+10	+ 9	+ 8	− 2	− 3	−10
8	−18	−11	+ 2	+ 7	+ 6	+ 5	+ 8	+11	+ 9	+ 6
6	+ 4	+ 3	+ 2	+ 2	0	− 3	− 5	− 5	− 5	− 4
3	+ 4	+ 2	+ 4	0	− 2	− 4	− 5	− 4	− 2	0
2	+ 3	+ 2	0	+ 2	− 1	− 1	− 4	− 5	− 3	+ 1
4	− 2	− 2	+ 2	+ 2	+ 2	+ 2	+ 2	− 4	+ 1	+ 2
6	+ 4	+ 6	0	+ 1	+10	− 3	− 6	−11	− 5	− 3
3	+ 3	+ 3	+ 2	− 2	0	− 1	− 3	− 3	− 2	+ 3
8	+ 1	+ 5	+ 6	+ 3	− 4	− 2	− 6	−10	− 3	− 4
7	+ 6	+ 3	+ 2	− 2	0	− 2	− 2	− 5	0	− 1
2	+ 3	+ 1	+ 1	− 2	− 1	− 1	− 2	− 2	− 2	+ 2
2	+ 4	+ 3	+ 3	− 2	− 3	− 4	− 2	− 1	− 1	+ 1
0	− 5	− 6	− 4	− 7	− 2	0	0	+ 4	+ 7	+12
1	− 5	−10	−14	− 8	− 1	+ 5	+ 8	+ 9	+ 6	+16
6	− 7	− 7	− 8	− 6	+ 1	+ 5	+20	0	+ 9	+ 3
2	+ 1	− 1	− 2	− 2	0	+ 2	+ 5	+ 3	+ 3	− 2
7	− 7	− 3	− 2	− 2	0	+ 1	+ 2	+ 6	+ 7	+ 6
3	+ 4	+ 8	+ 5	+ 2	+ 4	+ 5	+ 3	+ 2	− 5	−11
7	− 5	− 5	+ 4	+ 5	+ 7	+ 7	+ 5	+ 1	− 1	− 3
8	+ 2	+10	+11	+ 7	+ 2	+ 1	+ 1	− 2	− 6	− 5
5	− 6	− 1	− 1	+ 4	+ 8	+10	+ 8	+ 9	+ 4	− 4
3	− 4	− 1	− 1	− 4	+10	+11	+ 7	+ 3	− 1	− 7
8	+ 2	+ 6	−12	− 2	+ 2	+13	+ 4	+ 1	+ 5	+ 2
1	− 7	− 7	− 7	−16	− 4	+ 9	+11	+ 7	+13	+ 1

(cont.)

TABLE I. Station Locations a

No.	*Place*	*Latitude*	*Longitude*	*Operator*	*Ye*
C288	Hilo	19°44′N	155°03′W	USCGS	IG
C278	Honolulu	21°18′N	157°52′W	USCGS	IG
C282	Kahului	20°45′N	156°28′W	USCGS	IG
C408	Mokuoloe	21°26′N	157°47′W	USCGS	IG
C275	Nawiliwili	21°58′N	159°21′W	USCGS	IG
C262	Midway	28°13′N	177°22′W	USCGS	IG
–	Hanasaki	43°17′N	145°35′E	UGGI	IG
C178	Aburatsubo	35°09′N	139°37′E	UGGI	IG
E499	Naze	28°23′N	129°30′E	UGGI	IG
62	Takao	22°37′N	120°16′E	PMRS	19
E552	Manila	14°35′N	120°58′E	UGGI	IG
E607	Davao	07°05′N	125°38′E	UGGI	IG
58a	Menado	01°32′N	124°50′E	PMRS	19
55(1)	Port Moresby	09°26′S	147°06′E	PMRS	19
55(2)	Guadalcanal	09°25′S	159°59′E	PMRS	19
–	Cairns	16°55′S	145°43′E	UGGI	IG
–	Townsville	19°20′S	146°50′E	UGGI	IG
–	Gladstone	23°53′S	151°12′E	UGGI	IG
–	Coff's Harbour	30°20′S	153°00′E	UGGI	IG
–	Camp Cove	33°53′S	151°15′E	UGGI	IG
C929	Lord Howe I.	31°31′S	159°07′E	UGGI	IG
–	Williamstown	37°52′S	144°58′E	UGGI	IG
–	Cape Sorrell	42°13′S	145°13′E	UGGI	IG
70	Auckland	36°51′S	174°49′E	PMRS	1917–23, 19
71	Bluff	46°35′S	168°22′E	PMRS	19

Table

Number When available, the number designated by Comité Spécial de l'Année Géophysi Internationale has been used to identify the station. Stations for which data h been taken from Pattullo, *et al.* (1955) are given the number assigned to the stat group by these workers. Several times an additional number is added in parenthe to distinguish between different members of the same station group. In some ca neither CSAGI nor PMRS numbers apply.

Place Name of city or island at which each tide guage was located.

Operators The operator or source of data are identified as follows:

USSR: data collected by Russian workers; transmitted to Scripps Institut by personal communication.

USCGS: stations operated by United States Coast and Geodetic Survey. D obtained through World Data Center (A) Oceanography, A & M Coll of Texas.

PMRS: Data taken directly from Pattullo, *et al.*, 1955.

Chile: IGY stations operated by the National IGY Committee of Chile. D transmitted to Scripps by the Chilean IGY Committee.

OM MEAN SEA LEVEL (cm) (cont.)

M	*A*	*M*	*J*	*J*	*A*	*S*	*O*	*N*	*D*
+ 1	— 7	— 2	0	— 1	+ 4	+ 5	+ 7	+ 2	+ 1
— 1	— 7	— 4	— 4	+ 3	+ 5	+ 5	+ 6	+ 6	+ 2
— 2	— 6	— 3	— 1	+ 1	+ 4	+ 7	+ 6	+ 6	+ 2
+ 1	— 8	— 3	— 5	+ 3	+ 5	+ 5	+ 7	+ 5	+ 3
— 4	— 2	— 1	— 6	+ 1	+ 1	+ 9	+ 8	+ 9	+ 3
— 9	—15	— 3	— 5	— 7	+ 1	+ 7	+ 5	+ 1	— 1
+ 2	— 4	— 1	— 2	+ 1	+ 2	+ 4	— 1	— 3	0
— 6	—11	— 2	+ 6	+ 6	+ 1	+ 8	+ 6	+ 5	+ 1
—20	—16	+ 3	+ 7	+17	+16	+18	+ 9	+ 3	— 6
— 7	— 4	0	+ 5	+10	+13	+11	+ 7	0	—10
— 8	— 5	— 1	+ 6	+10	+12	+17	+ 4	— 4	— 9
— 3	+ 1	+ 4	+ 8	+ 8	+ 6	+ 5	+ 1	— 2	—18
+ 3	+ 4	+ 1	0	+ 1	— 3	— 5	— 2	— 1	+ 2
+10	+10	+10	+11	— 5	—12	— 5	—10	— 6	— 6
+ 3	+ 8	+10	0	— 5	— 4	— 2	— 1	0	— 3
+10	+21	+ 4	+ 5	— 7	— 6	— 9	— 6	— 8	— 4
+13	+26	+ 5	0	— 8	— 7	—10	—10	— 8	— 3
+ 9	+14	0	+ 7	— 3	— 5	— 9	—11	— 5	— 1
+ 6	+ 9	+13	+ 2	+ 6	— 2	+ 1	— 2	—10	— 3
+10	+ 5	+12	+ 3	+ 1	— 9	— 8	— 3	— 5	— 2
+23	+16	+11	—22	— 8	— 8	—13	— 7	+ 6	+11
+ 1	+ 2	+12	+ 2	+ 6	— 3	— 2	+ 1	+ 3	— 1
— 3	— 7	+23	+ 8	+11	— 4	— 3	— 2	— 1	— 5
+ 3	+ 2	+ 4	+ 5	0	— 2	— 5	— 3	— 5	— 1
+ 6	+ 3	+ 1	— 2	— 2	— 2	— 4	+ 2	0	+ 2

LANATIONS

France: IGY stations operated by National IGY Committee of France, in part with equipment and assistance from Scripps Institution. Data obtained directly from French IGY Officers in French Polynesia.

SIO/UK: stations operated by Scripps Institution personnel or island resident in co-operation with National IGY Committee of the United Kingdom.

Japan: stations operated by Japan; data provided by Japanese Hydrographic Department.

UGGI: Monthly means published by Union Géodesique et Geophysique Internationale.

Indicates the years during which observations were taken. IGY means 1957 and/or 1958.

Area of ocean in which gauge is located; if gauge is close to a boundary between zones, no number appears in this column. See Fig. 5 and the discussion of this figure in text.

M etc. Monthly mean sea level minus annual mean sea level at the gauge, in centimeters. This quantity is referred to in the text as the "deviation."

Figure 1. Locations of tide gauges that provided data used in this study. See Ta
for identification.

semiskilled observer. Further, the data had to be such that, v
reasonable care, they could be referred to a constant datum (refere
level) throughout the observational period. Standard tide gau
such as those used by the Coast Survey (Crouse-Hinds Instrum
Co., or D. Ballauf and Co., manufacturers), or water level recor
made by Leupold and Stevens, Inc. filled these requirements,
both were used at various locations.

Operation was provided by local residents whenever possi
When this was not feasible, special technicians were maintained
the islands, at least until residents could be trained. In almost

es the observers donated all or part of their efforts generously hout reimbursement. This and the exceptionally high level of ernational co-operation achieved were the deciding factors in king the observational program a success. Details of the trials l ingenuity of the operators at each station are impressive and y will be included in a mimeographed data report.[3]

Results. The seasonal deviation of sea level from its annual mean illustrated in Fig. 2 by four quarterly contour charts. Wherever ailable, values from the IGY data are used for these charts; most the values are from this period. Where IGY data have not become ailable or are lacking, data from earlier years have been used, but se instances are few. The problems raised by this combination of Y and non-IGY data will be mentioned later.

Let us look first at the chart centered around September (Fig. 2a). te particularly the unbroken zone of higher-than-average sea level oss the entire ocean from Asia to North America and from near e Equator to about 45° N. Zero deviation lines run east-west nearly ng the Equator and on a line slightly northwest-southeast at 45° 55° N. Outside of this band, *i.e.*, north of 50° N and south of the uator, all deviations are negative. There is a slight indication of other zero deviation line to the south of the sampled region: Puerto ntt, Chile, at 40° S, has a slight positive value, and gauges on New aland and southern Australia show only small negative values.

In addition to this principal feature we note that the coastal viations, at least in the northern hemisphere, are a little larger an those out at sea. We have a band of high sea level from Japan North America, but the level tilts up as the coastal edges are proached. Note also that the deviations in the southern hemisphere e generally smaller than those in the northern and that the near- ore deviations here are not particularly larger than those offshore. We can make nearly the same remarks about the chart for March ig. 2c) as we did for the September one, except that now the areas at had positive deviations had negative ones, etc. The two pictures e nearly mirror images of each other.

When we turn to the remaining pair of charts we find an immediate fference. Again the deviations are appreciable, but instead of east- st contours the isolines run largely north-south. For example,

[3] Island Observatories, Pacific, available from World Data Center (A), Oceanography, A. and M. College of Texas.

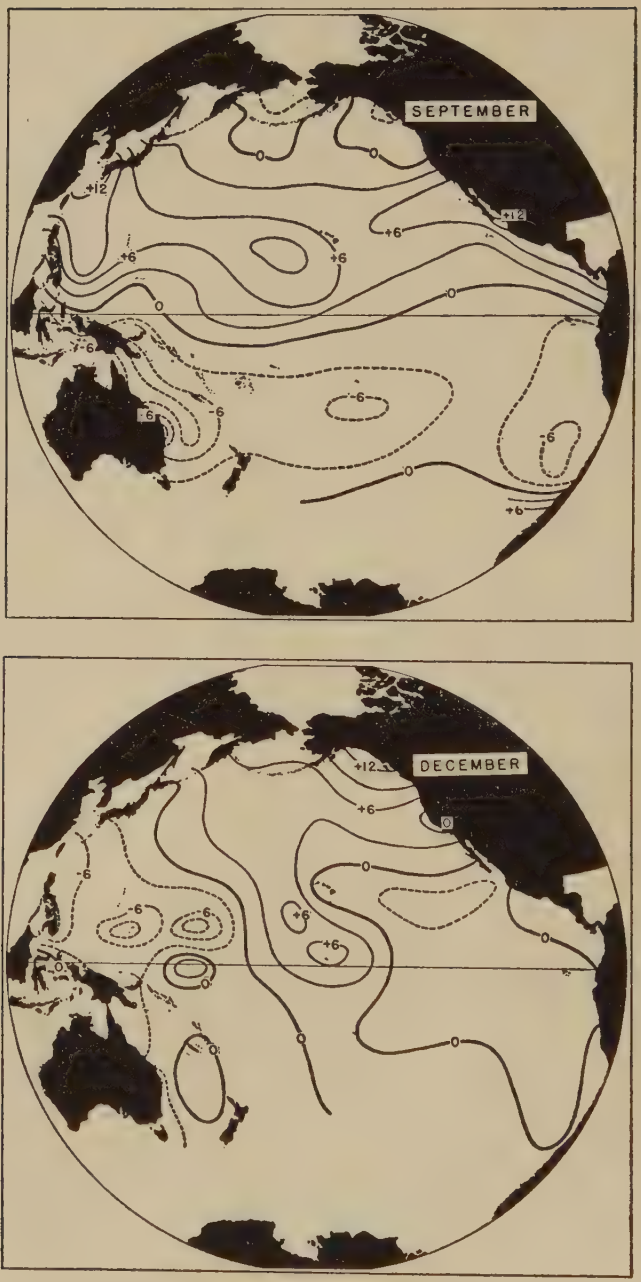

Figure 2. Deviations from mean annual sea level, by quarters, drawn for an average o
values in: (a) August, September, October; (b) November, December, January; (c) February, Ma

(d) May, June, July. Contour interval, 2 cm. Light solid lines indicate positive deviations
than annual mean); dashed lines negative deviations; heavy solid lines zero deviations.

in November, December, and January the largest positive deviati is found along the shores of the Gulf of Alaska while a strong rid of high sea level sweeps southward across the Line Islands and in the southern hemisphere. At the same time, off the continent coasts, sea level is low in both hemispheres. The oceanic maximu and offshore minima are all particularly well marked just north the Equator. In the southern hemisphere the western boundary the area of positive deviation seems poorly delineated; two isolat areas of higher-than-average sea level appear, one in the Tasm Sea and one to the north of it near the Equator.

The June picture (Fig. 2d) shows the same pattern as the Dece ber one, but again there is a reversal of sign, with the Decemb negative areas taking on positive values six months later.

We are left with essentially two patterns, one of which we can c the September-March oscillation, the other the December-Ju oscillation. The nodal, or zero, lines of these two patterns are sho in Fig. 3. These lines are drawn at the average positions of the ze

Figure 3. Zero deviations. Solid lines indicate zero deviations on September and Ma charts; dashed lines represent zero deviations on December and June charts.

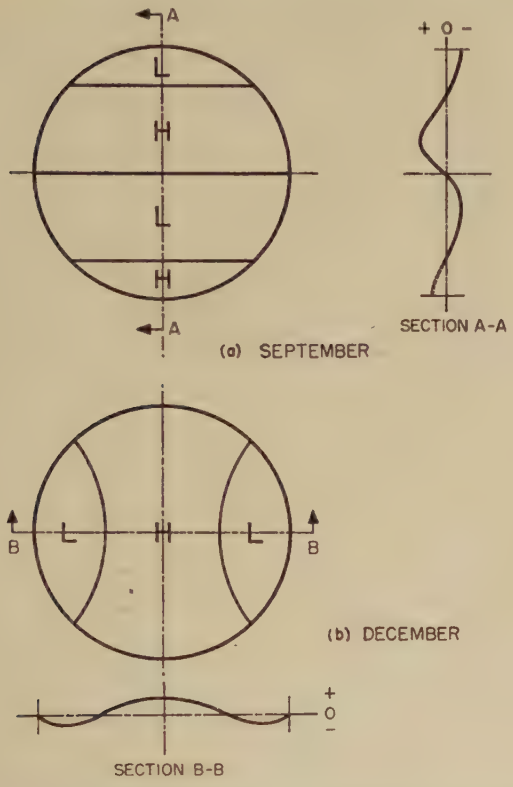

ure 4. Schematic representation of seasonal variation in sea level. (a) September
nd elevation section looking from the east; (b) December plan and elevation section
from the south.

of Fig. 2, and although their general positions and trends can
onsidered determined, obviously the details cannot be given
credence. For example, evidence given by Hamon and Stacey
uscript) indicates that the change of phase between the Austral-
oast and the central Tasman Sea is real. However, since it is
l on data from only one tide gauge located on Lord Howe
d, we will omit it from the present discussion.
nplified schematic representations of the September and Decem-
atterns are shown in Fig. 4. These would serve equally well for
h and June, respectively, if the high areas (H) were replaced by
areas (L) and vice versa. They include only the most basic

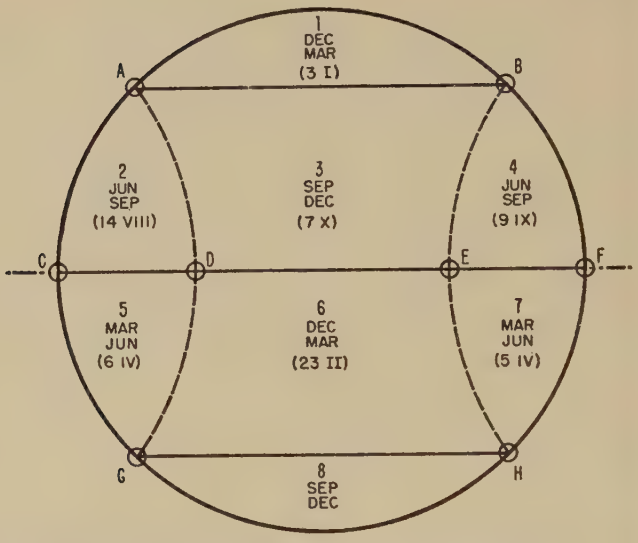

Figure 5. Schematic summary. Solid lines represent zero deviations in Septem dashed lines zero deviations in December. For discussion of lettered points, etc., see

features of the quarterly patterns, *i.e.*, in September there are e west zero lines along the Equator and at 45°N and 45°S; in Dec ber there are two nearly longitudinal zero lines and two zero po on the Equator at the coastlines.

These zero lines are combined in Fig. 5, which is the schem representation of Fig. 3. According to this model there are ei nodal points, lettered A to H, where the deviation in sea leve zero during *all four quarters of the year*. Also, since the equinoc nodal line on the Equator bisects the solstitial nodal lines, model ocean is divided into eight zones, two each of four poss kinds. Sea level is high in both December and March in zones 1 6, high in June and in September in zones 2 and 4, etc. The quarters of high level are always successive, of course, accordin our postulate that where sea level is high in one quarter it is two quarters later. The quarters of high level are indicated by names of the months lettered in each zone; the earlier of the tw given on top. We say, for example, December to March, *not* Ma to December.

We can examine the usefulness of this model as a description of variations in two ways: (1) verification of the nodal points, and

nparison of the expected time of maximum with the observed
ıe.

As one can see from Fig. 3 and from examination of the charts Fig. 2, the nodal points can be located, but only approximately. riations are low at all seasons along the coast of Kamchatka int A) and along California (point B). A zero line lies near the uator south of the Philippines on all four charts (point C) while nt F is identified nearly as well by an intersection of a zero line l the coast of South America at Ecuador on three of the charts. every season a zero line intersects the Equator just north of adalcanal (point D), and another intersection occurs between °W and 120°W (point E). A line twenty degress of longitude in ent can hardly be considered a point, but there are no islands ır the Equator between 90°W and 150°W to help us locate the

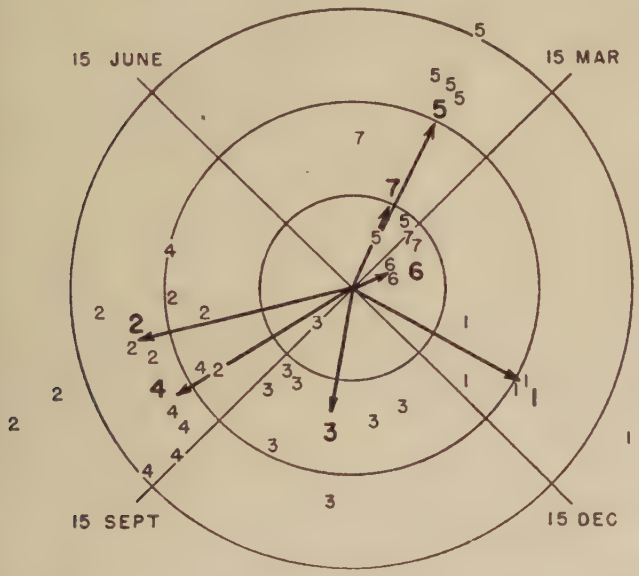

Figure 6. Phase and amplitude of the annual term for all localities within each zone. e of maximum is given by angular position: 15 March at top right, 15 June at top left, Amplitude is indicated by distance from center; the concentric circles show amplitudes , 10 and 15 cm. Each small number represents one locality within the zone indicated, ɔpting Hawaii, where all five gauge results were averaged before the harmonic analysis made. Vectors show mean phase and amplitude for all localities within the zone (vector n); the zone to which each applies is indicated by the large number placed near the end he vector.

intersection more accurately. Points G and H can be neither deter mined nor rejected with the present distribution of data.

Harmonic analyses of the data from each gauge lying within th zones were made, zones being delineated according to Fig. 3. Gauge lying on or near nodal lines were omitted; zone numbers as assigne are given in Table I. The vector mean date of maximum for th annual term for each zone is shown in parentheses in Fig. 5 an plotted as a vector in Fig. 6. From Fig. 5 we see that the time o maximum so computed lies within the expected months in all seve zones where data were available. Fig. 6 illustrates the fact that no only the vector means but the individual station vectors as wel agree with the expected times of maxima. We conclude that th schematic model is an adequate if not complete summary of th seasonal sea level variations in the Pacific Ocean during the IGY

This simple model has certain obvious weaknesses. The nodal line drawn from the data are by no means as simple as those on ou circular ocean, nor is the Pacific circular. The December midocea ridge actually has two maxima, one near Alaska and the othe around the Line Islands. Also, the hemispherical asymmetry of th variations has been neglected. However, further refinements of th model are probably not feasible at this time.

Representativeness of Results. One may reasonably ask if a shor time-series such as that of the 18-month IGY period is sufficient fo determination of the principal features of the average seasona variation. A further uncertainty is introduced by the fact that man of the IGY installations were made under somewhat unfavorabl conditions, so that some of the data cannot be considered as reliabl as those from well established gauges operated by experienced per sonnel. For example, at Arorae Island it was not possible to tak staff readings, therefore we have found it necessary to assume tha the position of the chart paper does not change appreciably and tha all readings refer to "chart zero". This is the worst situation, for a other stations have comparative staff readings, though on occasio parts of the records are missing and other difficulties have occurred

An estimate of the representativeness of the IGY data may b obtained from the five samples shown in Fig. 7, each representing different zone among the eight illustrated in Fig. 5. There is by n means exact agreement; month-to-month changes are appreciabl and sometimes erratic, and the range of heights observed at eac

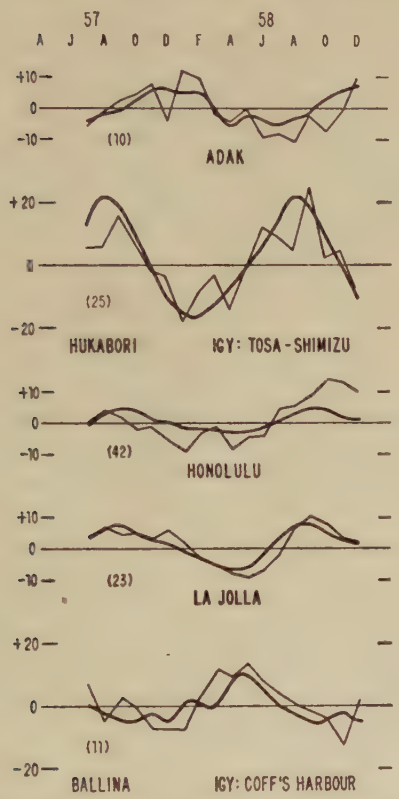

igure 7. Comparison of IGY results with long-term means at five localities. Light lines show monthly mean deviations (cm) during IGY; heavy lines show long-term thly means. The figures in parentheses indicate the number of years used in finding ong-term mean.

ation is larger during the IGY than when long-term monthly ans are compared. However, these differences are exactly what one ects when measuring climatological variables for only one year, we can see that the phase and amplitude relationships among the ions were much the same during the IGY as they were found to rom the long-term means. This implies that combination of and parison of data from different years is probably permissible, and can state with some confidence that the patterns shown in Fig. 2 typical of the average seasonal variations in sea level although her the details nor the relative slopes indicated should be given credence.

Causes of Observed Variations. The September-March oscillati has been described and discussed previously in some detail (Pattul *et al.*, 1955); at least in lower latitudes it is closely related to seasor changes in the density of the water column. This close relationsh does not in itself constitute an explanation of either the recorded the steric oscillation, nor does it identify the forces that must operative to maintain the variable slopes associated with the oscillations.

Lisitzin and Pattullo (manuscript) have found that both the Se tember-March and December-June oscillations are isostatic in t open ocean (total pressure at great depth does not vary). In l latitudes the principal factor is the steric term whereas in hi latitudes atmospheric pressure plays the dominant role. Howev the large deviations along some coastlines are apparently not isosta and an additional explanation must be sought; it probably lies in t relationships between sea slopes on the one hand and the effects winds and nonisostatic currents on the other.

Acknowledgment. This description has been made possible throu the efforts of many individuals, particularly Mr. J. D. Frautschy a Mrs. Elizabeth Parker, without whom the great amount of ordination and co-operation could not have been achieved. To al am grateful for the generous help.

REFERENCES

Hamon, B. V. and F. D. Stacey
Sea levels around Australia during the International Geophysical Ye Austr. J. Mar. Freshw. Res.

Lisitzin, Eugénie
1955. Les variations annuelles du niveau des océans. Bull. Inf. COEC, VII (235–250.

Lisitzin, Eugénie and June G. Pattullo
The principal factors influencing the seasonal oscillation in sea le Manuscript.

Pattullo, June, Walter Munk, Roger Revelle and Elizabeth Strong
1955. The seasonal oscillation in sea level. J. Mar. Res., *14* (1): 88–155.

UGGI, Union Géodesique et Géophysique Internationale
1959. Monthly and annual mean heights of sea level for the period of the Int national Geophysical Year (1957 to 1958) and unpublished data for ear years. Publ. sci. Ass. Océanogr. phys., No. 20. 65 pp.

DETERMINATION OF COBALT IN SEAWATER

By

HERBERT V. WEISS AND JOHN A. REED

U. S. Naval Radiological Defense Laboratory
Chemical Technology Division
San Francisco, California

ABSTRACT

obalt has been isolated from seawater by cocrystallization with α-nitroso-phthol. Quantitative determination by a nitroso-R-salt method for each of two ater samples has indicated the cobalt content to be 0.038 μg/l after radiometric ction for losses incurred in the isolation process.

he cobalt content of seawater has been variously estimated as μg/l (I. and W. Noddack, 1940) and 1.0 μg/l (Malyuga and Ma-ova, 1954); and a more definite range of 0.38 to 0.67 μg/l has n reported by Ishibashi (1953), but details of his analytical hod were not completely documented.

his report describes a procedure that determines accurately the centration of this element in seawater. It depends on the cocrys-ization of elements with organic reagents (Weiss and Lai, 1960), eneral process applicable to the isolation of ultramicroquantities an element from solution. After separation of cobalt along with ll amounts of certain other elements from seawater, the cobalt is ified by ion exchange and is determined quantitatively by color-tric analysis.

n preliminary study of the cocrystallization of minute quantities cobalt, the organic precipitant α-nitroso-β-naphthol was selected ause it forms an insoluble compound with cobalt, a condition ch satisfies the basic requirement for efficient cocrystallization. t solutions consisted of 0.1 l of seawater containing Co^{60} tracer h less than 10^{-10} g inert cobalt added. To these test solutions four erent weights of organic reagent dissolved in acetone, ranging n 0.4 to 3.2 mg, were introduced. The solutions were boiled for min. After cooling, the crystallized organic reagent was collected its radioactive content assayed in a gamma scintillation counter.

The cocrystallization of cobalt as determined by this measureme was quantitative when 1.6 to 3.2 mg of the reagent were us (Table I).

TABLE I. Recovery of Cobalt-60 From 0.1 Liter of Seawater by Cocrystallization With Various Concentrations of α-Nitroso-β-Naphth

α-Nitroso-β-Naphthol Added (mg)	*Co*^{60} *Recovery* (%)
0.4	89.0 ± 0.5
0.8	94.8 ± 0.5
1.6	99.4 ± 0.5
3.2	99.5 ± 0.5

This isolation procedure was subsequently applied to the det mination of cobalt in larger volumes of seawater. Surface seawa was collected in scrupulously cleaned 20 l polyethylene bottles miles due west of San Francisco in July 1959. To avoid contamin tion, the collection was made several hundred yards from the sh (It was previously established with radiotracer in seawater th cobalt does not adsorb on the surface of this polyethylene.)

Two samples, one 50 l and the other 100 l in volume, were su mitted to the following process. For convenience, each sample w subdivided into aliquots of one liter. Then 10^3 c/m of Co^{60} tra (specific activity, 19,500 mc/g) was added to each aliquot to perm final correction for chemical losses. One ml of 1.6% α-nitroso- naphthol in acetone was added, and the solution was boiled f 10 min, after which the beaker was placed on an ice-bath for 15 mi After the crystallized reagent was collected by filtration throu fine sintered glass, the filtrate was discarded. The walls of ea beaker were then washed with hot nitric acid and the wash w passed through the sintered glass funnel to dissolve the orga residue. This washing treatment was repeated twice. The washin and dissolved reagent of the aliquots from each of the origi samples were combined. To each of the combined samples 5 ml concentrated H_2SO_4 were added and the solution was evaporat until fumes of SO_3 appeared. Several milliliters of a 50:50 mixt of concentrated $HClO_4$ and HNO_3 were slowly added to the h solution to completely ash the organic residue. The samples we then heated to complete dryness, and each contained about 2 g inorganic residue. Radioactive count of the residue from the 5

ple, compared with a Co^{60} standard of the same volume, indicated 99% of the cobalt was isolated. Each ashed residue was dis-ed in distilled water. Only a small quantity of the solid was not ble, and since the undissolved material accounted for only 3 to of the cobalt, it was discarded.

ne dissolved samples were purified by ion exchange and enough entrated HCl was added to make the samples about 10N. um chloride, which crystallizes from solution with this treatment, separated from the supernatant liquid by centrifugation; it was washed several times with concentrated HCl and discarded. HCl wash was added to the main solution. The strongly acid-solution was passed through an anion exchange column in the form under previously described column conditions (Kraus and re, 1953). The column was first eluted with 6N HCl to remove el. Cobalt was then selectively eluted with 4N HCl while possible aminants (iron, zinc and copper) remained adsorbed on the mn. The recovery of cobalt was again determined radiometrically his stage of the analysis. The 50 l sample contained 87.0% of the inal quantity of cobalt, the 100 l sample 90.8%.

he eluted cobalt, evaporated to near dryness, was quantitatively yzed by a nitroso-R-salt method (Shipman and Lai, 1956). owing a blank correction for all chemicals that entered the ysis in the amounts used as well as adjustment for the cobalt l as determined radiochemically, the content of each of the vater samples was determined to be 0.038 μg/l of cobalt. The n errors in the analysis, attributable to the radioactive counting istics and the spectrophotometric measurements, were approx-tely 0.5% and 3%, respectively.

fter spectrophotometric analysis,[1] the samples were prepared for quivocal qualitative identification of the isolated material by trographic assay. The samples were combined and the nitroso-lt was removed by ashing with nitric and perchloric acid. Cobalt separated from residual salts introduced in the colorimetric ysis by adsorption on an anion exchange resin (as above) and eluted directly with 30 ml of 4N HCl. The eluate was evaporated small volume, deposited on copper electrodes and analyzed trographically. The results confirmed the presence of cobalt.

The authors wish to express their appreciation for the spectrographic analysis Conway and G. V. Shalimoff of the Lawrence Radiation Laboratory, University lifornia.

Traces of other elements (Al, Ca, Fe, Mg, Mn, Ni, Si, Ti, Zr) we also identified. However, the influence of these elements in t colorimetric determination of cobalt by this method was tested, a none interfered at concentrations far in excess of the trace quanti which was present. Thus, the quantitative value given for ea seawater sample analyzed is presented with reasonable reliabilit

REFERENCES

Ishibashi, M.

1953. Minute elements in seawater. Rec. oceanogr. Works Japan, *1*: 88–92.

Kraus, K. A. and G. E. Moore

1953. Anion exchange studies, VI. The divalent transition elements manganese zinc in hydrochloric acid. J. Amer. chem. Soc., *75*: 1460–1462.

Malyuga, D. P. and A. I. Makarova

1954. Cobalt content of soils and plants ashes of tuva. Doklady Akad. Na SSSR, *98*: 811–813.

Noddack, I. and W.

1939. Die Häufigkeiten der Schwermetalle in Meerestieren. Ark. Zool., 32A(1 1–35.

Shipman, W. H. and J. R. Lai

1956. General photometric microdetermination of cobalt with nitroso-R-s Anal. Chem., *28*: 1151–1152.

Weiss, H. V. and M. G. Lai

1960. The cocrystallization of ultramicroquantities of alkaline earth eleme with potassium rhodizonate. Anal. Chem., *32*: 475–478.

DETERMINATION AND OCCURRENCE OF COBALT IN SEA WATER

By

THOMAS G. THOMPSON AND TAIVO LAEVASTU[1]

Department of Oceanography
University of Washington
Seattle, Washington

ABSTRACT

ethods have been investigated to ascertain the most desirable procedure for mining the trace concentrations of cobalt in sea water. The nitroso-R-salt od of Sandell was adopted and modified for sea water analysis. Samples of water secured with the nonmetallic water sampler of Thompson and Chow. Prelimi- studies of the waters of the San Juan Archipelago and of Puget Sound showed lt concentrations ranging from 0.0039 to 0.0054 μg-at Co/l.

nce little is known of the biogeochemistry of cobalt in the n, study of a method to determine its amount in sea water was ated with the view of eventually investigating its role in the sea. available data on the occurrence of cobalt in sea water are marized in Table I. These data vary by more than one order nagnitude and this variation may be due to local conditions, to onal changes, or to deviations resulting from the analytical hods employed.

TABLE I. Concentrations of Cobalt in Sea Water According to Previous Investigators

Place of Collection	*μg-at/kg*	*Investigator*
Black Sea	0.059	Malyuga, 1945
Barents Sea	0.025	Malyuga, 1945
Skagerrak (Gullmarsfjord)	0.0017	I. & W. Noddack, 1939
Pacific Ocean	0.0085	Ishibashi, *et al.*, 1951
English Channel	<0.005	Black and Mitchell, 1952

Contribution No. 240, Department of Oceanography, University of Washington, le, Washington.

ortions of this work were performed under contract Nonr-477(10), Project 083–012, Office of Naval Research.

It is known that Vitamin B_{12} is a cobalt complex, and it is s
that marine animals and plants are important as sources of t
vitamin (Ivey, 1950). Bertrand and Mâcheboeuf (1925) stated t
animals have far less nickel than cobalt in their tissues, but la
I. and W. Noddack (1939) showed that the concentration of cob
in marine animals is about one-tenth that of the nickel conte
Black and Mitchell (1952) found that the concentration of cobalt
seaweeds was equivalent to about one-fourth that of nickel. Malyu
in his systematic work on algae (Vinogradov, 1953), found cob
and nickel in relatively high quantities, equivalent to about 9
at/kg of living matter or ten times this amount in the ash;
cobalt and nickel were present in 1:1 concentrations. Tsuchiya a
Makuta (1951) and Maxwell (1952) have made extensive studies
cobalt in marine products, finding from 0.2 to 6 μg-at/kg of mate
examined.

METHOD OF ANALYSIS

Reagents. All should be of reagent grade quality and should
tested for absence of cobalt.

Ammonium Hydroxide: – Dilute the concentrated reagent w
an equal volume of water.

Buffer Solution: – Dissolve 35.6 g disodium phosphate dihydr
and 6.2 g boric acid in 500 ml 1N NaOH and dilute to one lit

Citric Acid: – Dissolve 42 g of the crystals in 100 ml of wat

Distilled water: – Use redistilled water prepared in an all-gl
still for all operations.

Dithizone: – 0.02% solution in pure carbon tetrachlor
(= 200 mg/kg).

Hydrochloric Acid: – Dilute one part 12N HCl with two parts wat

Nitric Acid: – Concentrated reagent grade.

Nitroso-R-Salt: – Prepare 0.2% aqueous solution; store in c
and dark.

Perchloric Acid: – 70% reagent grade.

Sodium Carbonate: – Dissolve 50 g of reagent grade anhydr
sodium carbonate in one liter of redistilled water.

Sodium Citrate: – Dissolve 10 g of sodium citrate in 100 ml of wat

Sodium Hydroxide: – Dissolve 40 g in water and then dilute
one liter in volumetric flask.

Sulphuric Acid: – Concentrated reagent grade.

ıdard Cobalt Sulphate Solutions:
olution A. Weigh out exactly 1.2811 g of $CoSO_4 \cdot 7H_2O$, dissolve in water and dilute to one liter in a volumetric flask.
olution B. Pipet 100 ml of Solution A into a volumetric flask and dilute to exactly one liter.
olution C. Pipet 10 ml of Solution B into a volumetric flask and dilute exactly to one liter. This solution has a concentration of 0.001 μg-at Co/ml of water solution.
olutions B and C should be freshly prepared immediately before use.

cedure. Six to ten liters of freshly collected sea water were ıed with a nonmetallic sampling device (Thompson and Chow, in order to avoid contact of the water with any metal. The e was then filtered through millipore filters (H.A. type). The in the filtrate was coprecipitated with the naturally occurnagnesium in the waters by adding 50 ml of sodium carbonate ɔn per liter of collected sea water. Filtration and precipitahould be performed immediately after collecting in order to ıt changes in the cobalt content of the water by biological ty (Laevastu and Thompson, 1956).
precipitate was allowed to settle for 8 to 10 hours and the ıatant solution was then decanted through a millipore filter. ulk of the precipitate remaining in the container as well as that ed on the filter was dissolved in hydrochloric acid.
nitroso-R-salt method for the determination of cobalt (San-950) was modified to obtain an estimate of the element in sea Procedure with the modifications was as follows:
er the solution was complete, 15 ml of sodium citrate solution dded and the pH was adjusted to 8.4 to 8.5 with ammonium xide; the final volume should approximate 90 ml. The cobalt moved from this solution by adding 20 ml of dithizone reagent haking the solution in a wrist-action shaker for 20 minutes. ithizone carbon tetrachloride was separated from the solution. er portion of the dithizone reagent was added and the solution gain shaken for the same length of time. This process was ed a third time. The carbon tetrachloride extracts were com- and evaporated at a low heat; the residue was treated with l of concentrated sulfuric acid and one ml of perchloric acid, eating continued until it was colorless. When it had cooled,

one ml of citric acid and 1.5 ml of phosphate-boric acid buffer
added; the pH was adjusted to 8.0 with ammonium hydrox
then 0.5 ml of nitroso-R-salt solution was added and the resul
mixture was boiled for one minute. One ml of concentrated n
acid was then added and the mixture was boiled again for ano
minute. The solution was cooled and diluted to exactly 30 ml
distilled water. The color resulting from the presence of cobalt
stable for at least nine hours. The optical density was measure
a Beckman DU Spectrophotometer in 10 ml cells at a wavelengt
415 mμ. If any suspended material was present in the final solu
it was removed by filtration before measurements were made
the Beckman Spectrophotometer.

Calibration of Beckman DU Spectrophotometer. The follo
volumes of the cobalt standard solution C were taken: 1.00, 2
3.00, 5.00, 10.00, 15.00 and 25.00 ml; each was pipetted into a s
rate container. Then 15 ml sodium citrate was added and the s
tion was diluted to 90 ml. The solutions were then treated with
thiozine reagent and the procedure was continued in exactly
same manner as that outlined above. From the different read
obtained with the Beckman Spectrophotometer, a calibration c
showing the optical densities for various concentrations of co
was prepared for a wavelength of 415 mμ.

SUMMARY OF RESULTS

Preliminary studies on several samples of water collected in
San Juan Archipelago and on other samples from Puget Sound
a mean value of 0.0048 μg-at Co/kg, the values ranging from 0.
to 0.0054. Using previous data for nickel (Laevastu and Thomp
1956) for waters in the same regions, a nickel-cobalt ratio of
0.14 is obtained. This ratio approximates that obtained by o
investigators for marine animals and plants and also for ma
deposits (Young, 1954). More extensive studies on the occurrenc
cobalt with respect to localities, seasonal variations, marine organi
and deposits are contemplated. From present data and those repo
elsewhere, it is expected that the cobalt concentrations will var
different localities and depths and will show variations relate
biological activities and to seasons, particularly for waters at
surface and at depth.

REFERENCES

RAND, G. AND M. MÂCHEBOEUF

5. Presence of nickel and cobalt in animal tissues. C. R. Acad. Sci., Paris, *180*: 1380–1383.

K, W. A. P. AND R. L. MITCHELL

2. Trace elements in the common brown algae and in seawater. J. Mar. biol. Ass. U.K., *30* (3): 575–584.

ASHI, M., T. SHIGEMATSU AND Y. NAKAGAWA

1. Quantitative determination of nickel and cobalt in seawater. Bull. Inst. chem. Res., Kyoto, *26*: 68.

I. E.

0. Sources of Vitamin B_{12} in feed. Feedstuffs, *22* (33): 26, 66, 70–71.

ASTU, TAIVO AND T. G. THOMPSON

6. The determination and occurrence of nickel in sea water, marine organisms and sediments. J. Cons. int. Explor. Mer, *21* (2): 125–143.

UGA, D. P.

5. Content of copper, nickel, cobalt and other elements of the iron family in native water. Doklady Akad. Nauk, USSR, *48*: 113–116.

VELL, B. E.

2. The distribution of Vitamin B_{12} substance in some marine invertebrates of British Columbia. J. Fish. Res. Bd. Canada, *2* (3): 164–168.

ACK, I. AND W.

9. Die Häufigkeit der Schwermetalle in Meerestieren. Ark. Zool., *32A* (4): 1–35.

ELL, E. B.

0. Colorimetric determination of traces of metals. Interscience Publ. Inc., N.Y. 673 pp.

PSON, T. G. AND T. J. CHOW

5. A non-metallic water sampler. Deep-Sea Res., *2* (3): 200–203.

HIYA, Y. AND T. MAKUTA

1. Occurrence of cobalt in marine products. Tohoku J. agric. Res., *2*: 113–117 (Chem. Abstr., 1952, 11264a).

GRADOV, A. P.

3. The elementary chemical composition of marine organisms. Mem. Sears Found. Mar. Res., II; 647 pp.

G, E. I.

4. Trace elements in recent marine sediments. Annu. Meet. Geol. Soc. Amer. (1954), p. 125.